



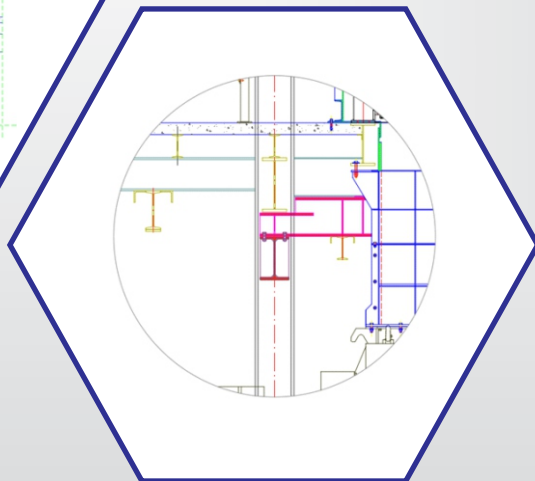
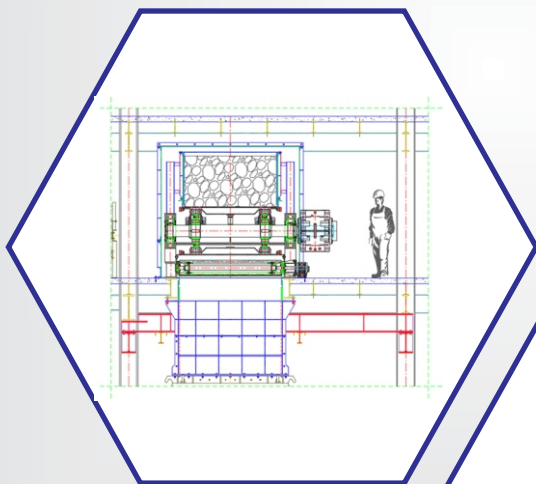
UDC 622

ISSN 2334-8836 (Štampano izdanje)

ISSN 2406-1395 (Online)

Mining and Metallurgy Engineering Bor

1/2025



Published by: Mining and Metallurgy Institute Bor

Mining and Metallurgy Engineering Bor

1/2025

MINING AND METALLURGY ENGINEERING BOR is a journal based on the rich tradition of expert and scientific work from the field of mining, underground and open-pit mining, mineral processing, geology, mineralogy, petrology, geomechanics, metallurgy, materials, technology, as well as related fields of science. Since 2001, published twice a year.

Editor-in-chief

Dr Ana Kostov
Principal Research Fellow
Mining and Metallurgy Institute Bor
Orcid: 0000-0001-6436-9091
E-mail: ana.kostov@imbor.co.rs
Phone: +38130/454-108; +38130/454-110

Deputy editor-in-chief

Dr Vesna Marjanović
Research associate
Mining and Metallurgy Institute Bor, Serbia
Orcid: 0000-0001-8005-5244

English Translation

Nevenka Vukašinović, prof.

Secretary of Editorial Board

Suzana Cvetković

Preprinting

Vesna Simić

Printed in: Grafomedtrade Bor

Circulation: 100 copies

Web site

www.imbor.co.rs

Journal is financially supported by

The Ministry of Science, Technological
Development and Innovation of the Republic Serbia
Mining and Metallurgy Institute Bor

ISSN 2334-8836 (Printed edition)

ISSN 2406-1395 (Online)

*Journal indexing in SCIndex and ISI.
All rights reserved.*

Published by

Mining and Metallurgy Institute Bor
19210 Bor, Alberta Ajnštajna 1
E-mail: institut@imbor.co.rs
Phone: +38130/454-101

**Scientific – Technical Cooperation with
the Engineering Academy of Serbia**

Editorial Board

Ignjatović Miroslav
Senior Research Associate
*Chamber of Commerce and Industry, Belgrade,
Serbia*

Kemal Gutić
Full professor
*University of Tuzla, Faculty of Mining, Geology
and Civil Engineering, Tuzla, Bosna and
Herzegovina*

Komljenović Dragan
Full professor
*Hydro-Quebec's Research Institute,
Montreal, Canada*

Milanović Dragan
Principal research fellow
Mining and Metallurgy Institute Bor, Serbia
Orcid: 0000-0002-5589-9127

Rakić Dragoslav
Full professor
*University of Belgrade, Faculty of Mining and
Geology, Belgrade, Serbia*
Orcid: 0000-0001-5375-3506

Staletović Novica
Full professor
*University of Union - Nikola Tesla, Faculty of
Ecology and Environmental Protection,
Belgrade, Serbia*
Orcid: 0000-0001-8450-5564

Trumić Biserka
Principal research fellow
Mining and Metallurgy Institute Bor, Serbia
Orcid: 0000-0001-8328-7315

Vuković Boško
Full professor
*Mine and Thermal Power Plant Gacko, Bosnia
and Herzegovina*

CONTENS

<i>Dragoslav Rakić, Marija Milosavljević, Tina Đurić, Anđelko Matić, Milenko Ljubojev</i> SETTLEMENT ANALYSIS OF THE LARGE-DIMENSIONAL SHALLOW FOUNDATIONS FOUNDED ON SAND	1
<i>Dragana Savić, Dušan Tašić, Katarina Milivojević, Dragan Ignjatović</i> IMPACT OF THE MECHANIZED EXCAVATION ON THE SLOPE STABILITY OF THE "GACKO" OPEN PIT	13
<i>Ivan Jovanović, Dušan Tašić, Miomir Mikić, Vladanka Presburger Ulniković, Novica Staletović, Violeta Nikolić</i> CLEAN ENERGY TECHNOLOGIES: THE IMPACT OF RENEWABLE SOURCES ON THE ENVIRONMENT AND ENERGY SECURITY	21
<i>Zoran Avramović, Milan Antonijević, Ljiljana Avramović, Dragana Božić, Vanja Trifunović</i> THE EFFECT OF CUPRIC IONS ON THE CORROSION BEHAVIOUR OF BRASS CuZn42 IN AN ACID ENVIRONMENT	33
<i>Ivan Stojičić, Miljan Gomilanović, Daniel Kržanović, Stefan Milanović, Tanja Stanković</i> SELECTION OF THE OPTIMAL FEEDING VARIANT FOR HAMMER CRUSHERS IN ORDER TO ACHIEVE THE DESIGNED PARAMETERS OF CRUSHED COAL	41
<i>Dejan Bugarin, Ivan Stojičić, Igor Svrkota, Miljan Gomilanović, Miloš Stojanović</i> DETERMINATION OF OPERATING AND MAINTENANCE COSTS OF TRANSPORT EQUIPMENT IN THE DEVELOPMENT OF EXPLORATORY MINE WORKINGS IN A LEAD AND ZINC MINE	53
<i>Nikola Miljković, Ivan Stojičić, Miloš Živanović, Nikola Jovanović, Jelena Stefanović</i> LIMESTONE AGGREGATE PURIFICATION AS A PART OF THE CRUSHING AND SIEVING AT THE "KAONA" QUARRY	63
<i>Miloš Živanović, Ivan Stojičić, Nikola Miljković, Jelena Stefanović, Nikola Jovanović, Miloš Marković</i> TECHNOLOGICAL AND STRUCTURAL SOLUTION FOR THE STRENGTHENING OF THE LOAD-BEARING STRUCTURE OF THE CRUSHER FACILITY DRMNO	69
<i>Jelena Stefanović, Zoran Avramović, Silvana Dimitrijević, Jelena Đorđević, Miloš Živanović, Nikola Jovanović</i> EVALUATION OF THE CORROSION RESISTANCE OF STEEL ELEMENTS FROM ELECTROLYTIC REFINING PLANT	75
<i>Nikola Jovanović, Jelena Stefanović, Miloš Živanović, Zlatko Pavlović, Nikola Miljković, Zoran Avramović</i> METHODOLOGICAL APPROACH TO MANAGING THE DEVELOPMENT OF A MAIN MINING DESIGN: A CASE STUDY OF THE X-RAY PLANT AT THE GACKO OPEN-PIT MINE	81
<i>Marija Jonović, Lidija Barjaktarović, Dejan Bugarin</i> MAXIMIZING OPPORTUNITIES BY LEVERAGING THE STRATEGIC RISK MANAGEMENT WITHIN THE SCIENTIFIC INSTITUTE	85

*Dragoslav Rakić^{*1}, Marija Milosavljević^{*}, Tina Đurić^{*},
Anđelko Matic^{**}, Milenko Ljubojev^{***}*

SETTLEMENT ANALYSIS OF THE LARGE-DIMENSIONAL SHALLOW FOUNDATIONS FOUNDED ON SAND

Orcid: 1) <https://orcid.org/0000-0001-5375-3506>

Abstract

In practice, a number of methods have been developed for calculating the settlement of shallow foundations on sand, but in general it can be said that there is no standardized calculation method. The practice has shown that when calculating the settlement of mat foundation of large dimensions, significantly larger settlements are obtained compared to the measured ones. This may indicate certain shortcomings when using the usual empirical relations for settlement calculation. This work presents the most commonly used semi-empirical methods for calculating the foundation settlement on sandy soils, and it analyzes the results obtained using different approaches (Schmertmann et al., 1970, 1978; Schultze and Sherif, 1973; Janbu et al., 1956), including the numerical simulations in the Settle3 program, which combines the simplicity of one-dimensional settlement analysis with the visualization capabilities of more modern three-dimensional programs. The analysis was carried out on one specific facility that was built in Novi Sad. During its construction, geodetic monitoring of settlement was performed, which enabled a comparison between the calculated and measured values.

Keywords: *elasticity theory, mat foundation, calculated settlement, geodetic measurement*

1 INTRODUCTION

The load on the foundation facility causes its vertical displacement - settlement. The settlement process can be caused by the momentary deformations of the soil, long-term consolidation or changes in the stress state in the soil, and the total settlement is typically divided into three components (Figure 1)

$$S = S_i + S_c + S_s \quad (1)$$

where:

s - total settlement

s_i - initial (current, elastic) settlement

s_c - consolidation settlement

s_s - secondary settlement

A similar equation is used in the EC7 regulations where for the settlement calculation in partially saturated and saturated soil, three components are also analyzed

$$S_{Ed} = S_i + S_c + S_s \leq S_{Cd} \quad (2)$$

where:

S_{Ed} - total settlement caused by the action effects

S_{Cd} - limit value of settlement, i.e. allowable value of settlement

^{*} University in Belgrade, Faculty of Mining and Geology, Belgrade, Đušina 7, 11000 Belgrade, Serbia
E-mail: dragoslav.rakic@rgf.bg.ac.rs

^{**} Geoda doo, Novi Sad, Serbia

^{***} Mining and Metallurgy Institute Bor, Alberta Ajnštajna 1, 19210 Bor, Serbia

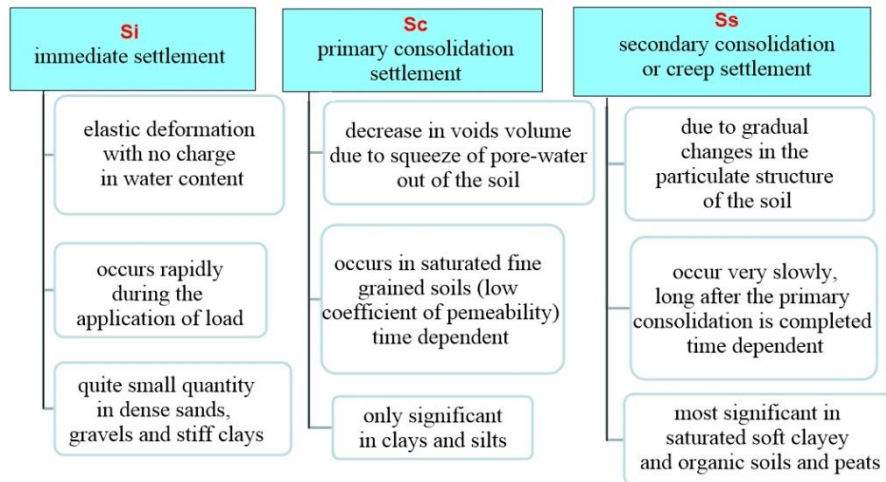


Figure 1 Schematic representation of the settlement components of different soil types

The listed components of settlement occur in all types of soil. However, in granular soils, such as sandy soils, the water permeability is very high, so the majority of settlement occurs almost entirely during the ap-

plication of the load (Figure 2). For this reason, in sandy (i.e., coarse-grained) soils, typically only the initial (elastic) settlement is calculated.

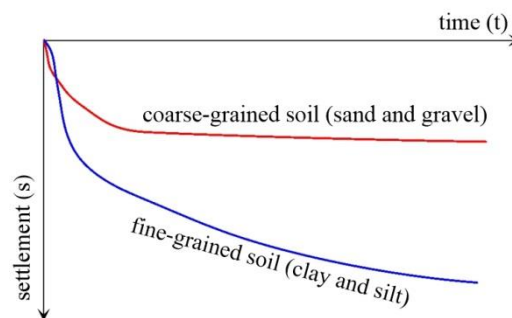


Figure 2 Schematic representation of the temporal settlement of foundations in different types of soil

The initial settlement of a shallow foundation can be estimated using the theory of elasticity, and depends on soil properties, foundation type (rigid or flexible), and the location of the observed point (center or corner). Numerous methods have been developed for calculating the initial settlement of founda-

tions founded on sand, but in general it can be said that there is no reliable "standardized" method that implies the consistent and accurate settlement forecasting. The methods, used for calculating the initial settlement of foundations on sandy soils, can generally be classified into three categories [1, 2, 3]:

- methods based on measurements/ observations of settlement of facilities or large-scale models (these methods are empirical in nature and are correlated with the results of the standard field tests, such as cone penetration test (CPT) and Standard Penetration Test (SPT). This group includes the following methods: Tercaghi and Peck (1948, 1967); Mayerhoff (1956, 1965); De Beer and Martens (1957); Peck and Bazara (1969); Burland and Bulbridge (1985).
- semi-empirical methods based on a combination of observed settlement behavior and theoretical analysis. The most commonly used methods in this category included: Schmertmann (1970, 1978); Schultz and Sheriff (1973); Bridjud (2007); Akbas and Kulhawi (2009).
- methods based on theoretical foundations, derived from the theory of elasticity.

Many methods rely on the results of in-situ tests such as SPT or CPT, and therefore it is not possible to satisfactorily study the theoretical relationships between the different methods. Estimates obtained using various methods are typically evaluated through comparisons with measured settlements, based on a large number of actual observations. The settlement of foundation mats of large dimensions can be evaluated using the methods based on the theory of elasticity, assuming that the load is transferred to the soil in a manner similar to that of classical shallow foundations of smaller dimensions, and considering that the settling layer has finite thickness.

This paper aims to analyze and compare the settlement results, obtained using different methods, in order to evaluate their reliability and precision in the assessment of behavior the foundation soil, when it comes to the foundation mats of large dimensions. As a case study, the settlement of the Court of Appeal building in Novi Sad, which is founded on sandy soil, was analyzed. Geodetic moni-

toring of settlement was conducted during the construction period of this facility, providing valuable data for comparison. Settlement calculations were performed using several methods, based on elasticity theory, with a provisional definition of the final thickness of the settling layer.

In addition, a numerical settlement analysis was carried out using Settle3 software, which included the time-dependent progression of elastic settlement by phases, where each phase was defined according to the geodetic measurements. This analysis made it possible to identify the potential differences between the methods used, as well as to determine the factors that affect the accuracy of settlement values obtained, which can contribute to a better understanding the application of these methods when analyzing the shallow foundations of large dimensions.

2 THE MOST COMMONLY USED METHODS OF SETTLEMENT CALCULATION ON SANDY SOIL

In practice, the equations from elasticity theory are most commonly used to calculate the settlement of sandy soil, despite the fact that the soil is not truly elastic and does not exhibit a linear stress-strain relationship. Nevertheless, settlement calculation based on the elasticity theory, is the simplest approach, as it requires only two soil parameters (E_s – Modulus of elasticity and ν – Poisson's ratio). This simplicity is the main reason for the frequent use of these equations. In cases where a rigid (non-deformable) layer exists at a certain depth below the foundation base, and the soil is considered homogeneous, the settlement of a shallow foundation according to elasticity theory is given by [2]:

$$s_e = \frac{(1-\nu^2)}{E_s} \cdot I_s \cdot I_f \cdot q_n \cdot (\alpha B') \quad (3)$$

where:

s_e – elastic (initial) settlement
 q_n – additional applied load

B – foundation width ($B' = B/2$ – for the central point of foundation)

B' – B – for the corner point of foundation

E_s – modulus of elasticity of the soil (due to the multi-layer environments and inhomogeneous nature of soil, the value of E_s may vary with depth. For this reason, a weighted average of the modulus is recommended)

ν – Poisson's ratio

I_f – depth influence factor

I_s – shape influence factor (these factors depend on the Poisson's ratio, and the ratios between foundation dimensions and thickness of the settling layer)

α – factor that depends on the analyzed point and on the type of foundation through which the load is transferred.

Regardless of the number of available methods based on elasticity theory, the methods proposed by Schmertmann (Schmertmann et al., 1970, 1978), Schultz and Sherif (Schultze and Sherif, 1973) and Burland and Burbridge (Burland and Burbridge, 1985) are the most widely used in worldwide. This is due to the fact that their results show the highest accuracy when comparing calculated and measured settlements, as well as their simplicity of use [4]. This paper focuses on the Schmertman's method and the Schulz and Sherif method, as these two methods have proven to be particularly accurate and reliable.

The Schmertman's method is a semi-empirical approach based on elasticity theory, by means of which the distribution of deformations is modeled in a homogeneous, isotropic, linearly elastic half-space. It assumes that coarse-grained soil (sand) behaves elastically, meaning that deformations occur in proportion to the applied load. Based on numerous experimental studies, Schmertman proposed the following equation for calculating the settlement of foundations founded on sand:

$$s_e = C_1 \cdot C_2 \cdot q_n \cdot \sum_{z=0}^{z=2B} \frac{I_z \cdot \Delta z}{E_s} \quad (4)$$

where:

C_1 – correction factor for the embedment of foundation

C_2 – correction factor to account for creep in soil

Δz – layer thickness

I_z – strain influence factor of vertical deformations in the middle of layer

The strain influence factor I_z increases linearly from zero at the foundation level, reaches a maximum value of approximately 0.6 at a depth of $B/2$ (half the foundation width) below the foundation base, and then decreases linearly back to zero at a depth of $2B$ below the foundation level. Due to these reasons in practice, it is often called the "2B-0.6 distribution" (Figure 3a). The correction factors C_1 and C_2 are determined as follows

$$C_1 = 1 - 0.5 \cdot \frac{\gamma \cdot D_f}{q_n} \geq 0.5 \quad (5)$$

$$C_2 = 1 + 0.2 \cdot \log\left(\frac{t}{0.1}\right) \quad (6)$$

where:

γD_f – weight of the upper layer at the level of foundation elevation (effective geostatic stress)

t – time from the application of load to the moment for which the settlement is calculated, expressed in years

Immediately after the construction of a facility, the correction factor C_1 is taken as 1. The elastic modulus E_s can be defined based on the results of in-situ tests, such as SPT and CPT. Schmertman suggests that E_s should be derived from the CPT static penetration test for each individual case, using the expression $E_s = 2q_c$ (q_c – average resistance of the static penetrometer tip in the sand layer whose settlement is determined).

Since the original approach did not account for the foundation shape, the method was partially modified (Schmertmann et al., 1978), with specific adjustments made for square and strip foundations. As a result, the shape of the influence diagram I_z (Figure

3b) and the corresponding equation for its determination were revised.

$$I_{z,\max} = 0.5 + 0.1 \cdot \sqrt{\frac{q_n}{\sigma'_{z,\max}}} \quad (7)$$

where:

$\sigma'_{z,\max}$ – maximum primary effective vertical stresses at the depth where the influence factor

I_z reaches its maximum value (i.e., at $B/2$ or B , depending on the foundation shape)

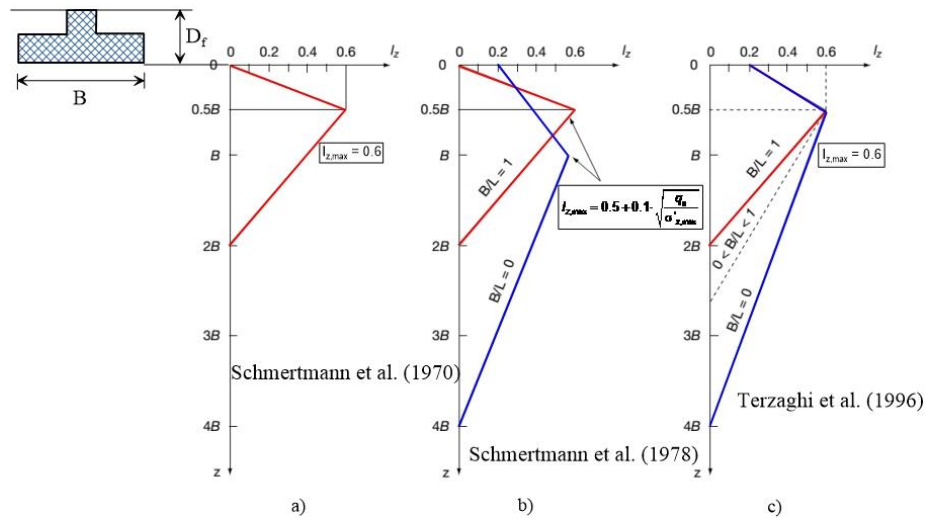


Figure 3 Different variations of the distribution diagram of the influence factor I_z

Considering that the stiffness is about 40% higher under plane strain conditions compared to axisymmetric loading, a different dependence between q_c and E_s was proposed. For square foundations $E_s = 2.5q_c$ while for the strip foundations $E_s = 3.5q_c$. As the dependencies are shown primarily for the square foundations ($L/B=1$) and strip-shaped foundations ($L/B>10$), when calculating the settlement of rectangular foundations ($1<L/B<10$), it is necessary to perform the interpolation in order to achieve the accurate results. This proposal was simplified by Tercagi [3], so the influence factor $I_{z,\max} = 0.6$ was proposed for both square and strip foundations as shown in Figure 3c, while for the rectangular foundations the influence depth is calculated on the basis of the following equation

$$z_l = 2B \cdot \left(1 + \log \frac{L}{B} \right) \quad (8)$$

Although the modified Shmertman method from 1978 is more complex than the original, it did not bring the significant improvements in practice, and due to this reason both variants of the Shmertman method are used in geotechnical practice.

The method proposed by Schulz and Sherif is also based on the equation for calculating the foundation settlement in an elastic isotropic subspace.

$$s_e = \frac{q_n \cdot B}{E_s} \cdot f_n \quad (9)$$

where:

f_n – influence factor that depends on ν - Poisson's ratio, the ratio of the foundation length to its width (L/B) the ratio of the thickness of the settling layer (H) to the foundation width (B) (Figure 4).

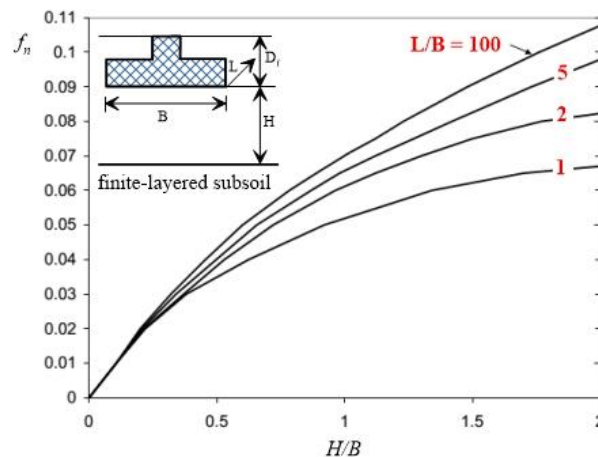


Figure 4 Diagram on the basis of which the influential factor f_n is defined

It should be noted that the original equation does not use the soil's modulus of elasticity directly. Instead, this value is estimated based on the results of the SPT test, specifically the N_{60} value, and was derived from empirical data. Additionally, an assumption was introduced that at depths greater than $2B$, the influence of the additional load becomes negligible. Therefore, when the ratio $H/B > 2$, a value of 2 is adopted.

Yanbu et al. [4] proposed a generalized equation for calculating the average elastic settlement of uniformly loaded foundations in the following form

$$s_e = \mu_0 \cdot \mu_1 \frac{B \cdot q_n}{E_s} \quad (10)$$

where:

μ_0 – influential factor that depends on the ratio D_f/B and L/B and is read from the diagram

μ_1 – influential factor that depends on the ratio H/B and L/B and is read from the diagram

This equation was originally derived for calculation the initial settlement in clay, but it can also be applied to sand, where the drained moduls of elasticity is used as the deformability parameter. It should be noted

that Christian and Carrier (1978) proposed partially corrected values of the coefficients μ_0 and μ_1 which were initially derived for flexible circular foundations [6], however, based on the conducted analysis, the adequate values were also proposed for the rectangular foundations.

The building analyzed for settlement behavior is located in the Novi Sad neighborhood of Stari grad, in Stražilovska Street. It consists of $2W+W+D+6$ floors, and has an approximately rectangular base, with dimensions $L \times W = 55.0 \text{ m} \times 20.0 \text{ m}$. The structure is supported by a foundation mat at depth of $D_f = 10.9 \text{ m}$ in relation to the projected terrain elevation.

The total gross load transferred from the base plate to the ground is $q = 225 \text{ kPa}$, while the net contact load used in the settlement analysis is $q_n = 35 \text{ kPa}$ ($q_n = q - \gamma D_f$, when calculating the effective geostatic stresses, the NPV at a depth of 3.0 m was also taken into account).

The terrain is built of alluvial sediments from the flood facies primarily composed of sandy dust and dusty sands with clay fraction content (saSiL). The bed facies include fine-grained to medium-grained sands inter-layered with dusty clay, with increasing depth revealing gravelly sands (saSa-SaP).

At depths of about 22 m, the sandy dusty clays (CIH-saSim) were found, likely corresponding to lake deposits of the upper Pliocene, formed in shallow freshwater conditions.

For the purpose of building the facility, two exploratory boreholes were drilled to a depth of 35 m, from which 15 soil samples

were collected. Additionally, 7 standard penetration tests-SPT and 2 static penetration tests-CPTu were performed. Based on the results of these field investigations and laboratory geomechanical tests, a geotechnical model of the terrain was defined (Figure 5), which served as the basis for calculating the settlement of facility.

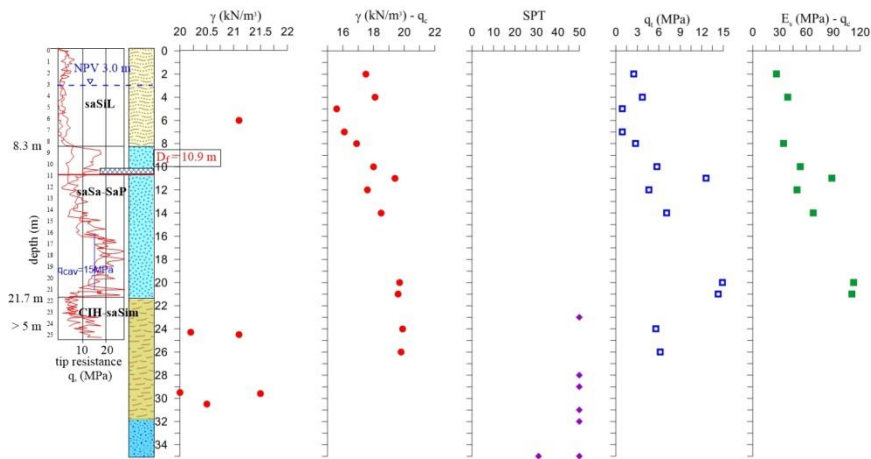


Figure 5 General geotechnical model of the terrain at the facility location

Analyzing the laboratory and field data, the values of soil parameters used for the

settlement calculation, were adopted, and are shown in Table 1.

Table 1 Soil parameters used in the settlement analyses

Layer designation	Bulk weight γ (kN/m ³)	Cone resistance q_c (kN/m ²)	Elasticity module $E_s = \alpha q_c$ (kN/m ²)	Poisson coefficient ν
saSiL	16.7	2000	4000	0.3
siSa-SaP	19.2	15000	30000	0.25
CIH-saSiL	19.8	9000	18000	0.3

4 ANALYSIS OF FOUNDATION SETTLEMENT

4.1 Analysis of settlement using the semi-empirical methods

The most commonly applied semi-empirical method for estimating the settlement of foundations founded on and is the Schmertmann method, which considers the

time elapsed from load application to the moment when settlement is calculated (t). Due to the existence of data related to the geodetic observations during the construc-

tion of the building, settlement calculations were performed for two time periods: $t = 3$ months and period of $t = 1$ year.

Considering the large foundation dimensions (width $B = 20$ m), instead of the usual depth of influence of $2B$ (which in this particular case would be 40 m in relation to the foundation height), an alternative proposal can be adopted. Specifically, for environments where the elasticity module E_s is greater than 10 MPa, the thickness of the layer is determined as follows [7]

$$H_e = m \cdot (z_0 + \xi \cdot B) \quad (11)$$

where m - the correction factor which for the sandy environments is $m = 0.5$ and the coefficients z_0 and ξ are tabulated depending on the ratio of length and width of the foundation L/B ($z_0=12.4$, $\xi=0.51$), so that the thickness of the elastic layer that settles is $H_e = 11.3$ m. This implies that at depths greater than 22 m relative to the ground surface, there is a non-deformable layer that corresponds to the contact with the sandy-dusty clays (CIH-saSim).

Based on the analysis, the estimated settlement for a period of 3 months is $s_{e1} = 2.89$ mm. In the case of analyzing twice the width of foundation for the impact depth ($H_e = 40$ m), the settlement value would be $s_{e2} = 12.37$ mm, which is more than four times the initial value. Over a longer period of 1 year, slightly higher settlement values are obtained ($s_{e1} = 3.21$ mm and $s_{e2} = 13.75$ mm).

The Schulz and Sherif method implies the use of a unique value of the elasticity module, for the previously defined thickness of the elastic layer of $H_e = 11.3$ m, its value is $E_s = 30$ MPa, and the settlement value obtained is $s_{e1} = 1.05$ mm without accounting for time-related effects. Otherwise, when analyzing the thickness of elastic layer that settles as twice the width of foundation, a layer of sandy-dusty clay is also taken into account, so it is necessary to adopt the weighted value of the elasticity module, which would be $E_s = 22.5$ MPa, and the settlement value would be $s_{e2} = 1.40$ mm.

In addition, the settlement was calculated on the basis of the method of Yanbu, Bjerum and Shansli, considering an influence depth of $H_e = 11.3$ m, where the settlement value of $s_{e1} = 8.07$ mm ($E_s = 30$ MPa), i.e. settlement $s_{e2} = 10.76$ mm, when the weighted value of elasticity module of $E_s = 22.5$ kPa is adopted, i.e. when analyzing the thickness of elastic layer of $H_e = 40$ m.

4.2 Settlement analysis based on 3D modeling in the Settle3 program

As a part of this analysis, the settlement calculations were performed using the Settle3 program, which is a part of the Rock Science software package. The Settle3 is an advanced program that includes a 3D analysis of soil settlement and consolidation, thus enabling the modeling of various geotechnical conditions, using the theory of elasticity and theory of consolidation [8].

The same geotechnical model was used for calculation, and as the Settle3 software package also provides insight into the time-dependent progression of settlement based on increasing supplementary load, the phased construction of the building was modeled. In this connection, the supplementary load was added gradually in three phases over time intervals of 18, 46 and 64 days, namely $q_n = 15 + 10 + 10$ kPa.

This approach enables a more realistic representation of development the subsidence over time and simulates a gradual increase in the load on soil. Monitoring of subsidence was carried out in phases, which partially coincided with the geodetic measurements, and in characteristic time intervals of increase in the supplementary load, i.e. $t = 18, 46, 64, 89$ and 365 days in relation to the beginning of construction.

Figure 6 shows the calculation of foundation settlement in different stages of loading, i.e. as a function of time, taking into account four characteristic periods: stage 1 - 18 days, stage 2 - 46 days, stage 3 - 64 days and stage 4 - 89 days. The settlement values, when the thickness of elastic layer is

limited to $H_e = 11.3$ m, change depending on the load intensity change, i.e. the application phase, and are: phase 1 - $s_e = 4.25$ mm; phase - 2 $s_e = 7.09$ mm; phases 3 and 4 are $s_e = 9.92$ mm.

In the Settle3 program, the simulation was also performed for a time period of 365 days, but the settlement size remained identical to that obtained in stages 3 and 4 ($s_{e1} = 9.92$ mm) and for these reasons these results are not shown in Figure 6. For the case without elastic layer thickness limit

($H_e = 40$ m), the calculated settlement value is $s_{e2} = 28.58$ mm.

Considering the time factor, the diagrams clearly show that the elastic settlement took place in a very short time interval, reaching maximum values between 46 and 64 days. Also, the final settlement value obtained by the numerical model in the Settle3 shows a relatively good agreement with the results obtained by the semi-empirical methods, when the thickness of elastic layer is limited.

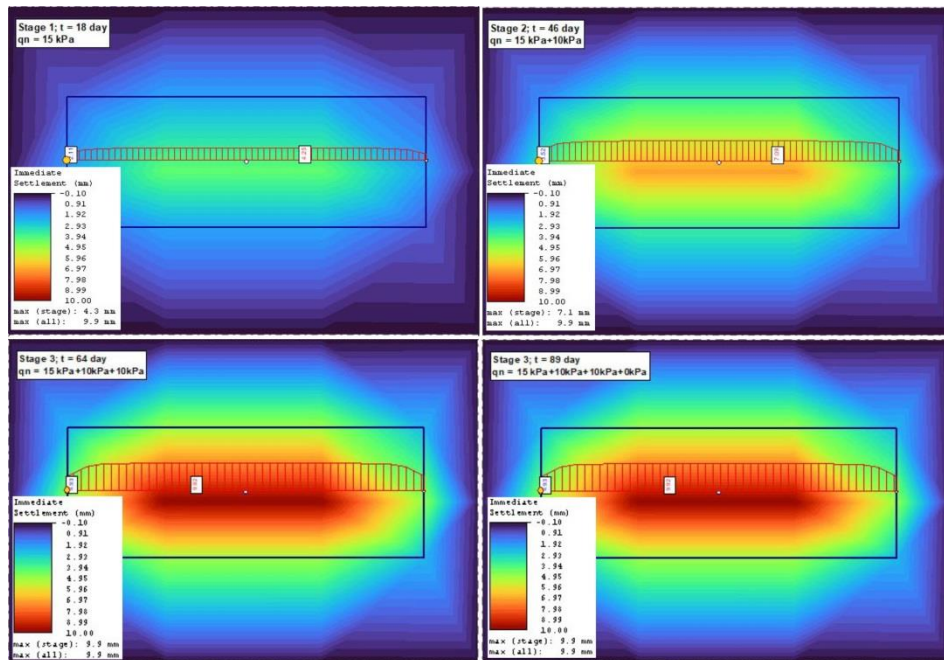


Figure 6 Graphic representation of settlement calculations in the Settle 3 program

4.3 Presentation the measured values of subsidence based on geodetic observations of benchmarks

During the facility construction, the six control geodetic benchmarks (R1-R6) were placed, on which observations were made (Figure 7). The accuracy of these measurements depends on several factors such as the environment, instruments, stability of

reference points, as well as the data processing methods. When it comes to the environment, it is necessary to pay attention to the atmospheric conditions such as temperature, humidity and pressure, which can affect the accuracy of measurement.

If the certain vibrations are generated in the vicinity of the site in question due to the operation of construction machinery, this can significantly affect the accuracy of measurement. Additionally, the stability of reference points is very important, so they should be placed on a terrain that is not subject to sliding or other types of deformation.

The monitoring period was relatively short lasting approximately 3 months (25/07 - 22/10/2022), and the observations were carried out within four series at time intervals of approximately one month, not taking into account the zero series.

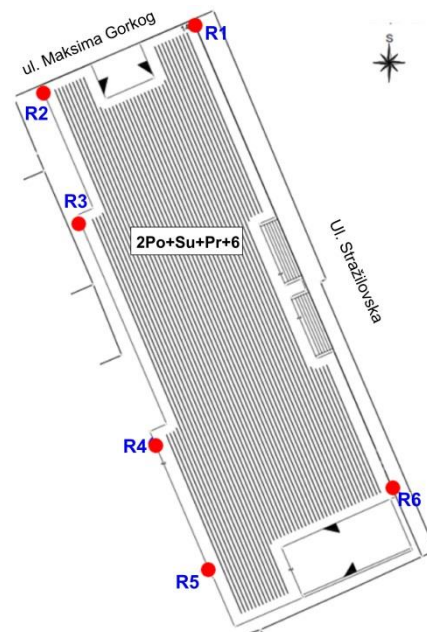


Figure 7 Locations of control benchmarks for geodetic observations

The measurement results are tabulated, with the indicated period of observation, individually for each benchmark (Table 2),

and are also shown graphically in Figure 8, together with the average settlement of all benchmarks.

Table 2 Presentation the results of geodetic observations of subsidence

series of observations	Bench mark - measured settlements s (mm)					
	R1	R2	R3	R4	R5	R6
0: 25.07.20222.	0.00	0.00	0.00	0.00	0.00	0.00
I: 12.08.20222.	0.30	0.40	0.10	0.50	0.30	0.40
II: 09.09.20222.	1.20	1.00	0.80	1.30	1.00	0.60
III: 27.09.20222.	2.00	2.20	2.10	2.70	2.10	1.60
IV :22.10.20222.	3.00	2.70	2.90	3.10	2.80	2.70

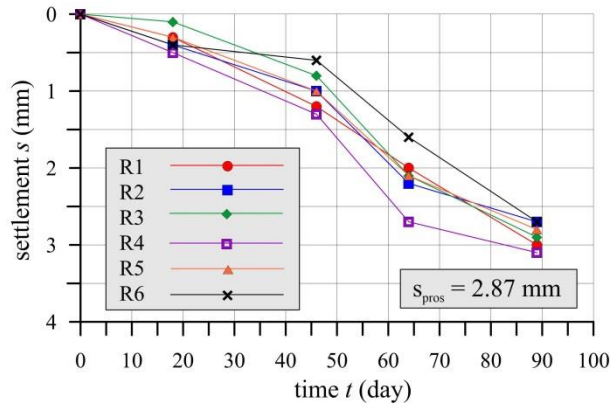


Figure 8 Graphic representation of the benchmark time subsidence

5 COMMENT AND CONCLUSION

The results of calculating the settlement of foundations of large dimensions highly depend on the adopted thickness of layer for which the settlement is calculated. The choice of thickness of this layer is influenced by several factors, such as: the dimensions of foundation, load that the foundation receives as well as the characteristics of the soil itself. The presented settlement results using the semi-empirical and numerical analyzes (Settle3 also uses a 3D model) were obtained based on the previously defined effective

thickness of layer (H_e), which is harmonized with the geotechnical model of terrain and geotechnical parameters (primarily the elasticity mode of the soil E_s), which are the key importance for the accurate assessment of settlement.

Figure 9 presents a comparative overview of all settlement calculation results and measured values, clearly illustrating the differences between geodetic observations and analytical predictions derived from semi-empirical methods, numerical analysis, and the Settle3 software.

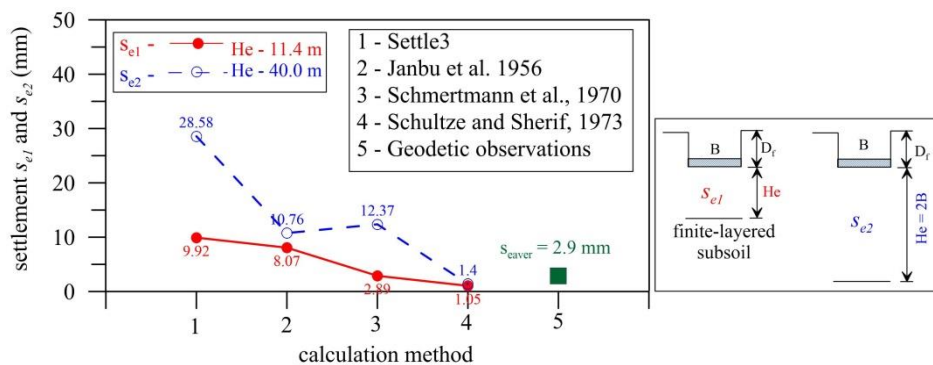


Figure 9 Results of settlement calculation based on different calculation methods

The analysis clearly shows that deviations are significantly larger when settlement calculations are performed without a predefined thickness for the elastic layer (H_e). There are several reasons for this, such as: changes in the lithological composition of the terrain and differences in the physical-mechanical parameters, i.e. the accuracy of the formed geotechnical model, climate changes at the time of conducting the explorations and possible changes during the geodetic observations (rainfall, temperature change and possible partial change of the groundwater level), as well as the fact that the geodetic measurements were performed in a short time interval and did not cover the entire construction period of the facility.

For large-dimension foundations, wherever possible, the thickness of the elastic layer should be limited by defining the depth to the conditionally non-deformable layer, particularly in environments with an elasticity modulus exceeding $E = 10$ MPa. Otherwise, if the effective settlement depth is assumed to be $H_e = 2B$ (twice the foundation width), significantly higher settlement values are obtained.

The analyzes also showed that considering the foundations of large dimensions, the closest estimate of settlement in comparison to measured values were obtained using the methods of Schmertman and Schulz and Sherif. In addition, based on numerical simulations performed with Settle3, where the phased load application is also included, it was concluded that the settlements occur relatively quickly and mainly during the construction phase when facilities are built in environments dominated by coarse-grained soils.

Ultimately, this research highlights the importance of employing multiple analytical methods for soil settlement assessment, which enhances result reliability, improves long-term foundation behavior predictions, and supports the optimization of engineering solutions.

REFERENCES

- [1] B.M. Das, Principles of Foundation Engineering, Publisher, Global Engineering, 2014, p. 946.
- [2] D.P. Coduto, Geotechnical Engineering - Principles and Practices, Prentice Hall, 1998, p. 759.
- [3] K. Terzaghi, R.B. Peck, G. Mesri, G., Soil Mechanics in Engineering Practice, 3rd Edition, Wiley, New York, 1996, p. 534.
- [4] N. Janbu, M. Bjerrum, B. Kaernsli, Veiledning Ved Losning Av Fundamentering Soppgaver, Norw. Geotech. Inst., 16 (1956) 30-32.
- [5] X.F. Chen, Settlement Calculation on High-Rise Buildings Theory and Application, Beijing: Science Press, 2011, p. 439.
- [6] L.B. Vinh, N.V. Nhan, L.B. Khanh, Study on the Settlement of Raft Foundations by Different Methods, MATEC Web of Conferences, 2018.
- [7] D. Rakić, N. Šušić, M. Ljubojev, Analysis of Foundation Settlement from Progressive Moistening of Silty Clay, Rudarski radovi/Mining Engineering, 1 (2012) 1-10.
- [8] Rocscience Inc. Settle3 – Settlement and Consolidation Analysis, Theory Manual, 2022, p. 61.

*Dragana Savić^{*1}, Dušan Tašić^{**2}, Katarina Milivojević^{***3}, Dragan Ignjatović^{***4}*

IMPACT OF THE MECHANIZED EXCAVATION ON THE SLOPE STABILITY OF THE "GACKO" OPEN PIT^{***}

Orcid: 1) <https://orcid.org/0009-0002-3396-9435>; 2) <https://orcid.org/0000-0001-8005-9640>;
3) <https://orcid.org/0000-0009-1306-4044>; 4) <https://orcid.org/0000-0003-2333-6853>

Abstract

Maintaining the open pit slopes in a stable condition requires compliance between the geometrical parameters of the open pit on one side and the pit-technical conditions, physical-mechanical properties of the rocks and hydrogeological properties of the deposit on the other side. When the underground activity is located below an open pit, deformation of the open pit slopes can be expected as a result of subsidence caused by the underground mining. For an adequate analysis of the stress-strain states in the massif, it is essential to consider the partial relaxation of the primary stresses in the excavation. Numerical analysis simulates the progress of mining works and stress changes and deformations in the vicinity of the underground room, the amount of subsidence on the ground surface depending on the chosen method of mechanized excavation, i.e. the impact on the open pit slopes. Numerous examples in the world provide a clear warning regarding the possible impact of underground works at the open pit. Analysis the impact of dimensions and spatial position of the wide front panel and column-chamber excavation on the stress-strain state, i.e. stability of the open pit slope, was done on the example of the "Gacko" open pit mine.

Keywords: open pit slopes, slope deformations, underground exploitation, numerical modeling, environment

1 INTRODUCTION

The Palabora copper mine in South Africa is one of the steepest and deepest open pits in the world, with a radius of about 1.5 km and a depth of about 800 m, Figure 1. [1].

A large-scale deformation of the final slope occurred in 2004 after the protection pillar deformed 400 m below the bottom of the pit.

Dimensions of the fracture were about 800 m high and 300 m wide. The frontal scar was 50 m behind the final open pit contour. It was estimated that 130 million tons of waste filled the northwestern side of the open pit as well as the bottom itself (Figure 2). The caused deformation affected the loss of 30% of the ore reserves [5].

^{*} Mining Institute, Batajnički put 2, 11080 Beograd – Zemun, Serbia,

E-mail: dragana.savic@ribeograd.ac.rs

^{**} Mining and Metallurgy Institute Bor, Alberta Ajnštajna 1, 19210 Bor, Serbia

^{***} The authors are grateful to the Ministry of science, technological development and innovation of the Republic of Serbia for financial support according to the Contract No. 451-03-136/2025-03/200052.

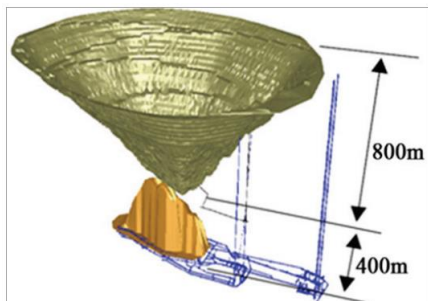


Figure 1 Three-dimensional model of the open pit and pit in the Palabora copper mine [1]

Another example is the example of undermining and interaction with the open pit in the Ernest Henry mine in eastern Australia [3].

Copper ore was surface exploited until 2011. The open pit had final dimensions: a diameter of about 1.5 km and a depth of 530 m.



Figure 2 Fracture on the slopes of the open pit in the Palabora copper mine [5]

Production by undermining started after the end of surface exploitation with a planned frame of undercutting of 220 m of pillars. The collapse of the pit began after the pillar was removed at the end of 2012. The big collapse happened two years later in December 2014. The fracture zone measured 200 m wide, 150 m high and 30 m thick (Figure 3).

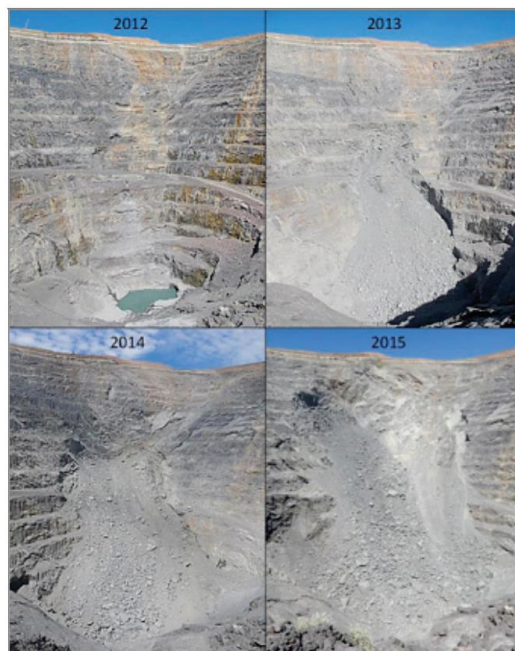


Figure 3 Fracture progression on the slopes of the Ernest Henry copper open pit as a function of time [3]

Analysis the impact of dimensions and spatial position of the wide front panel and column-chamber excavation on the stress-strain state, i.e. the slope stability of the open pit was done on the example of the open pit "Gacko". Due to the different geological conditions, depth of exploitation and applied technology of exploitation (the wide face method and column-chamber excavation), each method was considered individually.

2 THE IMPACT OF EXCAVATION BY DEVELOPING A WIDE-FACED PANEL ON THE SLOPE STABILITY OF THE OPEN PIT

The analysis of the open pit slope stability was done for the conditions that will prevail in the area of exploitation, according to the technical-technological characteristics of the excavation and transport machinery and based on the physical-mechanical properties of the working environment. The strength and deformability parameters of the

rock mass were determined on the basis of strength and deformability parameters of monolith and estimated GSI value.

The estimated value of the geological strength index (GSI) was obtained by correlation with the obtained values of RQD during the core mapping of the exploration drillholes.

All evaluations were carried out according to the recommendations of Hoek, and the residual values with the reduction of GSI [2], with the approximate ratio $GSI_r = 0.7 \text{ GSI}$ [7].

For the given characteristics of the rock mass, the Hoek-Brown strength criterion was obtained.

The rock mass parameters (Second bottom coal seam, roof and bottom sediments) shown in Table 1 and Table 2 were taken as the input data.

The calculation was made on the selected engineering geological profile west-east (profile I-I'-variant d), which is directed to the final slopes of the open pit.

Table 1 Strength and deformability parameters of the rock massif

Lithogenetic unit	γ (kN/m ³)	σ_p (MPa)	σ_z (MPa)	ϕ (°)	c (MPa)	E (MPa)	ν
¹⁰ Ng- ⁹ Ng	16.00	3.40	0.30	29°	0.67	488.50	0.32
⁸ Ng	19.91	3.77	0.41	31°50'	0.55	563.80	0.33
⁷ Ng	17.16	4.69	0.45	34°50'	0.61	705.60	0.29
⁶ Ng	13.54	10.05	0.89	31°	0.75	597.00	0.39
⁵ Ng	17.75	4.98	0.60	37°27'	1.72	963.50	0.27
⁴ Ng	14.81	7.82	0.77	32°	0.70	659.10	0.31
³ Ng	20.11	6.60	0.62	33°40'	1.31	899.00	0.33
² Ng	14.52	11.08	0.99	34°	0.96	794.00	0.33
¹ Ng	19.71	10.12	0.66	34°50'	1.91	1127.00	0.31

Table 2 Residual strength parameters

Lithogenetic unit	GSI	0,7 GSI	σ_z (MPa)	ϕ (°)	c (MPa)	mb	s	a
¹⁰ Ng- ⁹ Ng	45	34	0	25°79'	0.129	0.947	0.0007	0.517
⁸ Ng	45	34	0	27°29'	0.153	1.136	0.0007	0.517
⁷ Ng	45	34	0	25°79'	0.178	0.947	0.0007	0.517
⁶ Ng	45	34	0	24°	0.352	0.758	0.0007	0.517
⁵ Ng	45	34	0	30°	0.228	1.610	0.0007	0.517
⁴ Ng	45	34	0	24°	0.300	0.758	0.0007	0.517
³ Ng	45	34	0	25°79'	0.251	0.947	0.0007	0.517
² Ng	40	28	0	22°25'	0.342	0.611	0.0003	0.526
¹ Ng	45	34	0	27°29'	0.405	1.136	0.0007	0.517

The state of groundwater is variable in time and space and very important for the origin and development of all modern geodynamic processes on the slopes of technological profiles [9]. The hydrodynamic action of underground, that is, atmospheric water on rock masses, in the form of hydrostatic pressure and anisotropy of water permeability in the vertical direction, do not allow the draining of infiltrated water, thus lowering the value of physical-mechanical parameters.

Numerical analysis was performed using a modern method, using the program RS2, Version: 2019 10.010, Build Date: Build date: Jan 24 2020 12:11:17, License Information, License Key: Remote, WIN-B6CUU4CCJFS (147.91.181.157), Sentinel Key ID: 48329904298824269, Expiry: 2020-12-31, 23:59:59 GMT, Registered to: University of Belgrade, User ID: 11394- [8]

Calculation of the coefficient of critical stress state, SRF, was performed for different values of pore pressure, and the steps in

the stability analysis were: $r_u = 0.0$; $r_u = 0.2$ and $r_u = 0.4$ [6].

In the analysis of slope stability, the propagation of waves, caused by an earthquake in the most unfavorable direction was taken into account, i.e. perpendicular to the slope face, and the adopted seismicity coefficient was $K_s = 0.05$.

On the adopted model, the first working panel with a wide face is located 80 m behind the top of final slope, at a depth of 240 m (variant d). The slope of coal seam is 5°. The impact of making four panels with a wide face, moving away from the top of final slope of the open pit, was analyzed. The model with protected columns between the panels is 20.75 m.

Analyzing the results of geostatic calculations (Table 3), it can be seen that the existing geometry of slope with the height of general slope of $H = 225$ m and $\beta = 21^\circ$ satisfies the required safety in interaction with the underground mining works (Figures 4, 5 and 6).

Table 3 Coefficient of the critical stress state for the profile I-I'

Profile	Coefficient of the critical stress state (SRF)		
	Pore pressure coefficient		
	$r_u = 0.0$	$r_u = 0.2$	$r_u = 0.4$
I-I'	2.90	2.35	1.70

From the stability calculation results, shown in Table 3, it can be concluded that the determined coefficients of the critical

stress state (SRF) satisfy the condition for the final slope (≥ 1.30), for the analyzed values of pore pressure $r_u = 0.0$ $r_u = 0.2$ and $r_u = 0.4$.

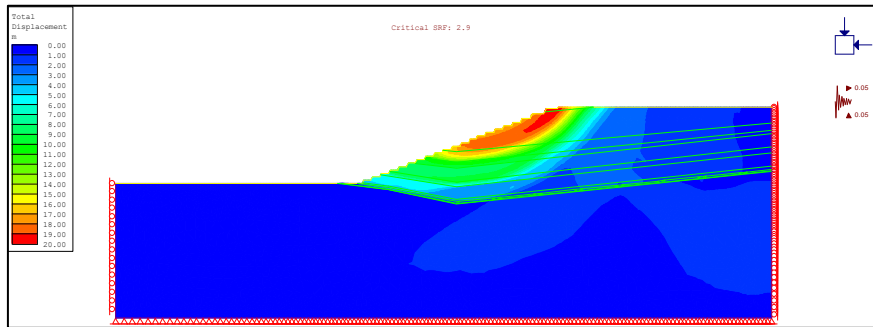


Figure 4 Critical sliding plane $SRF = 2.9$ ($r_u = 0.0$) with a view of total displacements

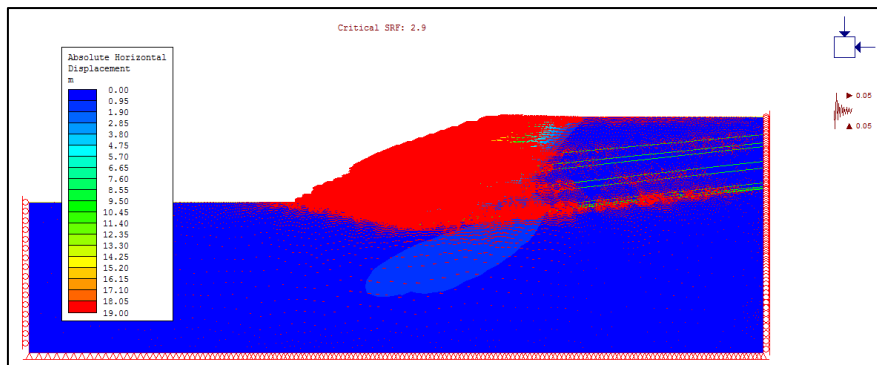


Figure 5 View of the horizontal displacement vectors for the critical sliding plane $SRF = 2.9$ ($r_u = 0.0$)

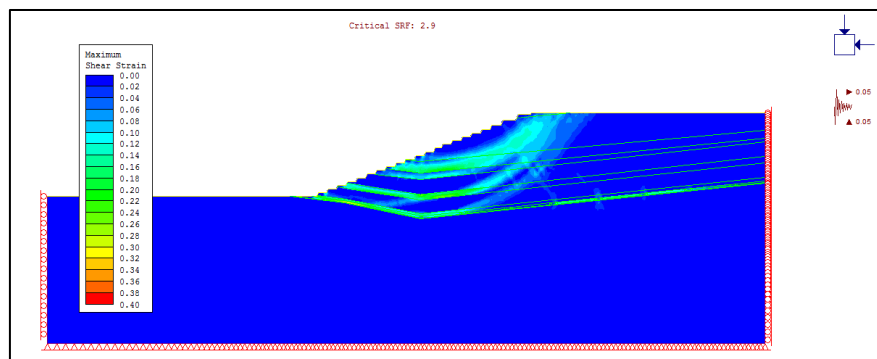


Figure 6 Critical sliding plane $SRF = 2.9$ ($r_u = 0.0$) with display of shear stresses

3 THE IMPACT OF MECHANIZED COLUMN-CHAMBER EXCAVATION ON THE SLOPE STABILITY OF THE OPEN PIT

The impact of mechanized column-chamber excavation on the slope stability of the open pit was checked through the analysis of the final slope stability. The analysis was done for the conditions that will prevail in the area of exploitation, according to the technical-technological characteristics of mining and transport machinery, and based on the physical-mechanical properties of the working environment. The calculation was made on the selected engineering-geological profile of south-north orientation (profile 1-1'), which was directed to the final slopes of the open pit, adopting the physical-mechanical parameters of the working environment (Table 1 and Table 2) [6].

Numerical analysis was performed using a modern method, using the program RS2, Version: 2019 10.010, Build Date: Build date: Jan 24 2020 12:11:17, License Information, License Key: Remote, WIN-B6CUU4CCJFS (147.91.181.157), Sentinel Key ID: 48329904298824269, Expiry: 2020-12-31, 23:59:59 GMT, Registered to: University of Belgrade, User ID: 11394- [8]

Calculation of the coefficient of critical stress state, SRF, was performed for different values of pore pressure, and the steps in the stability analysis were: $r_u = 0.0$; $r_u = 0.2$ and $r_u = 0.4$.

In the analysis of slope stability, the propagation of waves, caused by an earthquake in the most unfavorable direction was taken into account, i.e. perpendicular to the slope face, and the adopted seismicity coefficient was $K_s = 0.05$.

On profile 1-1', the coal seam slope is 12° per dip. From the bottom of the surface mine, a direct entry into the underground exploitation of the Second bottom coal seam is possible. The column-chamber excavation moves towards the urban area. The profile was analyzed with progression of a total of 27 underground rooms, between which there is a protective column of 20.75 m [6].

Analyzing the results of geostatic calculations (Table 3), it can be seen that the existing geometry of slope with the height of general slope of $H = 190$ m and $\beta = 18^\circ$ satisfies the required safety in interaction with the underground mining works (Figures 7, 8 and 9).

Table 4 Coefficient of the critical stress state for the profile 1-1'

Profile	Coefficient of the critical stress state (SRF)		
	Pore pressure coefficient		
1-1'	$r_u = 0.0$	$r_u = 0.2$	$r_u = 0.4$
	3.25	2.80	2.15

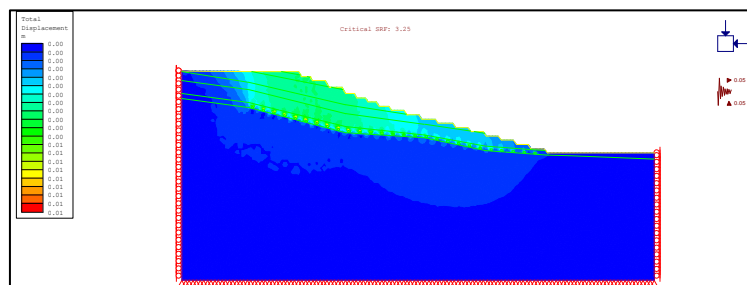


Figure 7 Critical sliding plane $SRF = 3.25$ ($r_u = 0.0$) with display of the total displacements

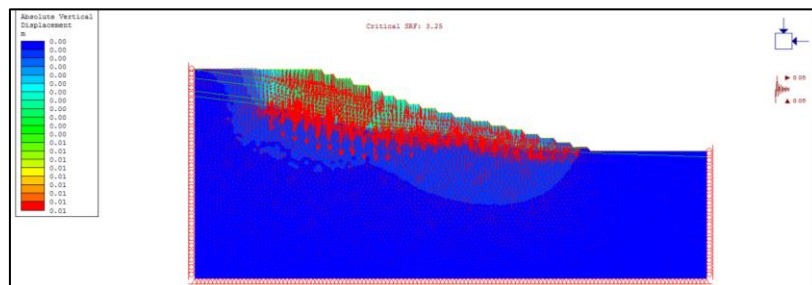


Figure 8 Display of the vector of vertical displacements for the critical sliding plane $SRF = 3.25$ ($r_u = 0.0$)

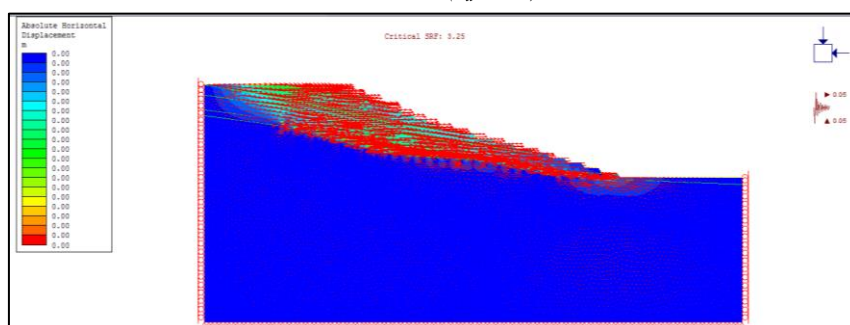


Figure 9 Display of the vector of horizontal displacements for the critical sliding plane $SRF = 3.25$ ($r_u = 0.0$)

4 CONCLUSION

From the stability calculation results, shown in Table 4, it is concluded that the determined coefficients of the critical stress state (SRF) satisfy the condition for the final slope (≥ 1.30) for the analyzed pore pressure values $r_u = 0.0$, $r_u = 0.2$ and $r_u = 0.4$, and that the analyzed open pit slope, observed in interaction with the underground mining works, is stable for all given criteria [6].

In addition to the possibility of applying the critical stress state coefficient (SRF) in checking the terrain stability in relation to the stress states that occur in the rock mass, this method can also be a control of the safety coefficient (Fs), obtained by some other calculation method, because it has been proven that the values of obtained coefficients for the same observed point are almost identical [4].

Since that the satisfactory geological conditions in the deposit "Gacko" (the thickness and slope of the second under-ground coal seam, the opening rooms directly enter the coal seam and all the preparation rooms are made in the coal seam), the possibilities and conditions of applying the new technologies for the exploitation of unused ore reserves were analyzed by developing a model of mechanized excavation and numerical modeling of interaction the mining machinery and rock mass, during the movement from surface to the underground exploitation of the second bottom coal seam. [6].

In geostatic calculations, the finite element method was used due to its ability to include the heterogeneity of environment, non-linear behavior of soil, complex

geometry of problem, interaction of the structure and soil, as well as the manufacturing method. For numerical modeling, a part of deposit at shallower depths and where there are the residential and other construction and infrastructure facilities (high-voltage and water supply network) was selected on the surface. During the analysis, the ground subsidence was assessed as a result of underground mining works.

The underground coal mining also has obvious advantages from the aspect of environmental protection (reduced negative impact on the air quality, noise level in the environment, impact of land degradation, occupation of space) because the excavated area gives the possibility to dispose the ash and slag from the "Gacko" Thermal Power Plant [6].

Modeling has considered the solution of disposing of this material in the underground mining rooms, thereby achieving the improvements in the physical and mechanical parameters of the working environment, which is especially manifested in the reduction of ground surface subsidence due to the excavation using a mechanized wide-faced complex with destruction of overburden ("sub-level" method), and consequently also in the reduction of deformations on the open pit slopes.

REFERENCES

- [1] R. Brummer, H. Li, The Transition from Open Pit to Underground Mining: an Unusual Slope Failure Mechanism at Palabora, Proceedings Int. Symposium on Stability of Rock Slopes, Cape Town, 2006.
- [2] M. Cai, P.K. Kaiser, Determination of Residual Strength Parameters of Jointed Rock Masses Using the GSI System, International Journal Of Rock Mechanics and Mining Sciences 44 (2007) 247-265.
- [3] A. D. Campbell, C. R. Lilley, Cave Propagation and Open Pit Interaction at the Ernest Henry Mine, Seventh International Conference and Exhibition on Mass Mining, Sydney, 2016.
- [4] D. Ignjatović, L. Đ. Ignjatović, Analysis and Relationship of Safety Coefficient (FS) and Critical Factor of Influence the Stress Reduction (SRF) in the Case of External Waste Dump of the East Waste Dump - Profile III-III' Open Pit "Gacko" Gacko, Mining & Metallurgy Engineering Bor, 1 (2015) 17-26.
- [5] S. Ngidi, P. Boshoff, Cave Management and Secondary Breaking Practices at Palabora Mining Company, 6th Southern African Base Metals Conference, The Southern African Institute of Mining and Metallurgy, 2011.
- [6] D. Savic, Development of a model for Mechanized Excavation of Coal Reserves Below the Town of Gacko, Doctoral Dissertation, Faculty of Mining and Geology, University of Belgrade, Belgrade, 2020.
- [7] X. C. Shi, Y. F. Meng, Numerical Study of Changes in Coal Permeability in a Mining Workface, Acta Montanistica Slovaca, 20 (2015) 234-241.
- [8] RS2, Version: 2019 10.010, Build Date: Build date: Jan 24 2020 12:11:17, License Information, License Key: Remote, WIN-B6CUU4CCJFS (147.91.181.157), Sentinel Key ID: 48329904298824269, Expiry: 2020-12-31, 23:59:59 GMT, Registered to: University of Belgrade, User ID: 11394
- [9] S. Vujić, V. Čebešek, Potential Traps and Risks in Slope Stability Calculations at Open Pit Mines, 4th Balkan Mine Congress, Slovenia, Ljubljana, 2011, pp.527-531.

*Ivan Jovanović^{*1}, Dušan Tašić^{**2}, Miomir Mikić^{*3}, Vladanka Presburger Ulniković^{**4},
Novica Staletović^{**5}, Violeta Nikolić^{**6}*

CLEAN ENERGY TECHNOLOGIES: THE IMPACT OF RENEWABLE SOURCES ON THE ENVIRONMENT AND ENERGY SECURITY^{***}

Orcid: 1) <https://orcid.org/0009-0000-5174-3734>; 2) <https://orcid.org/0000-0001-8005-9640>;
3) <https://orcid.org/0000-0001-7659-769X>; 4) <https://orcid.org/0000-0001-6144-3399>;
5) <https://orcid.org/0000-0001-8450-5564>; 6) <https://orcid.org/0000-0003-0933-3197>

Abstract

Renewable energy sources have a significant potential for improving the development of mankind. Energy obtained from the renewable sources, such as water, wind, solar and biomass, among others, can facilitate access to clean and safe energy for millions of people. It can provide an incentive for the social and economic development, contributing to the society tackling the environmental challenges. The clean energy technologies, impact of renewable sources on the environment and energy security should enable the general access to the modern energy services, increase the global rate of energy efficiency improvement, and increase the share of energy from the renewable sources within the global energy system. This achieves an integrated approach to the sustainable energy services, ensures the use of renewable energy sources and thus achieves more energy efficient solutions. The renewable energy technologies provide a unique opportunity to limit the carbon emissions into the atmosphere without compromising access to the energy, which has the significant implications for slowing down the climate changes. Also, development the renewable energy sources creates access to energy that is inexhaustible, thereby reducing a country's reliance on foreign resources and increasing its energy security. In addition, the renewable energy sources bring the great health benefits, providing the clean, safe energy, without the negative effects of using the fossil fuels.

Keywords: renewable energy, environment, energy sources, clean energy technologies

1 INTRODUCTION

The renewable energy sources represent the energy resources used for production the final energy, whose reserves are constantly or cyclically renewed.

The very name renewable comes from the fact that energy is consumed in an

amount that does not exceed the rate at which it is created in the nature. [1]

The renewable energy sources are found in the nature and renewed in whole or in part (Sun, biomass, water, wind, geothermal sources). [2]

^{*} Mining and Metallurgy Institute Bor, Bor, Alberta Ajnštajna 1, 19210 Bor, Serbia,
E-mail: ivan.jovanovic@irmbor.co.rs

^{**} "Union – Nikola Tesla" University, Faculty of Ecology and Environmental Protection,
Cara Dušana 62-64, 11158 Belgrade

^{***} The authors are grateful to the Ministry of science, technological development and innovation of the Republic of Serbia for financial support according to the Contract No. 451-03-136/2025-03/200052.

All the countries of the world are trying to increase the share of renewable energy sources in their energy balance, because the estimated reserves of the non-renewable energy sources (fossil fuels) are limited and insufficient to meet the growing energy needs. [3]

The theoretical potential of renewable energy sources is very large, but the technological level significantly limits the use of that potential. The development of technologies will increase the share of renewable energy sources in the total energy consumption.

The increase in the sale of renewable energy sources is not only caused by the increased awareness of the need to preserve the environment, but also by reduction the energy costs that these technologies make possible. Over time, these sources became competitive with the conventional (fossil) fuels. The price of conventional fuels is constantly increasing, regardless the occasional drops, so this is one of the reasons for using the renewable energy sources.

Certain countries adjust the prices of fossil fuels through their policies in order to encourage the use of renewable energy sources. By reducing the existing reserves of fossil fuels, their price increases. The renewable energy sources increase the energy sustainability of the system, improve the security of energy supply and reduce the dependence of certain countries on the import of energy raw materials (fossil fuels) and electricity. [4]

From the social aspect, the renewable energy sources require more employees per unit of energy produced compared to the conventional energy technologies.

The conventional energy technologies require large investments and constant investment in finding the new sources.

Also, the awareness of people in the environmental protection and reduction the carbon dioxide emissions into the atmos-

phere is developing, which is also the policy of the European Union. [5]

2 ENERGY SOURCES AND THE ENVIRONMENT

The energy can appear in several forms:

- potential energy: exists as a consequence of the object position of in relation to the other objects;
- kinetic energy: which is a consequence of the body movement;
- chemical energy: which is a consequence of the chemical bonds between the atoms of the object substance;
- electrical energy: which is a consequence of the object electrification;
- thermal energy: exists as a consequence of the body heating;
- nuclear energy: which exists as a consequence of the instability of the object atomic nuclei;
- electromagnetic energy: radiation energy, which can be the light, radio waves or some other form.

The basic types of energy that enable the functioning of today's civilization are mainly the thermal and electrical energy, which can be converted into the other types of energy in further technological procedures.

A large percentage of heat and electricity are obtained today from the non-renewable energy sources.

The term non-renewable energy sources refers to all potential carriers of some type of energy that were created in the past, and now cannot be renewed, i.e. they cannot be regenerated or reproduced.

The largest share of non-renewable energy sources are the fossil fuels, fuels created by the anaerobic digestion of dead organisms in the interior of the earth under the effect of high temperature and pressure for millions of years.

Fossil fuels are the main source with as much as 85-90% of energy. The fossil fuels include: coal, peat, oil and oil derivatives and natural gas.

The problems with non-renewable energy sources are firstly in their quantity and distribution. The stocks of fossil fuels are limited and rapidly disappearing, and due to the concentration of energy resources in only a few areas of the world, the use of non-renewable fuels has created a system of interdependence, so that the countries that depend on the import of fossil fuels are in the subordinate positions. Another problem is the human environment pollution. The burning of fossil fuels, especially those based on oil and coal, is the most likely cause of the global warming, thus creating the so-called greenhouse effect due to the emission of carbon dioxide, sulfur, nitrogen compounds and other polluting compounds and particles.

Changing the climate conditions threaten the Earth's ecological system, which can affect the food production. On the other hand, the use of nuclear energy represents a conditionally clean technology, but in the event of disasters, an extremely large pollution can occur with the enormous consequences for the humans and environment. Also, a disposal of radioactive waste is a big problem.

Unlike the non-renewable, the renewable energy sources represent a form of energy that is not expendable, i.e. it can partially or completely regenerate itself. This natural form of energy is found all around us, just like the nature itself.

The use of renewable energy sources reduces the emission of greenhouse gases, as well as the overall pollution of the environment and its media.

Some of the most used and well-known sources of this form of energy are:

- bio renewable sources (biomass);
- energy of small watercourses;

- wind energy;
- solar energy; and
- geothermal energy

Looking at the essence of these sources, it can be seen that these sources are, practically, only modalities of solar energy. Namely, the biomass is created through the photosynthesis on the basis of solar energy. The air flow - wind occurs due to differences in the air temperatures in different places as a result of solar radiation. Water circulation in the nature, as well as tides, are also a consequence of solar radiation. Due to the enormous amount of energy that the Sun radiates and the period of its life, it can be considered that the radiation of energy from the Sun will last a very long time from the aspect of our civilization.

There are three main primary sources of renewable energy: [6]

- Thermonuclear reactions on the Sun (solar energy, energy of biological origin, wind energy, etc.).
- Decay of isotopes in the depths of the Earth (geothermal energy, etc.).
- Gravitational action of the planets (energy of the sea waves, etc.).

Most other sources, for example, the energy from fossil fuels, water flows, wind, etc., come from the solar energy. Thermal energy that comes to the Earth from the Sun by radiation is the biggest source of energy. The potential of energy from the depths of the Earth is significantly lower than the atmospheric energy of the Sun, while the smallest potential is the action of the planets.

The renewable energy sources can be divided into several basic groups, and the most common division is: [7]

- Solar (the Sun energy);
- Wind energy;
- Energy of water flows;
- Hydrogen energy;
- Biomass energy;
- Energy from the environment.

The electrical, thermal and chemical energy are obtained from these primary energy sources.

3 CLEAN ENERGY TECHNOLOGIES

The clean energy technologies include the energy efficient technologies and technologies of renewable sources. Both technologies reduce the use of energy from the conventional sources and fossil fuels. The energy efficiency measures refer to the methods and means for reducing the energy consumption by improving the use of devices, improving the service and maintenance, replacing the control systems, etc.

The clean energy technologies that fall into the category of energy efficient necessarily include a combined heat and electricity production, efficient lighting system, ventilation system, frequency regulators for driving pumps and fans, insulation repair, highly efficient building envelopes and windows, and the other commercial and developing technologies. [8]

The renewable energy technologies transform the renewable energy resources into the useful thermal energy, cooling energy, electrical or mechanical energy. The renewable resources are those whose use does not affect the future availability. Some renewable resources cease to be renewable if they are misused. For example, burning wood as a renewable resource ceases to be one if it leads to the deforestation. It is typical that in every energy system there are various inefficiencies that can be eliminated with the minimal investments, while the same effect of reducing energy consumption using the renewable energy sources often requires the larger investments. The approach of first increasing energy efficiency and then applying the renewable energy sources reduces the investment for applica-

tion the renewable energy source technologies, because the energy needs are also lower.

An example of electric heating of a house located in a cold climate zone, the electricity consumption has to be reduced, the condition of the building envelope, insulation thickness, building sealing and thermal bridges should be considered first. After reaching the standards in heat losses, it is necessary to proceed to an analysis of the used heating system and to consider the possibilities of using the renewable energy sources such as solar. [9]

The economic reasons for using the cleaner technologies are primarily:

- Increase in the price of conventional (fossil) fuels;
- Reduction of the fossil fuel reserves;
- Development of technologies that use the "cleaner" technologies.

Social reasons for using the cleaner technologies are on the other hand:

- More job positions (require more employees per unit of the energy produced);
- Local interest (using the local resources of funds, so that money is not spent on importing the fossil fuels or electricity).

4 ADVANTAGES OF THE RENEWABLE ENERGY SOURCES

Providing access to the renewable energy is one of the most important long-term policy decisions which a country can make.

These are four key reasons why the renewable energy sources should be at the heart of every country's energy strategy: [10]

ECONOMIC DEVELOPMENT: access to the energy from the renewable sources means the creation of the new job positions.

Starting from the production of components and expansion the electric grid to the installation and maintenance the systems for energy production from the renewable sources, the use of local renewable sources has an important economic effect. This is especially important in places that have the limited or no access to energy and where the unemployment is a significant problem. The renewable energy sources can help to create four times as many jobs for every dollar invested as the fossil fuel industries – and those jobs tend to be better-skilled and higher-paying.

CLIMATE: There is consensus among the scientists that the human-caused carbon emissions are already contributing to changing the Earth's climate in dangerous and unpredictable ways. According to the latest research, if current trends are to be judged, the global average temperatures will increase by at least 4°C during this century. [11] The development of energy production from the renewable sources can significantly contribute to the reduction of carbon emissions, without jeopardizing the access to energy.

ENERGY SECURITY: countries that do not have their own energy sources are forced to import the foreign oil, gas and coal, so they are exposed to the risks of price shocks and are dependent on the political goodwill of their trading partners. This can result in budget deficits, public borrowing and fuel shortages when supplies are disrupted. Since the fossil fuel reserves are limited, their price will inevitably rise in the long term. By developing the renewable energy sources of your country, you can create the conditions for access to the inexhaustible energy, which would make each country less dependent on the foreign energy sources.

HEALTH: the development of renewable energy sources, in addition to the economic, safety and environmental benefits, also bene-

fits the health of population. Six million people die each year from air pollution, both inside and outside their homes, caused by the burning of fossil fuels and traditional biomass. [12] Energy from the renewable sources, whether used on a large scale, to power the entire cities, or on a small scale, to power the rural mini-grids, can provide the clean and safe energy, without any of the effects on human health that the fossil fuels produce. Even something as simple as providing the access to a small amount of electricity to light the home can go a long way toward eliminating the safety and health concerns of using kerosene. [13]

The world governments have set access to the energy, especially energy from the renewable sources, as an important goal to be achieved by 2030. The Sustainable Energy for All (SE4ALL) initiative has been supported by the governments around the world, [14] many of which are currently developing plans to provide the sustainable energy to their citizens. The Sustainable Energy for All initiative, led by an Advisory Board jointly chaired by the Secretary-General of the United Nations and the President of the World Bank, mobilizes all sectors of society for action to support the achievement of three interrelated goals to be achieved by 2030: [15]

- providing the general access to the modern energy services;
- doubling the global rate of increase in the energy efficiency; and
- doubling the share of energy from renewable sources in the global energy mix.

Technologies for the use of renewable energy sources promote the human development stimulating the economic development, mitigating the effects of climate change, contributing to the energy security and bringing the significant health benefits.

5 OBSTACLES IN THE USE OF RENEWABLE ENERGY SOURCES

The energy produced from the renewable sources brings the considerable long-term economic benefits for the environment, and awareness of the short-term benefits of adopting technologies for the use of renewable energy sources is also growing. However, there are still obstacles preventing the use of renewable energy technologies at the speed and scale that are necessary.

Five key obstacles prevent the full development of the use of energy from the renewable sources as an alternative to the use of energy obtained from the fossil fuels. They are: [16]

ECONOMIC OBSTACLES: the cost of electricity production is measured by the costs per produced kilowatt hour (kWh) or megawatt hour (MWh). The electricity from fossil fuels has historically been produced more cheaply than the electricity from the renewable sources. One of the key reasons for this is that the initial costs of building the infrastructure and facilities for the production of electricity from the renewable sources have until recently been significantly higher than the costs of building the power plants burning fossil fuels. Except in the case of market intervention, a company engaged in the production of electricity will, by the nature of things, decide for the production technology that has the lowest cost per kWh, regardless the potential long-term trends in production costs.

However, the costs of producing energy from the renewable sources have been drastically reduced in recent years and thanks to the implementation of technological innovations and economies of scale, they continue to fall. On the other hand, the fossil fuels

represent limited sources of energy. In the long term, the costs of using them can only increase. If the negative effects of burning the fossil fuels (for example the damage caused locally to the environment, impact on the health of the population and need for adaptation measures to the changed climatic conditions - adaptation) could be counted as the "external consequences", apparent competitive advantage of conventional energy sources would largely disappear.

The government subsidies are the second economic obstacle for the extraction and use of fossil fuels. According to the International Monetary Fund, in 2012, the fossil fuel subsidies on a global scale amounted to \$1.9 trillion, which is 2% of the global GDP and far exceeds the amount of \$88 billion in subsidies, given to support the use of renewable energy. Those subsidies included the reduced taxes and duties on the extraction of fossil fuels, controls on oil and electricity prices, and direct investment by the governments in the infrastructure used to extract and deliver the fossil fuels for the energy production.

TECHNICAL OBSTACLES: despite decades of research and development, the technical barriers have prevented the renewables from being competitive in the energy market.

An important technical problem was the fact that some renewable energy sources, especially the wind energy and solar energy, have uneven energy production over time (keeping in mind the unequal wind intensity and insolation), so it is not possible to deliver a guaranteed and constant amount of electricity. This phenomenon is known in the energy production as the supply vola-

tility. The supply of energy from these sources cannot be easily adjusted to demand, unlike the fossil fuel power plants, which are able to respond quickly to changes in the electricity grid, using less or more fuel, or changing the number of generating units currently operating. However, for most energy sources that produce energy unevenly, for example, the wind and solar, it is possible to predict what the situation will be like 24 hours in advance. An extended network, covering a larger territory, represents the best solution for balancing the uneven production from the renewable energy sources, which is characterized by the predictable unevenness.

The second technical problem is known as a dispersion, which means that the best renewable energy sources are often located far from the urban centers, where the energy demand is highest. For example, most of the technically usable water for the hydroelectric power plants is located in the mountain ranges. Since the distance of the power plant from the end user contributes to the increase in the amount of energy that is lost (within the system and to the increase in the costs of transmission and distribution the network infrastructure), there is a reduction in incentives for the use of renewable energy sources that are located in remote regions.

The electricity can now be efficiently transmitted over long distances using the high-voltage direct current (HVDC) cables, with an energy loss of only about 3 percent on every 1,000 km and less than 1 cent per kWh in the additional distribution costs. Those cables have already been used in China and India to connect the population centers with the distant hydropower sources. [17]

The HVDC cables can also be used to consolidate the renewable energy sources in the form of regional "super grids" that use the smart metering technology to manage and adjust the amount of energy in the grid. For example, the solar energy in the desert

can be connected to the remote wind turbines and hydroelectric power plants in the mountainous regions. By connecting the different renewable energy sources from the remote areas into one extended smart grid, the changes in energy supply can be balanced. The HVDC cables allow the production of energy from the renewable sources to be adjusted to the extent of the needs of the energy industry, cities, or even entire countries.

POLICY OBSTACLES: In many countries, the legislation and policies governing the markets of electricity, heating and transport fuel have been the biggest obstacle to the development of use the renewable energy sources.

The electricity markets are usually managed by a monopolistic organization, often a state-owned utility company, which fully controls the generation, distribution and sale of electricity to the consumers. The research has shown that where the electricity market is monopolized, energy producing companies have little or no incentive to advocate for the development of electricity produced from the renewable sources.

The challenge associated with this is the bureaucracy that must regulate and approve the development of electricity generation (or heating or transport fuel). Where there are many places where things are approved in several departments of the government (and in the federal and decentralized states, at more than one level of government), the costs of developing the use of renewable energy sources increase significantly, and the time required for this often significantly discourages its development.

Development of the use of renewable energy sources within the electricity grid can be accelerated if it is ensured that the political and legal framework is fully coherent and decision-making process is transparent.

COMMUNITY SUPPORT: with the local political challenges must be tackled even in situations where the government fully supports the need to encourage the development of use the renewable energy sources and has accepted the removal of economic and political barriers to their development.

While the renewable energy projects have proliferated over the past decade, some of them have met with the public opposition. It is important to ensure community buy-in and, where possible, the legal ownership of the renewable energy development as a way to reduce the opposition to development.

6 TECHNOLOGY OF USING THE RENEWABLE ENERGY SOURCES

The energy from renewable sources is produced from a source that is constantly replenished naturally. It is primarily used in one of three ways:

- electricity generation: renewable sources are used to generate the electricity that is distributed for the residential, commercial and industrial needs;
- production of thermal energy for heating: whether produced centrally or decentralized (in individual buildings), renewable resources, for example, water heated by the solar energy, can be used directly to the heat buildings; and
- production of transport fuels: fuels for privately owned motor vehicles, public transport and industrial and commercial use, for example for the freight trains, ships and aircraft, can be produced from the renewable sources.

During the past decade, the increased use of energy from the renewable sources is mainly due to the production of electricity and traditional way of using the biomass. If the world wants to slow the climate changes by reducing the carbon dioxide emissions, an effort must also be made to use the

sustainable energy sources to produce the heat and fuel for transportation. [18]

According to the data from the Energy Institute, in 2022, there was a 1% increase in the total primary energy consumption, reaching a level of approximately 3% above the pre-pandemic level of 2019. The share of renewable energy sources (excluding the hydroelectric power plants) in the primary energy consumption reached 7.5% in 2022, which represents an increase of almost 1% compared to the previous year, while the consumption of fossil fuels as a percentage of the primary energy remained stable at 82%. [19]

According to the data from the Energy Institute, from 2023, when it comes to the renewable energy (excluding hydro), it grew by 14% in 2022, reaching 40.9 EJ. Namely, the capacity of solar power plants and wind power plants continued to grow rapidly in 2022, while the largest part of capacity growth of the solar power plants and wind power plants was in China, which accounted for about 37% and 41% of the global increase in capacity. [19]

7 THE FUTURE OF RENEWABLE ENERGY SOURCES

In the future, the global development of society will depend to a significant extent on the state of the energy sector. The problems that all the countries of the world face to a lesser or greater extent are related to the provision of energy and preservation the environment. The issue of energy security and stability emerges as a cardinal issue related to the functioning of global economic, economic and social system.

The European Union, despite its high development and evolution of its attitude towards the issue of energy security, also faces the problem of reducing the environmental pollution, the application of renewable energy sources and its role in reducing the human impact on the climate. [20]

A connection of energy sector with the competitiveness of the European or any economy leads to an easy willingness to overrun the importance of struggle the sake of economic betterment to create the legal, institutional, technical, economic and social assumptions for a successful and sustainable fight against the climate changes. In the energy sector itself, the most important mechanisms for combating the climate changes are the energy efficiency and introduction the renewable energy sources in production, transmission, distribution and consumption. [21]

Unfortunately, neither the old nor the new members of the European Union, which had far more favorable market and political conditions for implementation the European regulations in the area of promotion the renewable energy sources and energy efficiency, security of supply and level of environmental protection, have not yet succeeded in fully implementing the European laws in this sector and the use of renewable energy sources.

The growing concerns about the global warming and energy dependence are forcing the countries of the European Union to modernize their approach to the energy production and consumption. The locally available renewable energy sources can significantly help with this problem with negligible or no carbon dioxide emissions. [22]

The water mills and windmills, used earlier, produced the mechanical energy from the renewable energy source of water. Today, the modern versions of these devices convert the water or wind into electricity. The European electricity production from the wind energy, which has made a significant progress in the last few years, is today at the level of electricity needs in Denmark and Hungary. [23]

Several technologies, especially the wind energy, small hydropower plants, biomass energy and solar energy, are economically

competitive. The other technologies depend on a market demand to become economically viable compared to the conventional energy sources. The process of accepting the new technologies is very slow, where the initial cost is a key problem for installation the new plants. [24]

The renewable energy sources, not including hydropower, provide less than 1% of the total required energy. [25] That share should be significantly increased in the future because there are fewer and fewer non-renewable sources of energy, and their harmful impact has become more and more pronounced in the last few decades.

8 CONCLUSION

The renewable energy sources and new technologies for using these sources are becoming an increasingly important segment in all fields, especially affecting the environment. Using the renewable energy sources reduces the consumption of non-renewable energy resources. The use of these sources is therefore very important from the aspect of environmental protection.

The development of renewable energy sources (especially wind, water, solar and biomass energy) is important for several reasons.

The renewable energy sources play a very important role in reducing the emission of carbon dioxide into the atmosphere. Also, increasing the share of renewable energy sources increases the energy sustainability of the system, as it helps to improve the security of energy supply by reduction a dependence on the import of energy raw materials and electricity.

The renewable energy sources are expected to become economically competitive with the conventional energy sources over a longer period of time.

A clear example is the energy itself, which as an area of the economy, on which the development of all other areas of the

economy is based, is the biggest polluter of the environment, without whose protection it is not possible to achieve the sustainable development of the human species and living world on the planet.

The environmental pollution knows no national borders, which is the reason for the further development of a new area of law - the law of environmental protection, which, in the same way as the law of energy, has an international character by its nature. All the countries of the world have a difficult task: how to reduce the use of fossil fuels and emission of harmful gases that cause the greenhouse effect, global warming, climate change, natural disasters and occurrence of acid rain, while at the same time preserving the achieved level of technological and economic development.

The only way is to reduce the use of fossil fuels and develop technologies for the use of renewable energy sources.

Replacing the fossil fuels with the renewable energy sources has a great impact on successfully solving global environmental problems. Today, the application of renewable energy sources is gaining more and more importance, especially for reasons of the environmental protection and the use of resources available on one's own territory.

Mitigation the climate changes is currently the most serious global problem, of which we are also a part. The time to stop the weather changes, which can cause a catastrophe like no man has ever seen, is getting shorter every day.

The solutions exist, and the renewable energy sources are the most important and unavoidable factor. The technologies of using the renewable energy sources are becoming more economically profitable and competitive on the market every day, which eliminates fears that the transition from fossil fuels will threaten the economies of the countries that use them.

REFERENCES

- [1] Dragoljub Todić, Mladenka Ignjatić, Milica Tomanović, Katarina Butkovska, Kamil Vilić, Guides Through the EU Policies - Environment (Loznica: European Movement in Serbia; Mladost Group, 2010), 25 (In Serbian)
- [2] Umair Shahzad, The Need for Renewable Energy Sources, Information Technology & Electrical Engineering (2012): 16-18.
- [3] N.L. Panwar, S.C. Kaushik, Surendra Kothari, Role of Renewable Energy Sources in Environmental Protection: A Review, Renewable and Sustainable Energy Reviews 15 (2011): 1513.
- [4] Marija Petrović-Randelović, Nataša Kocić, Branka Stojanović-Randelović, The Importance of Renewable Energy Sources for Sustainable Development, Economics of Sustainable Development 4, 2 (2020): 15.
- [5] National Action Plan for the Use of Renewable Energy Sources of the Republic of Serbia (Belgrade: Republic of Serbia, Ministry of Energy, Development and Environmental Protection, 2013) 1-161 (In Serbian)
- [6] D. Savić, D. Tašić, K. Milivojević, V. Đurđević, Multidisciplinary approach to the analysis of suitability the location intended for construction the solar power plants on the area of a mining waste dump, Mining and Metallurgy Engineering Bor 1 (2024) 7-16.
- [7] Antonia V. Herzog, Timothy E. Lipman, Daniel M. Kammen, Renewable Energy sources, Encyclopedia of Life Support Systems (EOLSS) Forerunner, Volume: Perspectives and Overview of Life Support Systems and Sustainable Development, Part 4C: Energy Resource Science and Technology

- Issues in Sustainable Development – Renewable Energy Sources, (Berkeley, USA: University of California, 2020) 9.
- [8] Law on Integrated Prevention and Control of the Environmental pollution, Official Gazette RS, No. 135/2004, 25/2025 and 109/2021 (In Serbian)
- [9] Law on Energy, Official Gazette RS, No. 145/2014-3, 95/2018-267 (other law), 40/2021-1, 35/2023-79 (other law), 62/2023-8 and 94/2024-204 (In Serbian)
- [10] R. Pollin, J. Wicks-Lin, H. Garrett-Peltier, Green Prosperity: How Clean-Energy Policies Can Fight Poverty and Raise Living Standards in the United States (Amherst: Department of Economics and Political Economy Research Institute (PERI), University of Massachusetts, 2009) 8.
- [11] Turn Down the Heat: Why a 4°C Warmer World Must be Avoided, (Washington, DC, USA: World Bank, 2012)
<http://documents.worldbank.org/curated/en/865571468149107611>
- [12] Christopher J.L. Murray, Alan D. Lopez, A Comparative Risk Assessment of Burden of Disease: A Systematic Analysis for the Global Burden of Disease Study 2010 (Boston MA, USA: World Health Organization, 2013) 31.
- [13] Regulations on Energy Permits, Official Gazette RS, No. 15/2015, 44/2018 (other laws) and 99/2024 (In Serbian)
- [14] SEforALL, Sustainable Energy for All, 2023, <https://www.seforall.org>.
- [15] European Environment Agency, Energy Subsidies in the European Union: A Brief Overview, Technical Paper, 1 (2004): 13.
- [16] Ieva Baršauskaitė, Background Note on Fossil Fuel Subsidy Reform, International Institute for Sustainable Development, (2022): 8.
- [17] Benjamin R.T. Cotts, Jay R. Prigmore II, Kevin L. Graf, HVDC Transmission for Renewable Energy Integration, The Power Grid - Smart, Secure, Green and Reliable, (2017): 171.
- [18] Tze-Zhang Ang, Mohamed Salem, Mohamad Kamarol, Himadry Shekhar Das, Mohammad Alhuyi Nazari, Natarajan Prabakaran, A Comprehensive Study of Renewable Energy Sources: Classifications, Challenges and Suggestions, Energy Strategy Reviews 43, 9 (2022): 100939.
- [19] Trends, III Quarter (Belgrade: Republic Institute of Statistics, 2023) 19-20 (In Serbian)
- [20] United Nations Capital Development Fund and United Nations Development Programme, Clean Start – Microfinance Opportunities for a Clean Energy Future (New York: UNCDF/UNDP, 2012).
- [21] United Nations Development Programme, Handbook for Conducting Technology Needs Assessment (TNA) for Climate Change (New York: UNDP and the United Nations Framework Convention on Climate Change Secretariat (UNFCCC), 2010).
- [22] Renewable Energy Policy Network for the 21st Century, Renewables Global Future Report 2013 (Paris: REN21 2013).
- [23] Erdiwansyah, Mahidin, H. Husin, Nasaruddin, M. Zaki, Muhibbuddin, A Critical Review of the Integration of Renewable Energy Sources with Various Technologies, Protection and Control of Modern Power Systems, 6(3) (2021), <https://doi.org/10.1186/s41601-021-00181-3>.

- [24] UNDP, Transforming On-Grid Renewable Energy Markets (New York, Washington DC: Global Environmental Facility, 2012).
- [25] UNDP, Example of Inclusive Green Economy Approaches in UNDPs Support to Countries (New York: UNDP, 2012).

Zoran Avramović^{*1}, Milan Antonijević^{**2}, Ljiljana Avramović^{*3},
Dragana Božić^{*4}, Vanja Trifunović^{*5}

THE EFFECT OF CUPRIC IONS ON THE CORROSION BEHAVIOUR OF BRASS CuZn42 IN AN ACID ENVIRONMENT^{***}

Orcid: 1) <https://orcid.org/0009-0006-7585-976X> 2) <https://orcid.org/0000-0002-2201-066X>
3) <https://orcid.org/0000-0002-3747-1530> 4) <https://orcid.org/0000-0003-1055-8449>
5) <https://orcid.org/0000-0003-4839-8751>

Abstract

This paper presents the results of research on the corrosion behavior of brass CuZn42 in an acidic environment, in the presence of copper ions. Based on the recorded anodic polarization curves, it was concluded that as the concentration of copper ions in the tested solution increases, the corrosion current densities also increase. This is reflected in the occurrence of the decinking process of brass, during which zinc is deposited on its surface, while the remaining porous copper stays within the brass mass.

Keywords: brass, deformation, copper (II) ion, corrosion, polarization, decinking

1 INTRODUCTION

The corrosion behavior of brass has been mostly tested in terms of the mechanisms of dezincification and stress corrosion. Dezincification is a well-known (delegating) process that refers to the loss of zinc from brass, and is considered as an important physical-mechanical property leading to the surface destruction [1-4]. It occurs in solutions containing the specific chemical compounds. The Cu-Zn family includes brass alloys. Dezincification (delegation, alloy separation) has a significant impact on these alloys due to the large difference in the equilibrium potential between Cu and Zn. Dezincification can occur as a

generalized form of corrosion or during crack propagation due to stress corrosion. The delegation of other Cu alloys is also an important example, such as the selective removal of Cu from Cu-Sn alloys or Al from aluminum bronze. During the corrosion of many technical aluminum alloys, the delegation of Cu-rich intermetallic particles (i.e., α -phase, Al_2Cu , or s-phase, Al_2CuMg) can occur as the first step. The delegation process can also be used to prepare functional, nanoporous Cu-based materials [5].

Previous studies have shown that ions such as the thiocyanates, bromides, and iodides do not participate in dezincification,

^{*} Mining and Metallurgy Institute Bor, Alberta Ajnštajna 1, 19210 Bor, Serbia,
E-mail: zoran.avramovic@irmbor.co.rs

^{**} University of Belgrade, Technical Faculty in Bor, VJ 12, Bor, Serbia

^{***} The authors are grateful to the Ministry of science, technological development and innovation of the Republic of Serbia for financial support according to the Contract No. 451-03-136/2025-03/200052.

while chlorides and sulfates, at certain concentrations, induce dezincification [6,7]. The effect of anions is reflected in their pronounced effect on the surface of sample. The observed differences in the dissolution kinetics and degree of dezincification in chloride and sulfate media may be influenced by the bond between copper and present anions.

Two main theories explain the mechanism of dezincification of brass: the first theory assumes the selective dissolution of zinc, which leaves the alloy and results in a porous residue rich in the metallic copper, while the second theory assumes the simultaneous dissolution of zinc and copper, with copper redeposition occurring to a certain degree.

There are still conflicting the opinions regarding copper redeposition, as well as the form and nature of the corrosion products of brass, deposited on the surface of sample during the selective dissolution of the alloy [8,9,10,11].

The corrosion behavior and dezincification process of the cold-deformed CuZn42 brass were investigated in an acidic sulfate solution at pH 2, with the addition of copper (II) ions, using the linear polarization method. The measured corrosion potentials and corrosion current densities were observed as characteristics of the dezincification process and corrosion resistance of the tested cold-deformed CuZn42 brass samples.

The obtained results show that the lower pH values of the tested solutions and increased copper (II) ion concentrations lead to an increase in corrosion current densities of the tested brass samples, which is a result of the selective dissolution of zinc and individual dissolution of zinc and copper, including the dezincification process.

The lowest corrosion current densities are observed in the brass samples with the highest degree of deformation (80%). The dezincification and anodic dissolution process of the cold-deformed brass samples occurs across the entire range of tested potentials.

The aim of this study was to show which of the tested cold-deformed brass samples exhibits an inhibitory effect. Additionally, the concentrations of copper ions were determined at which the tested brass samples show an active state towards the corrosion process.

2 EXPERIMENTAL PART

The sample of the tested brass, laboratory-produced, had the following chemical composition: Cu-57.95% (purity 99.997%), Zn-41.91% (purity 99.85%), and the rest-0.14%. The sample was embedded in cold-curing acrylic. A copper electrode was used as a reference sample. The samples for electrochemical measurements had a constant surface area of $P=0.38\text{cm}^2$. Before each polarization measurement, the samples were polished with a sandpaper of grade #1000 and aluminum oxide, then washed with distilled water and ethanol. A saturated calomel electrode (SCE) and platinum wire were used as the reference and counter electrodes, respectively, while the brass served as the working electrode in a classic three-electrode electrochemical cell. All potential values shown on the polarization curves are given relative to the saturated calomel electrode (E_{sce}). During polarization measurements, the following solutions were used: $1 \cdot 10^{-1}\text{M Na}_2\text{SO}_4$, $1 \cdot 10^{-1}\text{M Na}_2\text{SO}_4 + 1 \cdot 10^{-3}\text{M CuSO}_4$, $1 \cdot 10^{-1}\text{M Na}_2\text{SO}_4 + 5 \cdot 10^{-3}\text{M CuSO}_4$, $1 \cdot 10^{-1}\text{M Na}_2\text{SO}_4 + 1 \cdot 10^{-2}\text{M CuSO}_4$, and $1 \cdot 10^{-1}\text{M Na}_2\text{SO}_4 + 5 \cdot 10^{-2}\text{M CuSO}_4$. The working electrolyte was $10^{-1}\text{M Na}_2\text{SO}_4$ solution. Polarization measurements were performed from the open circuit potential to a potential of 1000 mV (SCE) with a polarization rate of 10mV/s, using the linear polarization method. The AMEL equipment was used, specifically: potentiostat-model 553, programmable function generator-model 568, interface-model 560/A/log, and digital x/y recorder-model 863.

3 RESULTS AND DISCUSSION

For the high concentrations of H_2SO_4 (1.0M) and low temperatures (298K), the copper surface is passivated, resulting in the low corrosion rates ($1.7 \cdot 10^{-3}$ mm/d). The phenomenon of copper passivation in 1.0M H_2SO_4 solution is explained in the literature by formation the $\text{CuSO}_4 \cdot 5\text{H}_2\text{O}$ and/or Cu_2O film [12]. The passivation film consists of a mixture of copper oxides on the inner side, while the outer layer is composed of copper sulfate hydrates [13]. The corrosion potentials for pH value of 2 and all tested samples are negative, with copper exhibiting the

most positive corrosion potential, as shown in Table 1. The most positive values for the copper electrode were also obtained in studies [14,15], when investigating the corrosion potentials of copper, tin, and bronze (Cu-10Sn) in Na_2SO_4 solution. In the study [16], the corrosion potential values and corrosion current densities for the copper electrode in $1 \cdot 10^{-1}$ M Na_2SO_4 solution at pH value of 3.5 were: -26 mV and $0.91 \mu\text{A}/\text{cm}^2$, with complete agreement in the shapes of polarization curves, as shown in Figure 1, as a result of our tests.

Table 1 Values for corrosion potentials (E_{corr}) and corrosion current densities (j_{corr}) for the tested brass alloys and copper in a $1 \cdot 10^{-1}$ M Na_2SO_4 solution, at pH 2 in the presence of copper ions

$1 \cdot 10^{-1}$ M $\text{Na}_2\text{SO}_4 + 1 \cdot 10^{-3}$ M Cu^{2+}						
Sample	Cu	CuZn42 (0%)	CuZn42 (20%)	CuZn42 (40%)	CuZn42 (60%)	CuZn42 (80%)
E_{corr} (mV)	-14	-53	-49	-58	-53	-68
j_{corr} (mA/cm ²)	0.679	0.817	0.865	0.981	1.121	0.745
$1 \cdot 10^{-1}$ M $\text{Na}_2\text{SO}_4 + 5 \cdot 10^{-3}$ M Cu^{2+}						
Sample	Cu	CuZn42 (0%)	CuZn42 (20%)	CuZn42 (40%)	CuZn42 (60%)	CuZn42 (80%)
E_{corr} (mV)	-6	-45	-25	-37	-40	-43
j_{corr} (mA/cm ²)	0.711	0.935	1.092	1.134	1.218	0.912
$1 \cdot 10^{-1}$ M $\text{Na}_2\text{SO}_4 + 1 \cdot 10^{-2}$ M Cu^{2+}						
Sample	Cu	CuZn42 (0%)	CuZn42 (20%)	CuZn42 (40%)	CuZn42 (60%)	CuZn42 (80%)
E_{corr} (mV)	2	-30	-28	-49	-24	-29
j_{corr} (mA/cm ²)	0.867	1.057	1.17	1.304	1.342	1.015
$1 \cdot 10^{-1}$ M $\text{Na}_2\text{SO}_4 + 5 \cdot 10^{-2}$ M Cu^{2+}						
Sample	Cu	CuZn42 (0%)	CuZn42 (20%)	CuZn42 (40%)	CuZn42 (60%)	CuZn42 (80%)
E_{corr} (mV)	31	-16	10	10	-10	10
j_{corr} (mA/cm ²)	0.947	1.238	1.333	1.378	1.448	1.211

It can be seen from Table 1 that the values of corrosion current densities are lowest for the copper electrode. For brass CuZn42, the values of corrosion current densities increase with the increase in deformation degree (Table 1). The highest values of co-

rosion current densities are observed for brass CuZn42 with a deformation degree of 60%, while the lowest values are for brass with a deformation degree of 80%. This is explained by the greatest disorder in the crystal lattice and easier formation of the

protective CuO/Cu₂O film on the surface of brass [17-20]. Copper(II) ions play an important role in the occurrence of stress

corrosion in brass over a wide range of solution pH values [21-23].

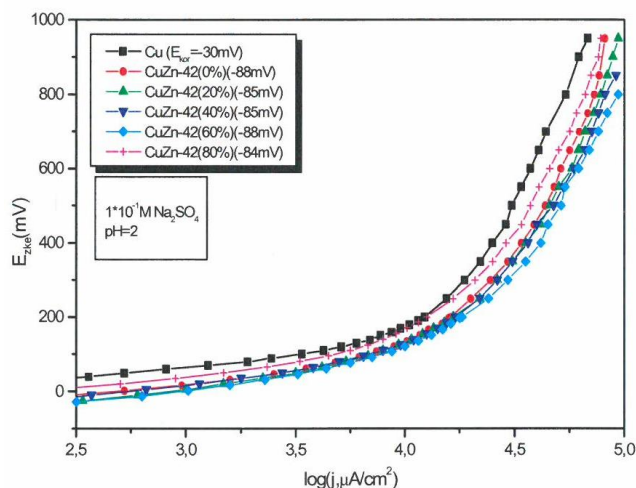


Figure 1 Polarization curves for deformed brass CuZn42 and copper in a $1 \cdot 10^{-1} \text{M Na}_2\text{SO}_4$ solution

The effect of Cu²⁺ ions on the corrosion process of copper and CuZn42 brass was tested by addition the following concentrations of Cu²⁺ ions: $1 \cdot 10^{-3} \text{M}$, $5 \cdot 10^{-3} \text{M}$, $1 \cdot 10^{-2} \text{M}$, and $5 \cdot 10^{-2} \text{M}$ to a $1 \cdot 10^{-1} \text{M Na}_2\text{SO}_4$ solution. The tests were conducted at pH 2.

The values for corrosion potentials (E_{corr}) for copper and CuZn42 brass "shift" over time into the more positive region with increasing concentrations of Cu²⁺ ions (Tables 2 and 3), with the most positive values observed at the Cu²⁺ ion concentration of $5 \cdot 10^{-2} \text{M}$.

Table 2 Corrosion potential values for copper electrode in a Cu²⁺ ion solution at pH 2

Cu electrode					
	Solution				
	$1 \cdot 10^{-1} \text{M Na}_2\text{SO}_4$	$1 \cdot 10^{-1} \text{M Na}_2\text{SO}_4 + 1 \cdot 10^{-3} \text{M Cu}^{2+}$	$1 \cdot 10^{-1} \text{M Na}_2\text{SO}_4 + 5 \cdot 10^{-3} \text{M Cu}^{2+}$	$1 \cdot 10^{-1} \text{M Na}_2\text{SO}_4 + 1 \cdot 10^{-2} \text{M Cu}^{2+}$	$1 \cdot 10^{-1} \text{M Na}_2\text{SO}_4 + 5 \cdot 10^{-2} \text{M Cu}^{2+}$
E_{corr} (mV)	-30	-14	-6	2	31

The zinc content in the brass results in lower corrosion potential values even in alkaline solutions, with the following measured values: for copper: -0.05V, for CuZn10: -0.10V, CuZn40: -0.14V and pure zinc: -0.54V [7]. Additionally, the increased zinc concentrations in brass alter the chemical composition of the passive film on its surface, changing from the typical Cu₂O/CuO film to a ZnO/Cu₂O/CuO film with an increased ZnO content [24,25,26].

At the same time, the thickness of the zinc-oxide layer increases, while the thickness of the copper-oxide layer decreases.

The lowest corrosion current densities are observed for the copper electrode. A decrease in deformation degree leads to a reduction in the values for corrosion current density (j_{corr}) for all tested samples, with the highest values occurring in brass CuZn42(60%) and the lowest in brass CuZn42(80%), which is explained by the

stability of the formed $\text{Cu}_2\text{O}/\text{CuO}$ film on the electrode surface. In this case, a high degree of deformation of the electrode has an inhibitory effect on the corrosion process.

Table 3 Values for corrosion potential for brass CuZn42 at five deformation degrees and copper, in Cu^{2+} ion solution at pH 2

$1 \cdot 10^{-1} \text{M Na}_2\text{SO}_4 + 1 \cdot 10^{-3} \text{M Cu}^{2+}$						
Sample	Cu	CuZn42 (0%)	CuZn42 (20%)	CuZn42 (40%)	CuZn42 (60%)	CuZn42 (80%)
E_{corr} (mV)	-14	-53	-49	-58	-53	-68
$1 \cdot 10^{-1} \text{M Na}_2\text{SO}_4 + 5 \cdot 10^{-3} \text{M Cu}^{2+}$						
Sample	Cu	CuZn42 (0%)	CuZn42 (20%)	CuZn42 (40%)	CuZn42 (60%)	CuZn42 (80%)
E_{corr} (mV)	-6	-45	-25	-37	-40	-43
$1 \cdot 10^{-1} \text{M Na}_2\text{SO}_4 + 1 \cdot 10^{-2} \text{M Cu}^{2+}$						
Sample	Cu	CuZn42 (0%)	CuZn42 (20%)	CuZn42 (40%)	CuZn42 (60%)	CuZn42 (80%)
E_{corr} (mV)	2	-30	-28	-49	-24	-29
$1 \cdot 10^{-1} \text{M Na}_2\text{SO}_4 + 5 \cdot 10^{-2} \text{M Cu}^{2+}$						
Sample	Cu	CuZn42 (0%)	CuZn42 (20%)	CuZn42 (40%)	CuZn42 (60%)	CuZn42 (80%)
E_{corr} (mV)	31	-16	10	10	-10	10

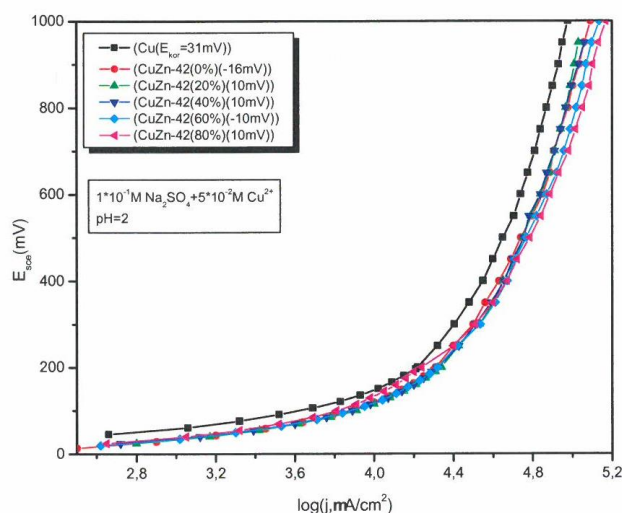


Figure 2 Polarization curves for the tested samples in $10^{-1} \text{M Na}_2\text{SO}_4 + 5 \cdot 10^{-2} \text{M Cu}^{2+}$

In Figure 2, the polarization curves of copper and brass CuZn42 are presented, with five degrees of deformation, in $1 \cdot 10^{-1} \text{M Na}_2\text{SO}_4$ solution, with the addition of the highest tested concentration of copper ions, $5 \cdot 10^{-2} \text{M Cu}^{2+}$, along with the displayed values for corrosion potentials and corrosion current densities.

For comparison the curve shapes as well as the values for E_{corr} and j_{corr} , Figure 3 and Table 4, show the polarization curves for the tested brass samples in $1 \cdot 10^{-1} \text{M Na}_2\text{SO}_4$ solution with the addition of $5 \cdot 10^{-2} \text{M Cl}^-$ ions.

Based on the presented curves (Figure 3) and values from Table 3 and Table 4, it can be concluded that the Cl^- ion has a less co-

rosive effect on the tested brass compared to Cu^{2+} ion solution. This is explained by the inhibitory effect of chloride ions and stability of the formed Cu(I)-chloride complex (CuCl_2^-), which is formed by the primary reaction:

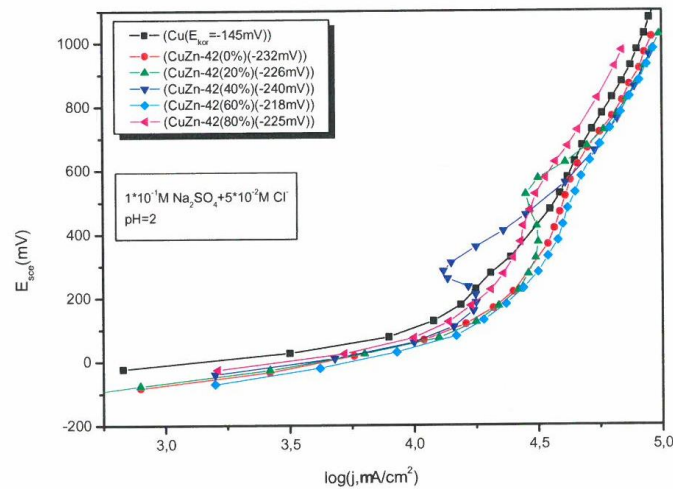
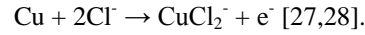


Figure 3 Polarization curves for tested samples in $10^{-1} \text{M Na}_2\text{SO}_4 + 5 \cdot 10^{-2} \text{M Cl}^-$

Table 4 Values of corrosion potentials and corrosion current densities for CuZn42 brass and copper in solution of $5 \cdot 10^{-2} \text{M Cl}^-$ ions, for pH 2

$1 \cdot 10^{-1} \text{M Na}_2\text{SO}_4 + 5 \cdot 10^{-2} \text{M Cl}^-$						
Sample	Cu	CuZn42 (0%)	CuZn42 (20%)	CuZn42 (40%)	CuZn42 (60%)	CuZn42 (80%)
E_{corr} (mV)	-145	-232	-226	-240	-218	-225
j_{corr} (mA/cm ²)	0.678	1.083	1.122	1.182	1.197	1.008

Based on the experiments conducted, it can be said that the inhibitory effect on corrosion is observed with a deformation degree of 80% for CuZn42 brass. The formed $\text{Cu}_2\text{O}/\text{CuO}$ film is unstable in a solution with a pH 2 leading to the increased values for corrosion current densities. The study in [10] found that the passive protective film, composed of Cu_2O compounds, is more unstable at pH 4 than at pH 7. A decrease in concentration of the Cu^{2+} ions and degree of deformation leads to a reduction in the values for corrosion current density (j_{corr}) for all tested electrodes.

A deformation degree of 80% has an inhibitory effect on the corrosion process of CuZn42 brass in all solutions. Tests have shown that the corrosion current densities for copper at pH 2 are lower than those for CuZn42 brass. This is explained by the poor stability of the surface film on CuZn42 brass in highly acidic solutions, or rapid disruption of the formed film on the brass surface, as well as the initial process of dezincification, during which zinc is more intensely leached from CuZn42 brass into solution at lower pH values [28, 29, 30].

The increased values for corrosion current density are a result of the initial stage of dezincification process and zinc leaching from the brass surface.

4 CONCLUSION

In Cu^{2+} ion solutions:

- CuZn42(60%) brass has the highest corrosion current density value.
- CuZn42(80%) brass has the lowest corrosion current density value.
- In acidic solutions, the protective layer formed on the brass surface is unstable, which is explained by the dezincification process of the tested brass.
- Increased corrosion current densities indicate an intensive dezincification process of brass, where zinc leaches from an alloy, leaving a porous copper residue with poor corrosion resistance.
- An effective method of protecting brass from the corrosion and dezincification process is the application of corrosion inhibitors.
- From the presented tables and graphs, the inhibitory effect of chloride ions is evident, which is explained by formation the stable Cu(I)-chloride complex (CuCl_2^-) on the surface of tested samples. The formation of this complex can lead to a decrease in availability the reactive surface sites for further processes (such as corrosion, oxidation, or other electrochemical reactions), as a layer is formed on the surface that protects metal from further damage or interaction with the surrounding environment.

REFERENCES

- [1] P. Lapitz, J. Ruzzante, M. G. Alvarez, AE Response of α -BRASS During Stress Corrosion Crack Propagation, *Corrosion Science*, 49 (2007) 3812-3820
- [2] W. Li, D. Y. Li, Variations of Work Function and Corrosion Behaviors of Deformed Copper Surface, *Applied Surface Science*, 240 (2005) 388-396
- [3] Y. J. Zou, D. H. Wang, W. Qiu, Solid-State Diffusion During the Selective Dissolution of Brass: Chrono-amperometry and Positron Annihilation Study, *Electrochimica Acta*, 42, 11 (1997) 1733-1741
- [4] H. G. Park, K. Jung-Gu, Ch. Yun-Mo, J. G. Han, S. H. Ahn, C. H. Lee, A Study on Corrosion Characterization of Plasma Oxidized 65/35 Brass with Various Frequencies, *Surface and Coatings Technology*, 200 (2005) 77-86
- [5] P. Zhou P., K. Ogle, The Corrosion of Copper and Copper Alloys. In: Wandelt, K. (Ed.) *Encyclopedia of Interfacial Chemistry: Surface Science and Electrochemistry*, 6 (2018) 478-489
- [6] R. Soenoko, P. H. Setyarini, S. Hidayatullah, M. S. Maarif, Corrosion Characterization of Cu-Based Alloy in Different Environments, *P. Metalurgija*, 59, 3 (2020) 373-376
- [7] I. Milošev, The Effect of Various Halide Ions on the Passivity of Cu, Zn, and Cu-xZn Alloys in Borate Buffer, *Corrosion Science*, 49 (2007) 637-646
- [8] H. Lu, K. Gao, W. Chu, Determination of Tensile Stress Induced by Dezincification Layer During Corrosion for Brass, *Corrosion Science*, 40, 10 (1998) 1663-1670
- [9] K. Marshakov, Corrosion Resistance and Dezincing of Brasses, *Protection of Metals*, 41, 3 (2005) 205-213
- [10] G. A. El-Mahdy, Electrochemical Impedance Study on Brass Corrosion in NaCl and $(\text{NH}_4)_2\text{SO}_4$ Solutions During Cyclic Wet-Dry Conditions, *Journal of Applied Electrochemistry*, 35 (2005) 347-353
- [11] A. Romaine, M. Crozet, N. Mary, B. Normand, M. Chassagne, F. Dufour, Importance of the Surface and environmental conditions on the Corrosion Behavior of Brass, Steel, and

- Brass-Coated Steel Wires and Brass-Coated Steel Cords, *Corrosion Science*, 177 (2020) 108 966
- [12] H. Otmačić, E. Stupnišek-Lisac, Copper Corrosion Inhibitors in Near Neutral Media, *Electrochimica Acta*, 48 (2003) 985-991
- [13] D. Tromans, T. Ahmed, Active/Passive Behavior of Copper in Strong Sulfuric Acid, *Journal of the Electrochemical Society*, 145 (1998) 601-612
- [14] A. Moreira, A. Benedetti, P. Cabot, P. Sumodjo, Electrochemical Behavior of Copper Electrode in Concentrated Sulfuric Acid Solutions, *Electrochimica Acta*, 38 (1993) 981-993
- [15] E. Sidot, N. Souissi, L. Bousselmi, E. Triki, L. Robbiola, Study of the Corrosion Behavior of Cu-10Sn Bronze in Aerated Na₂SO₄ Aqueous Solution, *Corrosion Science*, 48 (2006) 2241-2253
- [16] J. Telegdi, T. Rigo, E. Kalman, Molecular Layers of Hydroxamic Acids in Copper Corrosion Inhibition, *Journal of Electroanalytical Chemistry*, 582 (2005) 191-203
- [17] P. Rothenbach, On the Dezincification of Recrystallized and Statically Loaded Copper-Zinc Alloys with 30 at%-Zinc, *Corrosion Science*, 10 (1970) 391-407
- [18] S. Mayanna, T. Setty, Effect of Benzotriazole on the Dissolution of Copper Single Crystal Planes in Dilute Sulfuric Acid, *Corrosion Science*, 15, 6 (1975) 627-638
- [19] L. Burzynska, Z. Zembura, Dezincification of γ -Brass During Spontaneous Dissolution with Hydrogen Depolarization. Part I. Kinetics, *Polish Journal of Chemistry*, 66 (1992) 503-512
- [20] N. Nunez, E. Reguera, F. Corvo, E. Gonzales, C. Vasquez, Corrosion of Copper in Seawater and its Aerosols in a Tropical Island, *Corrosion Science*, 47 (2005) 461-469
- [21] M. Alvarez, C. Manfredi, M. Giordano, Anodic Rate-Controlling Steps in Transgranular Stress Corrosion Cracking of α -Brass in NaNO₂ Solutions, *Corrosion Science*, 24, 9 (1984) 769-780
- [22] L. Burzynska, J. Stoch, Z. Zembura, Kinetics of Spontaneous Dissolution of Cu-47.3 Atom Zn Brass with Hydrogen Depolarization. An XPS Study of the Surface Composition, *Solid State Ionics*, 38, 3-4 (1990) 179-186
- [23] X. J. Guo, K. Gao, L. Qiao, The Correspondence Between Susceptibility to SCC of Brass and Corrosion-Induced Tensile Stress with Various pH Values, *Corrosion*, 44 (2002) 2367-2375
- [24] I. Milošev, H. Strehblow, Electrochemical Behavior of Cu-xZn Alloys in Borate Buffer Solution at pH 9.2, *J. Electrochem. Soc.*, 150 (2003) 517-526
- [25] Z. Avramović, M. Antonijević, Corrosion of Cold-Deformed Brass in Acid Sulfate Solution, *Corrosion Science*, 46 (2004) 2793-2802
- [26] R. Heidersbach, E. Verink, The Dezincification of Alpha and Beta Brasses, *Corrosion*, 28, 11 (1972) 397-418
- [27] A. Beccaria, E. Mor, G. Poggi, F. Mazza, A Study of the Corrosion Products of Al-Brass Formed in Sodium Sulfate Solution in the Presence of Chloride, *Corrosion Science*, 27, 4 (1987) 363-376
- [28] S. Torchio, The Stress Corrosion Cracking of Admiralty Brass in Sulfate Solutions, *Corrosion Science*, 26, 2 (1986) 133-141
- [29] T. Hoar, C. Booker, The Electrochemistry of the Stress Corrosion Cracking of Alpha Brass, *Corrosion Science*, 5 (1965) 821-829
- [30] Lj. Krstulović, B. Kulušić, Corrosion Processes of α -Brass in Sodium Chloride Solution and Seawater, *Chemical Industry*, 45, 5 (1996) 177-186

Ivan Stojičić^{*1}, Miljan Gomilanić^{*2}, Daniel Kržanović^{*3},
Stefan Milanović^{*4}, Tanja Stanković^{*5}

SELECTION OF THE OPTIMAL FEEDING VARIANT FOR HAMMER CRUSHERS IN ORDER TO ACHIEVE THE DESIGNED PARAMETERS OF CRUSHED COAL ***

Orcid: 1) <https://orcid.org/0009-0005-0571-1172> ; 2) <https://orcid.org/0000-0002-1209-7423> ;
3) <https://orcid.org/0000-0003-3841-8667> ; 4) <https://orcid.org/0000-0003-4761-8716> ;
5) <https://orcid.org/0000-0002-2714-7016>

Abstract

The process of coal crushing for the Kostolac "B" Thermal Power Plant is carried out at the "Drmno" crushing plant using two hammer crushers of Czechoslovak production (PSP Engineering a.s. Prerov), type KDV 1137, with a nominal capacity of 1350 t/h, an electric motor power of 1000 kW, and a rotational speed of $n = 593 \text{ min}^{-1}$ (the circumferential-peripheral speed of the hammers is approximately 49 m/s).

This type of crusher requires a specific feeding regime, meaning that the material must be delivered to a designated space between the impact rollers and the rotor. Additionally, the height from which the material falls into the crusher is limited to 2.2 times the rotor diameter. It is crucial that the feeding speed of the crusher remains below 2 m/s and that the material falls precisely into the designated crushing zone.

This study examines the selection of the optimal variant for uniform crusher feeding to reduce the uneven wear of the hammers.

Keywords: Coal, hammer crushers, crushing, thermal power plant

1 INTRODUCTION

The capacity of the "Drmno" open-pit mine is 9,000,000 tons per year of raw coal, and the distribution of this coal to the thermal power plants "A" and "B" is shown in Table 1.

From the data presented in Table 1, it can be concluded that achieving the annual

capacity of 6,300,000 tons of raw coal for the needs of Thermal Power Plant Kostolac "B" is enabled by operating two crushers with a capacity of 1,200 t/h, which corresponds to approximately 2,625 hours per year of effective operation of the Drmno crushing plant. [1]

* Mining and Metallurgy Institute Bor, Alberta Ajnštajna 1, 19210 Bor, Serbia,
E-mail: ivan.stojicic@irnbob.co.rs

** Faculty of Mining and Geology, University of Belgrade, Dušina 7, 11120 Belgrade, Serbia

*** The authors would like to thank Electric Power Industry of Serbia A.D. – Branch "Thermal Power Plants and Mines Kostolac", Open-Pit Mine "Drmno". This work was financially supported by the Ministry of Science, Technological Development and Innovation of the Republic of Serbia, Contract No. 451-03-136/2025-03/200052.

Table 1 Capacities of crushers and thermal power plants Kostolac A and B

Parameter	Thermal Power Plant „Kostolac B”	Thermal Power Plant „Kostolac A”
Annual Capacity (tons / year)	6.300.000	2.700.000
Working time	300 days x 3 shifts / day = 900 shifts / year	
Tons per day	21000	9000
Tons per shift	7000	3000
Average hourly capacity (tons/hour)	2400	1000
Effective working time	2625 h/y	2700 h/y
Maximum capacity (tons/hour)	2700 t/h	1200 t/h

This means that the crushers can occasionally operate with a capacity lower than the average, which is 1,200 t/h per crusher, and even as low as 1,000 t/h. With a combined capacity of 2,000 t/h (2 x 1,000 t/h), the required annual operating time for the Drmno crushing plant is 3,150 hours.

The increase in the capacity of the "Drmno" open-pit mine to 12,000,000 tons per year will be achieved through a new crushing line that is currently under construction. The bulk density of raw coal varies, depending on particle size and quality, within the range of 0.65 to 0.9 t/m³. [2] For calculation purposes, a value of 0.76 t/m³ has been adopted. For raw coal from the "Drmno" open-pit mine, a natural angle of repose of 38° has been adopted.

The operation of the crushing plant can be evaluated based on the fulfillment of requirements for the desired granulometric composition, i.e., the appropriate particle size of crushed coal. There are two primary requirements regarding the granulometric composition of the crushed product:

*Crushed coal 100% –50 mm, with the content of the –30+0 mm size class in the crushed coal being at least 85%, and the content of the –50+30 mm size class being a maximum of 15%.

*Requirement by A. Mazurkiewicz (Furnace and Boiler Designer from Poland): Crushed coal should have a particle size of

100% –60 mm, with the content of the –40+0 mm size class being at least 95%, and the content of the –60+40 mm size class being a maximum of 5%. [3]

To achieve the designed granulometric composition, according to the equipment manufacturer's requirements [4,5] and the technical manual for this crusher, the following conditions must be met:

- According to the manufacturer's specifications, the maximum input coal size must be 800 mm, or the volume of individual pieces must be less than 0.1 m³. However, the technical manual for this crusher specifies a maximum input coal size of –450 mm.
- Feeding must be continuous, with a coal flow speed of a maximum of 2 m/s, distributed evenly across the entire rotor width, entering the feeding zone which ranges from 20 to 40° (45°) in the direction of rotor rotation with hammers.
- The feeding capacity should range between 1250 and 1450 t/h. Within this capacity range, the electric motor current drawn by the crusher should be between 90 and 110 A.
- During crusher operation, the gap, which is adjusted by moving the third impact roller, should be regulated according to the degree of hammer wear.

2 COAL CRUSHING PROCESS FOR THERMAL POWER PLANT “KOS-TOLAC B”

All the coal arriving at the Drmno crushing plant is directed for crushing via chute S1. In the case of separating large coal pieces, only the oversize from the cylindrical sizing screens R3 and R4, installed above the belt feeders, is processed.

If all the coal arriving at the Drmno crushing plant is to be crushed, then after chute S1, the coal gravitationally falls onto chute S2, which evenly splits the coal stream into two halves and directs it onto belt feeders TR6 and TR7. Belt TR6 feeds coal into hammer crusher D1, while belt TR7 feeds coal into hammer crusher D3.

The original design planned for the installation of three hammer crushers: D1, D2, and D3. The function of the belt feeders TR6 and TR7 was to supply all three crushers, which was made possible through the reversible operation of the conveyors. The expected particle size after crushing was approximately 85% –30 mm.

Hammer crusher D2 was dismantled due to problems that occurred with feeding the crushers, as the installed feeders TR6 and TR7 did not provide an optimal material entry trajectory into the crushers.

Table 2 *Technical characteristics of crushers D1 and D3*

Crushers D1 and D3	
Number of crushers	N = 2
Rotor diameter	D = 1600 mm
Rotor width	B = 2200 mm
Rotor speed	n = 600 o/min
Maximum input size	U _{max} = 800 mm
Output particle size	I = 0 – 40 mm
Motor power	P = 1000 kW
Capacity	Q = 1350 t/h

The total number of hammers on the crusher is 104 (Figure 1), which are arranged in 8 rows with 13 hammers each. The crusher housing does not have a grate,

and the particle size of the output product is regulated by adjusting the distance between the hammers and the impact rollers.



Figure 1 *Arrangement of hammers on the crusher shaft [1]*

The crushed coal is collected on conveyor belt TR10 and then, via a system of belt conveyors, it is deposited onto one of the crushed coal stockpiles (A, B, C, and D) located in front of Thermal Power Plant

Kostolac “B”, or it is directly transported to the bunkers of blocks B1 and B2 of the power plant, without intermediate storage.

Figure 2 shows the feeding zone of crushers KDV1137.

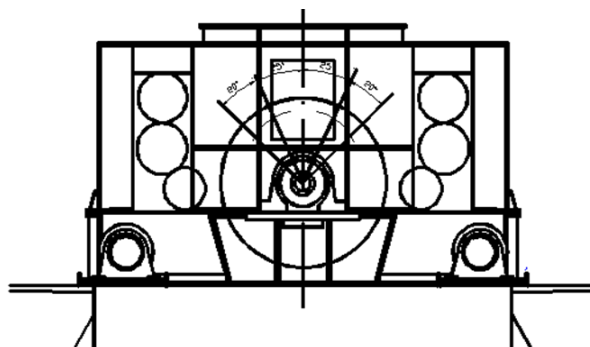


Figure 2 Hammer crusher KDV1137

The crushers are mounted on appropriate reinforced concrete foundations. Feeding of the crushers is performed using belt feeders TR6 and TR7, which handle raw coal with a particle size of $-400 (1000)+0$ mm directly from conveyor belt TR0 (via chutes S1 and S2, or from the oversize of screens R3 and R4, with a particle size of $-150+0$ mm).

The adjustment of the gap between the lower impact roller and the hammers on the rotor is performed depending on the degree of hammer wear. The method of hammer attachment allows them to be rotated after

wear, which enables better utilization of the hammers.

Figures 3 and 4 show photographs of the shaft with hammers and the lower impact roller, where the side walls of the discharge opening are visible. These walls are inclined inward, which is contrary to the manufacturer's recommendations.

The discharge opening of the crusher must have vertical side walls, perpendicular to the rotor axis, while the walls parallel to the rotor must be angled at 30° (inverted funnel).



Figure 3 and Figure 4 Shaft with hammers and lower impact roller [1]

Figure 5 shows the granulometric composition (% – mm) of raw coal and figure 6 shows granulometric composition

(% – mm) of crushed coal from open-pit mine "Drmno".

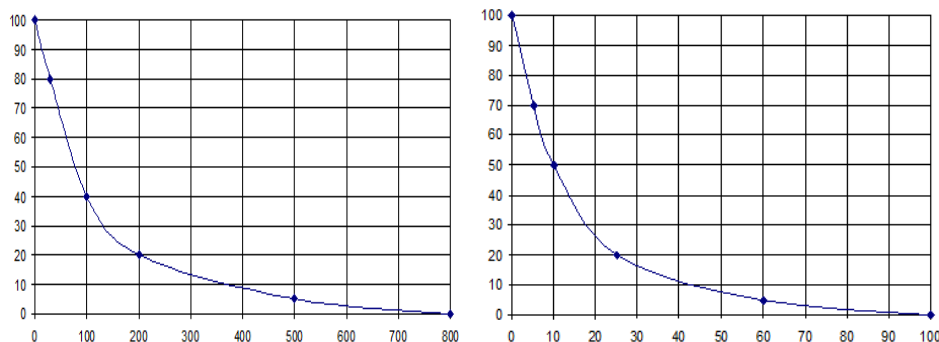


Figure 5 and Figure 6 Granulometric composition (% - mm) of coal from open-pit mine "Drmno" [2]

Periodic monitoring of the condition and operation of the crushing plant revealed the following:

- Feeding of the crushing plant is continuous, with capacity control in place.
- Coal pieces up to approximately 1000 mm in size are entering the crushers.
- Coal moisture content remained within a consistent range of about $40\% \pm 2.3\%$.
- The speed of the belt feeder feeding the crusher is below 2 m/s, thus satisfying the requirement for continuous feeding.
- The width of the belt feeder, $B = 2000$ mm, is slightly larger than the crusher's inlet opening, which is $B = 1900$ mm.
- The belt feeder has a trough-shaped cross-section, which means the material is unevenly distributed, with the thickness of the coal layer being greatest at the center of the cross-section.
- The impact plate, which is designed to direct material into the crushing zone, is positioned so that its center, where the material from the conveyor belt

primarily strikes, is located approximately 0.5 m from the vertical axis of the rotor and is installed at a height of over 2 m.

- The hammers wear unevenly and irregularly, with faster and more significant wear occurring at the center, which prevents proper adjustment of the lower impact roller. The particle size of the crushed coal depends on the degree of hammer wear, although this dependency cannot be clearly identified from the analysis of granulometric composition. A greater impact on the particle size of the crushed coal comes from the uneven hammer wear across the width of the shaft and the inability to properly adjust the gap between the hammers and the lower impact roller.

The general conclusion, considering both crushers in the Drmno crushing plant (D1 and D3), is that the hammers wear unevenly, specifically, they wear much faster in the middle of the shaft than at the ends. This results in difficulty adjusting the gap of the crusher's discharge opening.

The manner in which the hammers are mounted on the shaft attached on one side to a disc and on the other side to a sleeve also contributes to greater wear on the side facing the disc. After a certain period, the discharge opening can no longer be properly adjusted, which leads to a particle size that is larger than the designed specification.

This uneven hammer wear is primarily due to:

Uneven feeding of the crusher across the width of the rotor, and the type of material used for manufacturing the hammers.

The gap between the rotor and the lower impact roller is adjusted in steps, specifically in four steps of 20 mm each. In an ideal case, with uniform hammer wear, the gap would, through natural wear of the crushing bodies, range between 40 and 60 mm. After this, a new adjustment would reduce the gap to 40 mm. However, the mere increase of the gap over time indicates that it is impossible to continuously maintain the desired particle size of the crushed coal. Due to uneven hammer wear, the gap adjustment is made according to the longest hammers, i.e., the least worn hammers, which are located at the ends of the shaft. As a result, in the central crushing zone, the gaps cannot be adjusted to the appropriate size.

In that area, the hammers have reduced mass, which decreases their crushing potential. The larger gap and reduced hammer mass result in coarser crushed coal.

3 ALTERNATIVE SOLUTIONS FOR CRUSHER FEEDING

After analyzing the current state of coal crushing and the feeding of hammer crushers in the Drmno crushing plant, three

main new feeding solutions are proposed for consideration to achieve the designed particle size parameters of crushed coal, i.e., 15% –60+30 mm and 85% –30 mm:

1. Reconstruction of existing belt feeders, by reducing speed and increasing the coal layer height on the feeder, with adjustment of the entry trajectory into the crusher.
2. Replacement of existing belt feeders with chain scrapers.
3. Replacement of existing belt feeders TR6 and TR7 with plate feeders.

All three proposed solutions are feasible, each with its own advantages and disadvantages. This paper presents the basics of all three proposed solutions and the selection of the most optimal variant, which will be further developed by the equipment supplier in collaboration with the investor.

3.1. Reconstruction of existing belt feeders by reducing speed and increasing coal layer height on the feeder with adjustment of entry trajectory into the crusher

This solution involves replacing the existing belt feeders and acquiring new ones, with a flat profile rather than a trough profile, using more durable rubber and closely spaced rollers beneath the belt. The drive motor would be equipped with a frequency regulator to control the rotation speed, thus adjusting the belt speed. The belt speed would be significantly reduced, thereby increasing the coal layer height on the belt.

Figure 7 shows the appearance and capacity calculation of a belt feeder with a width of 2000 mm.


SELECTION AND CALCULATION OF BELT FEEDER					
					
Type of feeder	Belt feeder				
Feeder manufacturer	As per investor's choice				
Feeder width	B = 2000 mm				
Effective feeder width	B _{ef} = 1850 mm				
Coal layer height	H = 1200 mm				
Bulk density of coal	0,85 t/m ³				
Coal particle size	from + 0 to – 400 mm				
Feeder speed	12 m/min				
Feeder capacity	$Q = 60 \times 1,85 \times 1,2 \times 12 \times 0,85 \times 0,8 = 1086,9 \text{ t/h}$				
V [m/min]	5	10	12	14	15
V [m/s]	0,083	0,167	0,200	0,233	0,250
Q [t/h]	453	905,8	1086,9	1268,1	1358,6

Figure 7 Appearance and capacity calculation of a belt feeder

This requires reconstruction of the chute and checking the load-bearing capacity of the structural construction, due to the increased load, mainly caused by the coal layer on the feeders.

The belt feeder would be equipped with scrapers for the return side of the feeder belt.

By installing these feeders, the mass would increase due to the volume of coal above the belt by approximately 10 tons per feeder, plus an increase due to the expanded volume of the chute above the belt feeder. As seen from the calculations, a range of belt speeds has been adopted for a capacity of up to 1350 t/h, but the optimal capacity is set at 1000 t/h per crusher. This is done to ensure that the particle size of the crushed

coal is as close as possible to the designed specifications. The adopted capacity allows the processing of 6,300,000 tons per year over approximately 3150 hours of effective operation per year, which can be considered a very acceptable load for the equipment in the crushing plant.

3.2. Replacement of belt feeders with chain scrapers

Chain scrapers are of similar construction to the scrapers used in the reserve reception bunkers. They are characterized by a high material layer and low coal feeding speed. This solution involves the complete replacement of the existing belt feeders with chain feeders.

Figure 8 shows the appearance of the chain feeder and an approximate calculation of feeding capacity, which demonstrates that with a chain speed of 11 m/s and a

coal layer height of approximately 1.6 m, the desired capacity of around 1000 t/h is achieved.


SELECTION AND CALCULATION OF CHAIN FEEDER					
					
Type of feeder			Chain feeder		
Feeder manufacturer			As per investor's choice		
Feeder width			B = 2000 mm		
Effective feeder width			Bef = 1850 mm		
Coal layer height			H = 1600 mm		
Bulk density of coal			0,85 t/m3		
Coal particle size			od + 0 do – 400 mm		
Feeder speed			12 m/min		
Feeder capacity		$Q = 60 \times 1,85 \times 1,6 \times 12 \times 0,85 \times 0,6 = 1086,9 \text{ t/h}$			
V [m/min]	8	9	10	11	12
V [m/s]	0,133	0,150	0,167	0,183	0,200
Q [t/h]	724,6	815,2	905,8	996,3	1086,9

Figure 8 Appearance and capacity calculation of chain scraper

In this variant, in addition to the mass of the chain feeders, the mass of coal on the feeder also increases, which amounts to approximately 15 tons, plus an increase in the mass of the chute, whose side walls must correspond to the increased height of coal being fed into the crushers.

3.3. Replacement of belt feeders with apron feeders

As the third solution, the replacement of the existing belt feeders with plate feeders

was considered. The reason for this solution is the significant drop height of coal from chute S1 onto the feeders, and in this regard, the plates of the feeder provide the highest level of safety for operation. This machine also has disadvantages, including its significant weight and the necessity of installing cleaning devices beneath the return side of the feeder plates. Figure 9 shows the calculation of the apron feeder for the required capacity of 1000 t/h.


SELECTION AND CALCULATION OF PLATE FEEDER					
					
Type of feeder			Apron feeder		
Feeder manufacturer			As per investor's choice		
Feeder width			B = 2100 mm		
Effective feeder width			Bef = 2000 mm		
Coal layer height			H = 1100 mm		
Bulk density of coal			0,85 t/m ³		
Coal particle size			od + 0 do – 1000 mm		
Feeder speed			12 m/min		
Feeder capacity		$Q = 60 \times 2 \times 1,1 \times 12 \times 0,85 \times 0,8 = 1077,1 \text{ t/h}$			
V [m/min]	6	9	10	12	15
V [m/s]	0,100	0,150	0,167	0,200	0,250
Q [t/h]	538,6	807,8	897,6	1077,1	1346,4

Figure 9 Appearance and capacity calculation of plate feeder

4 SELECTION OF A NEW CRUSHER FEEDING SOLUTION

A brief comparative analysis of the proposed solutions revealed the following:

1. The proposed belt feeder has the disadvantage of receiving coal from a great height (chutes S1 and S2), which increases the risk of damage to the rubber belt. The return side of the belt is cleaned using scrapers.
2. The proposed chain feeder has an inconsistent coal height and requires a large height of about 1.6 m. There is not enough space for that height, and the discontinuity of the coal height entering the crusher is not favorable. The return side of the
3. feeder is cleaned by an additional scraper with a single plate on the underside.
4. The proposed plate feeders, despite having increased weight compared to the previous two solutions, offer an advantage due to the robustness of the machine. They maintain a continuous height that is adjusted and regulated by speed, allowing the feeding capacity to be kept constant. They have a low input speed of material into the central crushing zone, and they maintain a uniform height across their entire width, making

it realistic to expect uniform hammer wear in the crusher. The plate feeder requires the installation of a chain feeder for cleaning the return side of the plates.

After analyzing all three described proposals and consulting with the Investor, the decision was made to replace the existing belts TR6 and TR7 with appropriate plate feeders, which are robust and can meet the conditions for receiving coal through chutes S1 and S2, as well as enabling smooth feeding of the crushers into the center of the crushing area.

5 PRESENTATION OF THE NEW CRUSHER FEEDING SOLUTION

After replacing the existing belt feeders with new plate feeders, the designed parameters of the crushed coal were achieved. The new solution ensured even

feeding of crushers D1 and D3, resulting in uniform hammer wear [3].

With uniform hammer wear, it became possible to adjust the gap using the impact roller, which increased the service life of the hammers and reduced the number of hammer replacements on an annual basis.

Before the reconstruction, hammers were replaced two or three times per year, depending on the quality of the material. After the reconstruction, hammer replacement is performed during the planned maintenance of the crushing plant.

In addition to uniform hammer wear and extended hammer life, proper material delivery to the crushing zone was achieved, fulfilling the required parameters of the crushed coal.

Figures 10 and 11 show the new apron feeders PD6 and PD7 installed at the Drmno crushing plant during the trial operation and capacity verification phase.



Figure 10 Apron feeder PD6 [3]



Figure 11 Apron feeder PD7 [3]

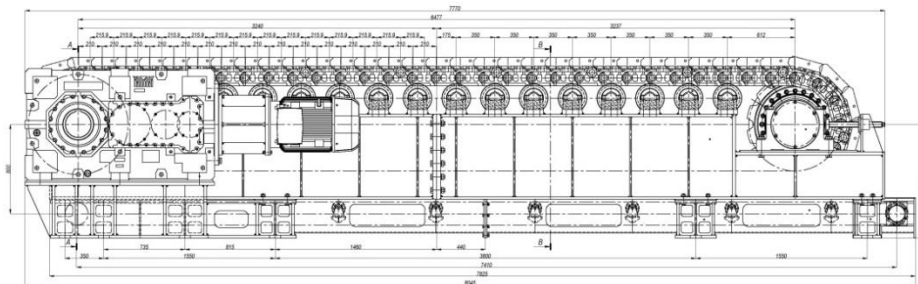


Figure 12 Apron feeder PD6/7 [3]

6 CONCLUSION

This paper presents the selection of the crusher feeding method aimed at achieving uniform hammer wear and the designed parameters of crushed coal.

First, a description of the existing state was provided, highlighting the issue of uneven hammer wear, which results in the inability to adjust the gap in the crusher. As

a consequence, it is impossible to achieve the designed parameters of the crushed coal.

The process of forming alternative solutions was presented, along with an analysis and evaluation of each variant.

Finally, the most optimal variant was selected, and a brief description of the state after installation was provided.

REFERENCES

- [1] I. Stojičić, M. Gomilanović, D. Kržanović, Technical Mining Project for the Reconstruction of the Feeding System of Existing Crushers at the Drmno Open-Pit Mine to Achieve the Designed Parameters of Crushed Coal – Technological and Mechanical Project.
- [2] Laboratory analysis of coal, Mining Institute Belgrade.
- [3] I. Stojičić, Technical Documentation of Plate Feeders, Technical Instructions, and Photographs from Assembly and Commissioning, Mining and Metallurgy Institute Bor, 2025.
- [4] B. Rajković, Z. Ilić, R. Rajković, Driving power verification of the apron feeder for ore transportation, Mining and Metallurgy Engineering Bor, 1-2 (2017) 63-70.
- [5] S. Tošić, Calculation of Continuous Transportation Appliances and Lifting Devices, Faculty of Mechanical Engineering Belgrade, 1994 (in Serbian).

*Dejan Bugarin^{*1}, Ivan Stojičić^{*2}, Igor Svrkota^{*3},
Miljan Gomilanović^{*4}, Miloš Stojanović^{*5}*

DETERMINATION OF OPERATING AND MAINTENANCE COSTS OF TRANSPORT EQUIPMENT IN THE DEVELOPMENT OF EXPLORATORY MINE WORKINGS IN A LEAD AND ZINC MINE^{**}

Orcid: 1) <https://orcid.org/0000-0002-9103-4614>; 2) <https://orcid.org/0009-0005-0571-1172>;
3) <https://orcid.org/0000-0002-3779-6327>; 4) <https://orcid.org/0000-0002-1209-7423>;
5) <https://orcid.org/0000-0003-0044-5491>

Abstract

This paper examines the costs of mechanized transport used in the construction of exploratory underground corridors over a three-year period. During the execution of the works, data were collected on fuel consumption and spare parts required for the uninterrupted operation of the machinery. Based on the analysis of the collected data on machinery operation, direct dependencies were established between the monthly length of the constructed underground corridors and the operational costs of machinery operation and maintenance for material transport.

Keywords – Underground corridor construction, Machinery operating costs, Maintenance

1 INTRODUCTION

Based on the positive results of geological exploration conducted through exploratory drilling, four prospective zones have been identified where further geological investigations [1] and the development of corresponding exploratory mine workings are required, with the aim of defining the boundaries of ore bodies.

Ore extraction is carried out from a polymetallic deposit composed of a large number of ore bodies (more than 90),

which, according to current findings, extend over an area approximately 3 [km] in length and more than 1.5 [km] in width. The general strike direction of the deposit is NW–SE.

Table 1 presents the basic physical and mechanical properties of the ores and the surrounding rocks of the ore bodies within the polymetallic deposit. It can be concluded that the geological environment is favorable for conducting exploratory, preparatory, and later exploitation works.

^{*} Mining and Metallurgy Institute Bor, Alberta Ajnštajna 1, 19210 Bor, Serbia,
E-mail: dejan.bugarin@irmbor.co.rs

^{**} This work was financially supported by the Ministry of Science, Technological Development and Innovation of the Republic of Serbia, Contract No. 451-03-136/2025-03/200052.

Table 1 Characteristics of ores and associated rocks in the deposit

Parametar	Sand stone	Skarn	Dacite	Lime stone	Breccia	Shale Marl	Kaolin	Lead-Zinc
Density [g/cm ³]	2,86	3,17	2,71	2,90	3,01	2,88	3,00	3,52
Bulk Density [g/cm ³]	2,71	2,94	2,59	2,75	2,81	2,72	2,87	3,33
Porosity [%]	5,06	6,83	4,51	5,26	6,67	5,56		6,23
Compressive Strength [MPa]	99,43	78,85	89,67	80,31	54,51	18,57	23,95	85,47
Tensile Strength [MPa]	10,83	8,44	10,21	7,17	7,20	2,02	5,00	11,04
Internal Friction Angle [°]	51,94	51,94	49,88	55,26	47,73	52,55	41,33	45,56
Elastic Modulus [GPa]	55,73	54,59	38,56	42,86	27,63		4,67	46,75
Seismic Wave Velocity [km/s]	5,11	5,16	5,29	5,02		2,54	4,55	4,59
Relative Humidity [%]	0,58	0,66	0,64	0,67				0,77
Poisson's Ratio	0,17	0,25	0,18	0,19	0,25			0,25
Cohesion [dN/cm ²]	199,7	157,1	106,9	152,3	170,3			193,4
Strength (Protodyakonov) Coefficient	9,94	7,88	8,70	8,03	5,45	1,86	2,40	8,55

The favorable geomechanical properties of the rock masses within the deposit are particularly evident during the excavation of horizontal, inclined, and vertical mine workings, as these typically do not require support, except in fault zones.

2 TECHNICAL DESCRIPTION OF EXPLORATORY DRIFTS

The elevation of 515 meters has been determined as the optimal level for driving

the drift from which all further geological exploration of the identified prospective zones will be conducted. This elevation simultaneously satisfies the positioning requirements for exploratory drilling in all zones and falls within the potential development range of a future mining level at –200 meters, given that it is located approximately 60 meters below the current lowest level at –150 meters. The plan includes the construction of four types of cross-sections of exploratory mine workings, namely:

- Type 1:** Profile 3.0×2.0[m], unsupported, $F_s = 7.05 \text{ [m}^2\text{]}$
- Type 2:** Profile 2.0×2.0[m], unsupported, $F_s = 4.00 \text{ [m}^2\text{]}$
- Type 3:** Profile 4.0×3.5[m], unsupported, $F_s = 12.84 \text{ [m}^2\text{]}$
- Type 4:** Profile 4.0×3.5[m], with steel support, $F_s = 12.84 \text{ [m}^2\text{]}$

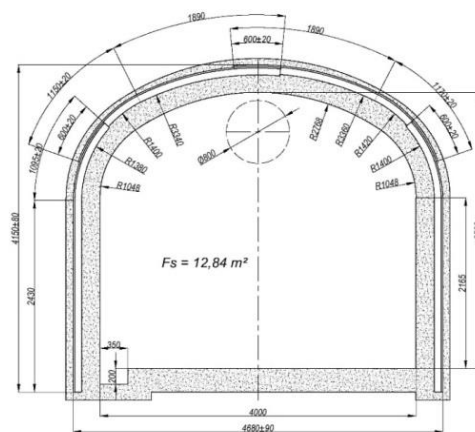


Figure 1 Profile 4.0×3.5[m], with steel support

Main Exploratory Decline GIN 200

The entry portal to the main exploratory decline GIN 200 is located on the plateau of the existing haulage adit at the -150 [m] level, for the following reasons:

- The plateau is equipped with complete infrastructure;
- A waste rock dump has already been formed, suitable for depositing material excavated during the development of exploratory workings;
- This location provides access approximately to the central part of the ore-bearing structure, which is highly favorable from the standpoint of future exploitation.

The main exploratory decline GIN 200 is a gently inclined underground opening intended to connect the surface with the exploratory drifts. It will serve for transporting the material excavated from the exploratory workings, personnel access, as well as the delivery of supplies and energy. Additionally, it will be used for workplace ventilation.

From the portal, GIN 200 proceeds horizontally for 15.0 [m], then continues for 430 [m] at a 10% decline down to an elevation of 513.0 [m]. From there, it advances sub-horizontally (with an upward gradient of 3.1%) for 630.1 [m] until it connects with the GIH 200/NW and GIH 200/SE drifts. The connection is made through two curves with a radius of 20.0 [m]. The total length of the main exploratory decline GIN 200, including the curves, is 1111.1 [m].

The cross-sectional dimensions were selected based on the size of the equipment used for drift development (drill rigs, loaders), and the clearance required for the mine truck planned for future ore and waste haulage. Consideration was also given to the positioning of ventilation ducts with a diameter of 800 mm during the decline development.

The cross-sectional area of the decline (without support) is $F_s = 12.84$ [m²]. The same clear area is maintained when using a four-piece steel arch support system, as

well as in the section supported with concrete lining.

Regarding ground support, based on data obtained from the technical borehole, it is estimated that the first 50 meters will be supported with concrete lining. It is also anticipated that approximately 20% of the total decline length (around 210 meters) will require steel arch supports. Along the entire section of the decline with a 10% gradient ($430 + 15 = 445$ meters), a 25 [cm] thick reinforced concrete floor slab will be installed, which will improve transport efficiency and reduce the operational costs of haulage.

Main Exploratory Drift GIH 200/NW

From its junction with the main exploratory decline GIN 200, this drift extends in a northwestern direction. The total length of the drift is 1707.3 meters, and it is being driven with an upward gradient of 3.51% .

The cross-sectional area of the drift (without support) is $F_s = 12.84$ [m²]. The same clear area is maintained when supported with a four-piece steel arch support system. The drift is largely unsupported.

Main Exploratory Drift GIH 200/SE

From its junction with the main exploratory decline GIN 200, this drift extends in a southeastern direction. The total length of the drift is 847.0 meters, and it is being driven with an upward gradient of 3.54% .

The cross-sectional area of the drift (without support) is $F_s = 12.84$ [m²]. The same clear area is maintained when supported with a four-piece steel arch support system. The drift is largely unsupported.

Excavation Technology of the Workings

The excavation of the aforementioned underground workings does not involve any particular specificities and does not differ from the standard procedures used in the development of production mine workings.

3 OVERVIEW OF DEPLOYED MACHINERY

The technological process of excavation consists of the following operational steps:

- Drilling of blast holes
- Charging and blasting
- Ventilation
- Loading and haulage of blasted material
- Ground support installation
- Drainage and auxiliary operations

An overview of the machinery used in the excavation of underground exploratory drifts is presented in Table 2. The overview includes equipment utilized for drilling, loading, and material transport operations [2].

Table 2 Overview of machinery used for operations execution

No.	Name	Type	Operating Period
1	Loader	GHH LF 4.1	X. 2019 – IV. 2021
2	Loader	GHH LF 4.1	X. 2019 – IV. 2021
3	Loader	GHH LF 6F	VI. 2020 – VIII. 2023
4	Loader	Atlas Copco ST3.5	III. 2021 – VIII. 2023
5	Drilling Rig	Tamrock HS105D	III. 2021 – VIII. 2023
6	Mine Truck	Aramine T1601C	V. 2021 – VIII. 2023

The objective of this study is to analyze the operational costs of operating and maintaining the machinery used for material transport and haulage from the mine.

Therefore, the data presented below refer specifically to the underground mine truck T1601C.

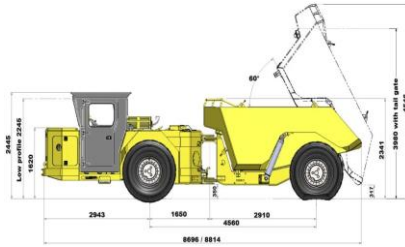
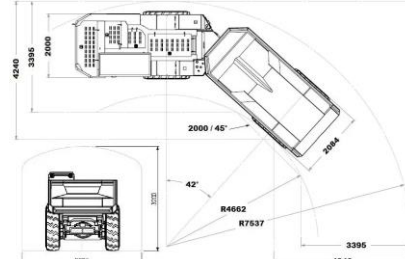
WORKING DIMENSIONS, MOVEMENT GEOMETRY, WORKING PERFORMANCE AND EQUIPMENT OF TRUCK T1601C								
DIMENSIONS		OPERAT. WEIGHTS	EMPTY	ALLOWED WEIGHT OF TRANSPORTED	MAXIMUM ALLOWED WEIGHT OF			
			17000 kg	15000 kg	17000 kg			
		CAPACITY	MAXIMUM LOADING CAPACITY	LOADING CAPACITY UP TO THE EDGE OF THE BED	LOADING CAPACITY WITH INCREASED BED			
			7,5 m³	6,7 m³	7,5 - 9,5 m³			
MOVEMENT GEOMETRY		DIESEL ENGINE	ENGINE MANUFACTURE	CUMMINS				
			MODEL / CODE	QSB6.7 WITH OIL COOLING				
			POWER	164kW				
			MAXIMUM TORQUE	959 Nm pri 1500 o/min				
		TIRES	14" R24	OPTIONALLY, 16" R25 TIRES CAN BE INSTALLED				
		TANK VOLUME	FUEL TANK	HYDRAULIC OIL TANK				
			220 liters	210 liters				
		DRIVING STABILITY CONDITIONS	MAX. MOVEMENT ANGLE	10° FOR A LOADED TRUCK WITH LOWERED BED				
			MAXIMUM SPEEDS ON INCLINE [km/h]	0%	10%	15%	20%	
			WHILE MOVING UNDER LOAD	20	9	7,5	4,5	
			WHILE MOVING WITHOUT LOAD	20	16	9	4,5	

Figure 2 Technical Specifications and Performance of the T1601C Truck

4 DATA ANALYSIS ON EXECUTION AND CONSUMPTION

The transport cycle includes loading, hauling the material to the dumping point, unloading, and returning to the loading point. The number of transport cycles completed within a given time period represents the only direct link between the realized work (i.e., the number of meters of mine workings excavated) and the incurred costs, since fuel consumption, lubricants, tire wear, truck depreciation, and similar expenses are determined based on the number of cycles.

In this case, the determination of transport cycles was carried out based on a detailed monthly specification of the constructed mine

workings. All the workings were developed with the same nominal profile of 4.0×3.5 meters, and therefore share the same clear cross-sectional area. This uniformity simplified the process, as it allowed for the summation of total lengths excavated each month to generate input data for calculating the number of transport cycles.

Based on the monthly excavation lengths and the cross-sectional area of the workings, the monthly volume of material requiring transportation and haulage to the surface was determined. The data specifying the executed work by working type on a monthly basis are presented in Table 3.

Table 3 Specification of executed works on a monthly basis

SPECIFICATION OF EXECUTED WORKS ON A MONTHLY BASIS															
Year	Month	Portal	GIN 200	GVS 1/N	RGVS 2/N	TS GIN 200	UK 1 DK 1 DK 2	SIH 0	SIH 1	SIH 2	GIH 200 SZ	TS 200SZ	VH 200	GIH 200 JI	Total per month [m]
2019	XI	7,00													
	XII	8,00													
2020	I		17,60												17,60
	II		25,58												25,58
	III		28,75												28,75
	IV		24,40												24,40
	V		22,34												22,34
	VI		37,10												37,10
	VII		34,31												34,31
	VIII		44,29												44,29
	IX		44,26												44,26
	X		61,73												61,73
	XI		53,14												53,14
	XII		41,24												41,24
2021	I		53,35												53,35
	II		63,01	18,10											81,11
	III		101,80	2,12											103,92
	IV		116,70		14,70		10,30								141,70
	V		129,80			9,40	12,80								152,00
	VI		99,40												99,40
	VII		102,90				13,50								116,40
	VIII											14,30		6,10	122,50
	IX											50,00		75,20	125,20
	X											84,20		79,90	164,10
	XI											49,00		81,00	130,00
	XII													38,50	38,50
2022	I								30,70	18,70					49,40
	II								77,30	23,00					100,30
	III								81,30	59,50					140,80
	IV									33,60					33,60
	V		27,70												27,70
	VI														
	VII														
	VIII						42,60				61,40				104,00
	IX						49,40				58,00				107,40
	X						62,20				34,90				97,10
	XI						3,70				77,40	16,90			98,00
	XII										35,60	42,40	6,80		84,80
2023	I										28,70	51,20	3,70		83,60
	II										19,40	42,30			61,70
	III											57,20			57,20
	IV											49,80			49,80
	V											48,90			48,90
	VI											96,30			96,30
	VII											20,30	30,90		51,20
	VIII											59,70			59,70
	IX											59,60			59,60
	X														
	XI														
	XII														
TOTAL			1.139,40	20,22	14,70	9,40	36,60	157,90	189,30	295,90	906,40	10,50	30,90	620,90	

The truck capacity was determined based on the allowable payload defined by the manufacturer, taking into account that the average bulk density of the transported material is 2.85 [g/cm³]. With this value and considering the loading capacity limit of 15,000 [kg], the truck loading capacity is calculated to be 5 [m³]. Based on the defined truck capacity and the previously specified volume of material to be transported, the required number of transport cycles per month is determined.

By defining the number of working days in each month, the monthly number of cycles is converted into the daily number of cycles. Considering the number of shifts, the number of transport cycles performed by the truck during a single shift is obtained. This is a critical piece of data, as it will be used in the following sections to define the number of operating hours and fuel consumption.

At the end of this section, which addresses transport cycles, the length of the transport route per cycle can be defined. For this determination, the input data includes the locations where the material is loaded into the truck. In the specific case analyzed, material loading was conducted either in the loading chamber UK1, located in the main exploratory decline GIN200 at a distance of 330 meters from the beginning of the ramp, or at the loading extension at the end of the main exploratory decline GIN200. Depending on these locations, the transport route length was defined for each possible scenario. The transport distances were further categorized based on the inclination of the drift.

All data calculated and described in the preceding text are presented in Table 4, which provides an overview of the total bulk volume of material for transport, the number of cycles, and transport distances.

Table 4 *Quantity of transported material and number of cycles*

QUANTITY OF TRANSPORTED MATERIAL AND NUMBER OF CYCLES															
Year	Month	Produced meters	Nominal profile (m)	Clear surface area (m²)	Material quantity (m³)	Truck capacity (m³)	Cycles per month	Number of work. days	Number of cycles per day	Number of shifts	Number of cycles per shift	Transport on flat section	Transport on upward incline	Movement outside	Return to loading
2021	V	152.00	4 x 3.5	12.85	1953.20	5.00	391	28	14	2	7	335.00	435.00	200.00	770.00
	VI	99.40	4 x 3.5	12.85	1277.29	5.00	255	28	9	2	5	335.00	435.00	200.00	770.00
	VII	122.50	4 x 3.5	12.85	1574.13	5.00	315	29	11	2	5	335.00	435.00	200.00	770.00
	VIII	158.70	4 x 3.5	12.85	2039.30	5.00	408	30	14	2	7	667.00	435.00	200.00	1102.00
	IX	125.20	4 x 3.5	12.85	1608.82	5.00	322	29	11	2	6	667.00	435.00	200.00	1102.00
	X	164.10	4 x 3.5	12.85	2108.69	5.00	422	30	14	2	7	667.00	435.00	200.00	1102.00
	XI	130.00	4 x 3.5	12.85	1670.50	5.00	334	29	12	2	6	667.00	435.00	200.00	1102.00
	XII	38.50	4 x 3.5	12.85	494.73	5.00	99	22	4	1	4	667.00	435.00	200.00	1102.00
	I	49.40	4 x 3.5	12.85	634.79	5.00	127	22	6	1	6	335.00	435.00	200.00	770.00
	II	100.30	4 x 3.5	12.85	1288.86	5.00	258	27	10	1	10	335.00	435.00	200.00	770.00
	III	140.80	4 x 3.5	12.85	1809.28	5.00	362	31	12	1	12	335.00	435.00	200.00	770.00
	IV	55.60	4 x 3.5	12.85	714.46	5.00	143	30	5	1	5	667.00	435.00	200.00	1102.00
2022	V	105.20	4 x 3.5	12.85	1351.82	5.00	270	29	9	1	9	667.00	435.00	200.00	1102.00
	VI	96.30	4 x 3.5	12.85	1237.46	5.00	247	30	8	1	8	667.00	435.00	200.00	1102.00
	VII	104.00	4 x 3.5	12.85	1336.40	5.00	267	31	9	1	9	667.00	435.00	200.00	1102.00
	VIII	107.40	4 x 3.5	12.85	1380.09	5.00	276	30	9	1	9	667.00	435.00	200.00	1102.00
	IX	97.10	4 x 3.5	12.85	1247.74	5.00	250	30	8	1	8	667.00	435.00	200.00	1102.00
	X	98.00	4 x 3.5	12.85	1259.30	5.00	252	31	8	1	8	667.00	435.00	200.00	1102.00
	XI	84.80	4 x 3.5	12.85	1089.68	5.00	218	30	7	1	7	667.00	435.00	200.00	1102.00
	XII	83.60	4 x 3.5	12.85	1074.26	5.00	215	22	10	1	10	667.00	435.00	200.00	1102.00
	I	61.70	4 x 3.5	12.85	792.85	5.00	159	23	7	1	7	667.00	435.00	200.00	1102.00
	II	57.20	4 x 3.5	12.85	735.02	5.00	147	27	5	1	5	667.00	435.00	200.00	1102.00
	III	49.80	4 x 3.5	12.85	639.93	5.00	128	31	4	1	4	667.00	435.00	200.00	1102.00
	IV	48.90	4 x 3.5	12.85	628.37	5.00	126	30	4	1	4	667.00	435.00	200.00	1102.00
2023	V	96.30	4 x 3.5	12.85	1237.46	5.00	247	30	8	1	8	667.00	435.00	200.00	1102.00
	VI	51.20	4 x 3.5	12.85	657.92	5.00	132	30	4	1	4	667.00	435.00	200.00	1102.00
	VII	59.70	4 x 3.5	12.85	767.15	5.00	153	31	5	1	5	667.00	435.00	200.00	1102.00
	VIII	59.60	4 x 3.5	12.85	765.86	5.00	153	30	5	1	5	667.00	435.00	200.00	1102.00
	IX	59.60	4 x 3.5	12.85	765.86	5.00	153	30	5	1	5	667.00	435.00	200.00	1102.00

The duration of a single transport cycle is determined based on the truck's travel speed across defined transport sections (e.g., flat sections, inclined sections).

According to the technical specifications of the T1601C truck, the maximum permis-

sible travel speeds are provided depending on whether the truck is loaded or empty, and on the gradient of the haul road.

For more detailed analyses of speed and rolling resistance, a traction force diagram (Figure 3) is used, showing the relationship

between tractive force (vertical axis in kN) and distance (horizontal axis in m) [3].

Under realistic loading and haulage conditions, the following travel speeds have been defined:

Loaded truck traveling on flat underground roadway: $v_1 = 7$ [km/h]

Loaded truck ascending a 10% incline underground: $v_2 = 4.5$ [km/h]

Loaded truck traveling on flat surface outside the mine: $v_3 = 8$ [km/h]

Empty truck traveling on flat underground roadway: $v_4 = 8$ [km/h]

Empty truck descending a 10% incline underground: $v_5 = 8$ [km/h]

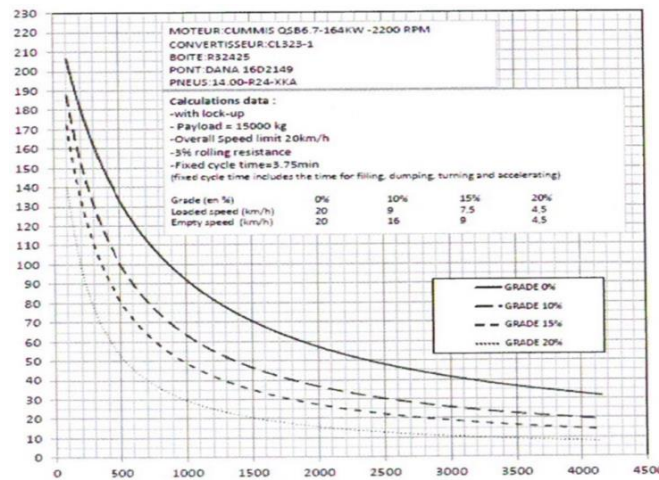


Figure 3 Diagram of the Relationship Between Tractive Force and distance

Depending on the loading location—either at the UK1 loading chamber or at the loading extension at the end of the main exploratory decline GIN200 - there are two distinct transport route lengths, and consequently, two different cycle durations for these characteristic haulage cycles.

Basic formula for calculating the transport cycle time is:

$$T_c = T_L + \frac{L_1}{v_1} + \frac{L_2}{v_2} + \frac{L_3}{v_3} + \frac{L_4}{v_4/5}$$

where are:

T_L – truck loading time [h]

L_1 – distance of transport on flat section [km]

L_2 – distance of transport on upward incline [km]

L_3 – distance of movement outside [km]

L_4 – distance of return to loading [km]

Cycle 1 represents loading at the UK1 loading chamber.

The transport cycle time is calculated as:

$$T_{c1} = 0.15 + (0.335 / 7) + (0.435 / 4.5) + (0.200 / 8) + (0.770 / 8) = 0.416 \text{ [h]} = 25 \text{ [min]}$$

Cycle 2 represents loading at the extension at the end of GIN200.

The transport cycle time is calculated as:

$$T_{c2} = 0.15 + (0.667 / 7) + (0.435 / 4.5) + (0.200 / 8) + (1.102 / 8) = 0.505 \text{ [h]} = 30 \text{ [min]}$$

With the defined transport cycle durations from the previous section, it is possible to determine (or verify from operation

nal records) the total number of truck operating hours on a monthly basis. Additionally, by summing up the transport dis-

tances and the number of cycles, the total distance traveled per month can be calculated. These figures serve as input data for determining the truck's monthly fuel con-

sumption, and subsequently, the average monthly fuel consumption during operational activities. The calculated data are presented in Table 5.

Table 5 Total mileage, operating hours, diesel fuel consumption

TOTAL MILEAGE, OPERATING HOURS, AND DIESEL FUEL CONSUMPTION									
Year	Month	Produced meters [m]	Quantity for export [m³]	Cycles per month	Cycle length [m]	Cycle duration [min]	Total mileage [km]	Operating hours [h]	Diesel fuel consumption [lit]
2021	V	152,00	1953,20	391	1740	25	680,3	162,9	2834
	VI	99,40	1277,29	255	1740	25	443,7	106,3	1848
	VII	122,50	1574,13	315	1740	25	548,1	131,3	2283
	VIII	158,70	2039,30	408	2404	30	980,8	204,0	4086
	IX	125,20	1608,82	322	2404	30	774,1	161,0	3225
	X	164,10	2108,69	422	2404	30	1.014,5	211,0	4226
	XI	130,00	1670,50	334	2404	30	802,9	167,0	3345
2022	XII	38,50	494,73	99	2404	30	238,0	49,5	991
	I	49,40	634,79	127	1740	25	221,0	52,9	921
	II	100,30	1288,86	258	1740	25	448,9	107,5	1870
	III	140,80	1809,28	362	1740	25	629,9	150,8	2624
	IV	55,60	714,46	143	2404	30	343,8	71,5	1432
	V	105,20	1351,82	270	2404	30	649,1	135,0	2704
	VI	96,30	1237,46	247	2404	30	593,8	123,5	2474
	VII	104,00	1336,40	267	2404	30	641,9	133,5	2674
	VIII	107,40	1380,09	276	2404	30	663,5	138,0	2764
	IX	97,10	1247,74	250	2404	30	601,0	125,0	2504
	X	98,00	1259,30	252	2404	30	605,8	126,0	2524
	XI	84,80	1089,68	218	2404	30	524,1	109,0	2183
2023	XII	83,60	1074,26	215	2404	30	516,9	107,5	2153
	I	61,70	792,85	159	2404	30	382,2	79,5	1592
	II	57,20	735,02	147	2404	30	353,4	73,5	1472
	III	49,80	639,93	128	2404	30	307,7	64,0	1282
	IV	48,90	628,37	126	2404	30	302,9	63,0	1262
	V	96,30	1237,46	247	2404	30	593,8	123,5	2474
	VI	51,20	657,92	132	2404	30	317,3	66,0	1322
	VII	59,70	767,15	153	2404	30	367,8	76,5	1532
	VIII	59,60	765,86	153	2404	30	367,8	76,5	1532
AVERAGE							532,7	114,1	2219

Tire consumption is presented in Table 6. Based on available data, tire usage is provided for the T1601C truck as well as for the GHH LF6 and ST3.5D loaders. This was done to ensure that the tire consumption overview can be used for further

analysis of operating costs and other machinery performance.

Table 7. presents the total monthly cost of spare parts required for the maintenance of the truck.

Table 6 Tire consumption

TIRE CONSUMPTION			
Year	Month	14" - T1601C	17,5" - GHH LF6 + ST 3,5
2020	VI - XII		10
2021	I - IV		9
	V - XII	16	18
2022	I - XII	12	13
2023	I - VIII	3	7
IN TOTAL		31	57

Table 7 Spare parts costs for maintenance

SPARE PARTS COSTS FOR MAINTENANCE OF THE T1601C TRUCK						
Number	Name	Code	Replacement period [h]	Monthly quantity	Unit price [€]	Monthly costs [€]
1	Primary air filter	8035212	125	1,00	99,30	99,30
2	Secondary air filter	8035213	250	0,50	85,40	42,70
3	Engine oil filter	8034231	250	0,50	17,00	8,50
4	Engine fuel filter	8034230	250	0,50	14,30	7,15
5	Water separator filter	7796975	250	0,50	29,65	14,83
6	Hydraulic tank filter	7702298	500	0,25	43,85	10,96
7	Belt on the engine	7785901	1000	0,25		
8	Tires	14.00 R24		31 / 28	1231,60	1363,60
IN TOTAL						1547,04

5 ANALYSIS OF OBTAINED RESULTS

The total monthly operating and maintenance costs are obtained by summing the costs of spare parts required for maintenance, fuel and lubricant costs, labor costs for both machine operators and maintenance personnel, and machine depreciation costs.

The average monthly fuel consumption is 2,219 [lit].

The unit price of one liter of Euro diesel is €1.60.

Therefore, the total monthly fuel cost is: $2,219 \times 1.6 = €3,550$

The monthly salary of the truck operator is €1,600.

The monthly salary of the maintenance mechanic is €1,000, but this amount is divided by the number of machines serviced by the same mechanic. In this case, the mechanic was responsible for maintaining four

machines operating simultaneously. Thus, the monthly cost allocated to the truck for mechanic labor is: $0.25 \times 1,000 = €250$

The average monthly consumption of SAE10W oil is 110 [lit].

The unit price per liter of SAE10W oil is €3.00.

Therefore, the total monthly cost for oil is: $110 \times 3 = €330$

Based on the previously determined data, the total monthly cost of operating and maintaining the T1601C truck is:

$$Tu = 547 + 3,550 + 1,600 + 250 + 330 = €7,277$$

Using this value, the unit operating and maintenance cost per meter of completed mining work and per unit volume of transported material can be calculated. The results are presented in Table 8 and diagram in figure 4.

Table 8 Operating costs of the T1601C truck

OPERATING COSTS OF THE T1601C TRUCK						
Year	Month	Produced meters [m]	Quantity for export [m³]	Operating costs [€]	Operating costs per meter of drift excavated [€/m]	Operating costs per unit of material volume [€/m³]
2021	V	152,00	1953,20	7277	47,88	3,73
	VI	99,40	1277,29	7277	73,21	5,70
	VII	122,50	1574,13	7277	59,40	4,62
	VIII	158,70	2039,30	7277	45,85	3,57
	IX	125,20	1608,82	7277	58,12	4,52
	X	164,10	2108,69	7277	44,34	3,45
	XI	130,00	1670,50	7277	55,98	4,36
	XII	38,50	494,73	7277	189,01	14,71
	I	49,40	634,79	7277	147,31	11,46
	II	100,30	1288,86	7277	72,55	5,65
	III	140,80	1809,28	7277	51,68	4,02
	IV	55,60	714,46	7277	130,88	10,19
2022	V	105,20	1351,82	7277	69,17	5,38
	VI	96,30	1237,46	7277	75,57	5,88
	VII	104,00	1336,40	7277	69,97	5,45
	VIII	107,40	1380,09	7277	67,76	5,27
	IX	97,10	1247,74	7277	74,94	5,83
	X	98,00	1259,30	7277	74,26	5,78
	XI	84,80	1089,68	7277	85,81	6,68
	XII	83,60	1074,26	7277	87,05	6,77
	I	61,70	792,85	7277	117,94	9,18
	II	57,20	735,02	7277	127,22	9,90
	III	49,80	639,93	7277	146,12	11,37
	IV	48,90	628,37	7277	148,81	11,58
2023	V	96,30	1237,46	7277	75,57	5,88
	VI	51,20	657,92	7277	142,13	11,06
	VII	59,70	767,15	7277	121,89	9,49
	VIII	59,60	765,86	7277	122,10	9,50
	AVERAGE				92,23	7,18

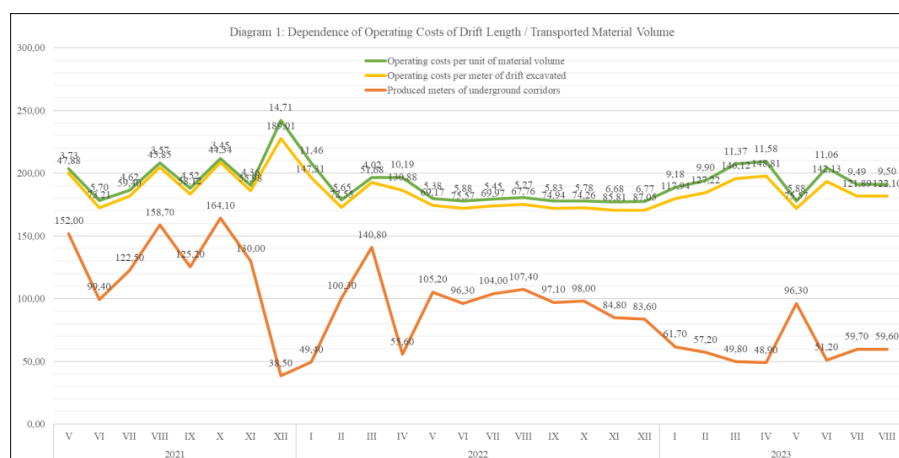


Figure 4 Dependence of operating costs of drift length / transported material volume

6 CONCLUSION

This study presents the methodology for determining the operational costs of equipment used for material transport during the excavation of exploratory underground drifts. Transport cycles were defined based on the total volume of material to be removed from the mine, in accordance with the technical specifications of the transport equipment.

Based on field-collected data, the actual consumption of spare parts for the underground truck was determined. By compiling the total operating and maintenance costs of the equipment, a correlation was established between the length of excavated underground workings and the operational costs.

The obtained data, expressed in €/m, can be used for cost estimation of operating and maintaining the same or similar equipment in future projects

REFERENCES

- [1] Z. Belić, Mining Project on the Exploration of Clastic Formation in the "Rudnik" Mine; Rudnik i flotacija "Rudnik" d.o.o., 2019.
- [2] Maintenance Reports by the Contractor "Carbon Mining Balkan", 2019 – 2023.
- [3] Technical Manual for the Aramine T1601C Truck, 2021.
- [4] B. Cavender, Mineral production costs: analysis and management, Society for Mining, Metallurgy, and Exploration, 1999.

*Nikola Miljković^{*1}, Ivan Stojičić^{*2}, Miloš Živanović^{*3},
Nikola Jovanović^{*4}, Jelena Stefanović^{*5}*

LIMESTONE AGGREGATE PURIFICATION AS A PART OF THE CRUSHING AND SIEVING AT THE “KAONA” QUARRY**

Orcid: 1) <https://orcid.org/0009-0009-2372-3942>; 2) <https://orcid.org/0009-0005-0571-1172>;
3) <https://orcid.org/0009-0006-3331-4294>; 4) <https://orcid.org/0009-0008-0982-2576>;
5) <https://orcid.org/0000-0001-6418-1814>

Abstract

As a part of the Main Mining Design for limestone processing at the Open Pit Kaona – Kučevo, a new Crushing Plant has been designed. This paper includes a part of technological process for additional cleaning of limestone with a fraction of -20+0 mm before the primary crushing.

Keywords: Kaona, crushing, screening, limestone, fraction

1 INTRODUCTION

Exploitation of limestone at the Open Pit Kaon near Kučevo is carried out according to the Main Mining Design. Part of the MMD is the Technical Technological-Mechanical Design for Limestone Processing at the Open Pit Kaona - Kučevo [1].

According to the project on the cadastral plot no. In 1539 KO Kučevo, the crushing and screening line was built. As a part of the requirements of the project task, it was requested that the waste be purified before the primary crushing, in order to obtain a commercial product of fraction: -20+5 mm and definitive waste of fraction -6+0 mm. The limestone crushing and screening line consists of the following subsystems:

1. Receiving part and primary crushing,
2. Secondary crushing and screening (Tower I) with the associated

transport lines and open warehouses of the final crushed material for the Lime Factory,

3. Tertiary crushing and screening (Tower II) with the associated transport lines and open warehouses of the final crushed commercial material,
4. Additional aggregate purification of limestone fraction -20 + 0 mm (Tower III) with the associated transport lines and open warehouses of purified limestone and definitive waste,
5. Dust removal systems.

The starting raw material in the processing process is the run-of-mine limestone - stone obtained by blasting and exploitation at the open pit - Kaona quarry. Limestone is brought in by trucks and

^{*} Mining and Metallurgy Institute Bor, Alberta Ajnštajna 1, 19210 Bor, Serbia,
E-mail: nikola.miljkovic@irnbor.co.rs

^{**} This work was financially supported by the Ministry of Science, Technological Development and Innovation of the Republic of Serbia, Contract No.: 451-03-136/2025-03/ 200052.

unloaded in the receiving bin. The receiving bin is equipped with a primary grid with openings # 750 x 750 mm (Figure 1), so

that limestone with a size below 750 mm (-750 mm) passes through the primary grid and enters the receiving bin. [2]



Figure 1 Receiving bin with the primary grid

At the bottom of the receiving bin is an apron feeder, which removes limestone from the receiving bin, i.e., its emptying. The drive group of the apron feeder has a variable number of revolutions, so the capacity of the apron feeder is also variable up to $Q_{max} = 400$ t/h.

Extracted limestone from the receiving bunker is delivered to the feeder/sieve with the disks (Wobbler feeder). Given that the input limestone is solid, the biggest impurities are found in the lowest granulations that are easily crumbled, so the purification is performed for granulation $-20 + 0$ mm. In addition to purification, the removal of granulation $-20 + 0$ mm from the main technological flow also relieves the primary jaw crusher.

In this paper, the physical methods of enrichment of low-quality limestone extracted from the Wobbler feeder were discussed, which can be [3]:

1. Washing and scrubbing, removes clay, silt and loosely attached impurities
2. Screening and classification, separates limestone by size and removes oversized or undersized impurities
3. Gravity separation (Dense media separation -DMS), removes heavy impurities or light contaminants
4. Magnetic separation, removes ferromagnetic impurities
5. Sensor - based sorting (optical/X-ray sorting), automatically removes impurities based on color, reflectance or atomic density

From the mentioned physical methods, the screening and classification [3] on a flip flow sieve was chosen, as the most technologically appropriate for the given case. Part of the technological scheme related to the processing of granulation $-20 + 0$ mm can be seen in Figure 2. [1]

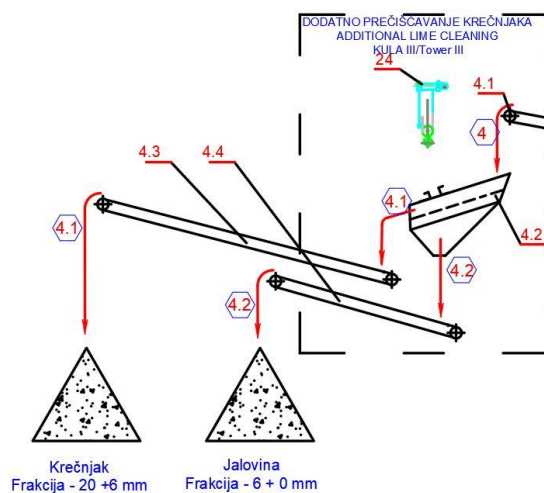


Figure 2 Technological scheme of the crushing and screening line

2 TECHNOLOGY OF ADDITIONAL LIMESTONE PURIFICATION

The fraction - 20 +0 mm is sent to the Tower III for purification, i.e., separation of definitive waste, fraction - 5 + 0 mm and purified limestone fraction - 20 + 6 mm, by means of a belt conveyor with a capacity of 120 t/h, engine power of 15 kW and adopted belt width of 800 mm [1]. The equipment for additional purification of limestone, that is,

the separation of waste - clay, is located in a separate facility - Tower III, as shown in Figure 3, on the left side of which a drawing from the project can be seen [1], while on the right side there is a photo of the finished state with a conveyor of fraction -20 +0 mm and external appearance of the Tower III as well as the disposal conveyors. [2]



Figure 3 Additional limestone purification – Tower III

To connect the equipment with screw connections, you should use screws of material quality class at least 8.8 according to SRPS EN 24015:2012 [4] and nuts 8 according to SRPS EN ISO 4032:2013. [5]

For connections exposed to vibrations during operation, use the elastic spring steel washers alloyed with silicon according to the SRPS M.B2.110 [6] and in other places the flat washers according to the SRPS M.B2.011. [7]

The welded connections that are performed on the construction site are mostly prefabricated type and are not intended for high loads, they are of the standard quality, they are mostly performed as the corner seams. The Tower III is a structure of a steel/frame construction, founded on a reinforced concrete grill. The base of the structure has a regular shape, dimensions 6.00x10.50 m. The working platforms are made of galvanized steel grid. Access to the work platforms is provided by stairs or ladders. Also, a monorail crane is installed in the Tower III for equipment maintenance and parts replacement.

Equipment for additional limestone purification consists of [1]:

1. Pos. 4.2 Vibrating flip-flow screen
 - Type: GFS-2060
 - Manufacturer: Winner, China
 - Capacity Q: 120 t/h
 - Passage through sieve Q1: 60 t/h
 - Cutting limit: 6 mm
 - Installed power P: 30 kW
2. Pos. 4.2.1: Oversize chute – purified limestone
3. Pos. 4.2.2: Undersize basket – definite waste
4. Pos. 4.3: Belt conveyor of purified limestone
 - Conveyor length: 36.5 m
 - Belt width: 800 mm
 - Inclination angle: 0°
 - Engine power: 11 kW
5. Pos. 4.4 Belt conveyor for definite waste
 - Conveyor length: 20.5 m
 - Belt width: 650 mm
 - Inclination angle: 0°
 - Engine power: 7.5 kW

Technologically, waste is separated on a single-level Flip-Flow sieve, pos. 4.2. The derived state of the vibro sieve can be seen in Figure 4. [2]

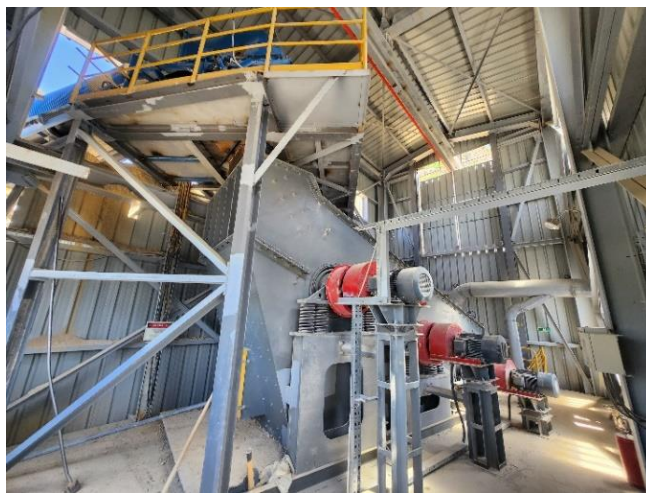


Figure 4 Extraction of waste with a Flip-Flow screen, the current state

The sieve oversize, fraction $-20 + 6$ mm, which represents the purified limestone, is transferred to the conveyor pos. 4.3 sending to the open storage as a commercial product. The derived state is shown in Figure 5 on the left. [2]

The sieve undersize, fraction $- 6+0$ mm, which represents the definitive waste, is transferred to the conveyor pos. 4.4 sending to the open waste storage, from where it is taken by trucks to the mine waste dump. The resulting state is shown in Figure 4 on the right. [2]



Figure 5 Storage of conveyors 4.3 and 4.4 with chutes with Flip-Flow sieves - finished state

3 ASSESSMENT OF INVESTMENTS

The economic indicators of mechanical equipment include the investments in conveyor belts, chute and flip-slow sieves. The investment in accompanying construction

works and steel and reinforced concrete structures are also given with mechanical equipment and are found in Table 1. The investments in electrical equipment are not a part of this work.

Table 1 Investments in mechanical equipment and construction works [1]

Order No.	Name of system part	Investment value (€)
1.	Mechanical purification equipment	100,000
2.	Construction AB works and steel structure	190,000
Total mechanical equipment and construction works:		290,000

4 CONCLUSION

This work presents the design of solutions for additional limestone aggregate purification as a part of the crushing and screening plant. The design of complete mechanical equipment, work technology and capacities are a part of a complex technical-mechanical undertaking that took into account all laws [8], rules of the profession as well as a detailed work in the software programs AutoCAD, SolidWorks, etc. The work shows the possibility of waste cleaning before the primary crushing with the fixed financial investments, in order to increase the percentage of utilization the commercial product from the input material, where, after sieving, the fraction: -20+5 mm is deposited separately from the definitive waste fraction -6+0 mm.

REFERENCES

- [1] Main Mining Design of Limestone Processing at the Open Pit Kaona - "Kučevo", Book 2, Volume 2.1 - Technological Machine Part, September 2019. (In Serbian)
- [2] Photos from Technical Reception the Limestone Crushing and Screening Line, June 2024, Kučevo (In Serbian)
- [3] A. Gupta, D. Yan, Mineral Processing Design and Operations, Elsevier, Edition 2, Chapter 9: Screening, 2016, p. 250.
- [4] Standard SRPS EN 24015:2012 – Hexagon Head Screws - Construction Class B, Date of Publication 03/30/2012. (In Serbian)
- [5] Standard SRPS EN ISO 4032:2013 – Regular Hexagon Nuts (Type 1), Manufacturing Class A and B, Date of Publication 11/29/2013. (In Serbian)
- [6] Standard SRPS M.B2.110:1981 – Elastic Coil Washers with Twisted and Flat Ends, Date of Publication 1/1/1981. (In Serbian)
- [7] Standard SRPS M.B2.111:1981 – Elastic Coil Washers with Twisted and Flat Ends, Date of Publication 1/1/1981. (In Serbian)
- [8] Law on Mining and Geological Explorations, Official Gazette RS, no. 101/2015, no. 95/2018 – other law and no. 40/2020. (In Serbian)

Miloš Živanović^{*1}, Ivan Stojičić^{*2}, Nikola Miljković^{*3}, Jelena Stefanović^{*4},
Nikola Jovanović^{*5}, Miloš Marković^{*6}

TECHNOLOGICAL AND STRUCTURAL SOLUTION FOR THE STRENGTHENING OF THE LOAD-BEARING STRUCTURE OF THE CRUSHER FACILITY DRMNO^{**}

Orcid: 1) <https://orcid.org/0009-0006-3331-4294>; 2) <https://orcid.org/0009-0005-0571-1172>;
3) <https://orcid.org/0009-0009-2372-3942>; 4) <https://orcid.org/0000-0001-6418-1814>;
5) <https://orcid.org/0009-0008-0982-2576>; 6) <https://orcid.org/0009-0007-8392-0636>

Abstract

This paper presents the technological and structural solution for the reinforcement of the main load-bearing steel structure of the crusher facility at the Drmno open-pit coal mine near Kostolac. The structure in question is part of a coal crushing plant exposed to dynamic and static loads over extended periods of operation. In order to achieve the designed and required granulation of the crushed coal, the crushing plant was reconstructed. As part of this reconstruction, the existing belt feeders intended for feeding the jaw crushers were replaced with plate feeders. Due to the increased load on the structure, the steel structure was reinforced. The reinforcement was carried out using prefabricated HEB steel profiles with welded stiffeners, providing additional load-carrying capacity and improving overall structural stability. The adopted solution enabled continued safe operation of the facility. The paper also discusses the methodology of structural assessment, the installation process, and the effectiveness of the applied reinforcement system.

Keywords: Crusher facility, Drmno surface coal mine, open-pit mining, steel structure reinforcement, industrial facility rehabilitation

1 INTRODUCTION

The process of coal crushing for the Kostolac "B" Thermal Power Plant is carried out at the "Drmno" crushing plant using two hammer crushers of Czechoslovak production, type KDV 1137, [1] with a nominal capacity of 1350 t/h, an electric motor power of 1000 kW, and a rotational speed of

$n = 593 \text{ min}^{-1}$. The circumferential-peripheral speed of the hammers is approximately 49 m/s. [2]

This type of crusher requires a specific feeding regime, meaning that the material must be delivered to a designated space between the impact rollers and the rotor. [2]

^{*} Mining and Metallurgy Institute Bor, Alberta Ajnštajna 1, 19210 Bor, Serbia
E-mail: milos.zivanovic@irmbor.co.rs

^{**} This work was financially supported by the Ministry of Science, Technological Development and Innovation of the Republic of Serbia, Contract No. 451-03-136/2025-03/200052. The authors would like to thank Electric Power Industry of Serbia A.D. – Branch "Thermal Power Plants and Mines Kostolac", Open-Pit Mine "Drmno".

2 TECHNOLOGY

Periodic monitoring of the condition and operation of the crushing plant revealed the following: [3]

- Feeding of the crushing plant is continuous, with capacity control in place
- The belt feeder has a trough-shaped cross-section, which means the material is unevenly distributed, with the thickness of the coal layer being greatest at the center of the cross-section.

The conclusion, considering both crushers in the Drmno crushing plant (D1 and D3), is that the hammers wear unevenly, specifically, they wear much faster in the middle of the shaft than at the ends. This results in difficulty adjusting the gap of the crusher's discharge opening. [4]

After analyzing described proposals and consulting with the Investor, the decision was made to replace the existing belts TR6 and TR7 with appropriate plate feeders, which are robust and can meet the conditions for receiving coal through chutes S1 and S2, as well as enabling smooth feeding of the crushers into the center of the crushing area.

After replacing the existing belt feeders with new plate feeders, the designed parameters of the crushed coal were achieved. The new solution ensured even feeding of crushers D1 and D3, resulting in uniform hammer wear.



Figure 1 and Figure 2 Apron feeders PD6 and PD7

The weight of one existing belt feeder is approximately 12 tons, which transports 2 tons of material (coal). The weight of one planned new apron feeder is approximately 36 tons (including accompanying bars and hopper), which will transport the projected quantity of coal of 12 tons (2.00 t/m). Due to the increase in both the self-weight and

operational weight of the new equipment compared to the existing one, it is necessary to reinforce the existing supporting structure of the platform in the “Drmno” crusher building at elevation +8.00 (relative), i.e. 85.20 mm (absolute), in order to enable the replacement of the aforementioned feeders.

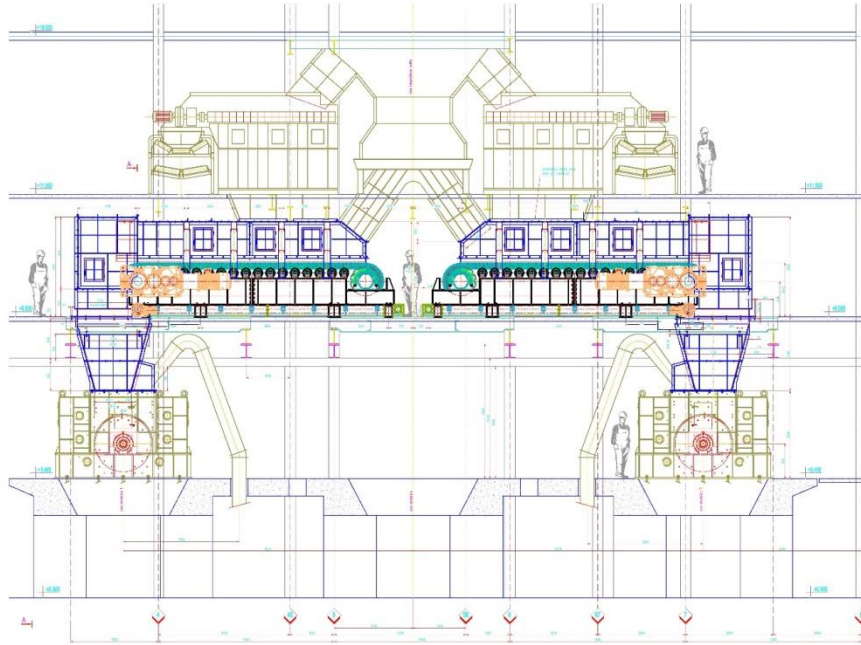


Figure 3 Technological layout of the "Drmno" crushing plant

Following the conducted control static calculation, it was established that the "weak links" on the subject platform are, in fact, the transverse beams supporting the longitudinal beams of the conveyor. Specifically, the conveyor's longitudinal beams are welded I-section beams with flange dimensions of 250x25 mm and web thickness of 390x12 mm, with a total height of 440 mm. The mentioned transverse beams are rolled INP400 profiles and are significantly weaker than the longitudinal conveyor beams, which they are meant to support.

The proposed reinforcement involves the addition of new beams beneath the existing transverse beams. The existing transverse beams are point-supported on the new reinforcement beams via three support plates, all in accordance with the graphical documentation. This method relieves the load on the existing transverse beams without weakening the connections between the existing beams, girders, and columns.

Since columns are not present at all the locations of the aforementioned transverse beams—meaning direct support for additional girder beams is not always available—new longitudinal beams are added as supports for the new transverse beams. These longitudinal beams are positioned to rest on the existing columns.

The newly designed transverse reinforcement beams are conceived as simply supported beams made from rolled HEB 400 profiles. The newly designed longitudinal beams, serving as supports for the new transverse beams, are also simply supported beams, made from rolled HEB 450 profiles. All joints for the newly designed beams are designed as pinned connections.

It is also planned to dismantle the existing monorail support beams between axes "B" and "C" and reinstall them onto the newly designed transverse reinforcement beams. Additionally, in axes "3" and "8", new transverse beams made of rolled INP340/400 pro

files will be added to serve as additional supports for the monorails.

3 STRUCTURAL REINFORCEMENT

The structural reinforcement was necessitated by a change in equipment configuration—specifically, the replacement of two belt feeders with two plate feeders in the crusher facility at the Drmno open-pit coal mine. The

new plate feeders introduced an additional 50 tons of load to the existing steel structure, exceeding its original design capacity.

To facilitate the reinforcement process, the belt feeders were disassembled, allowing unobstructed access to the structural members. Reinforcement was performed prior to the installation of the new equipment to ensure safety and integrity under the increased load.

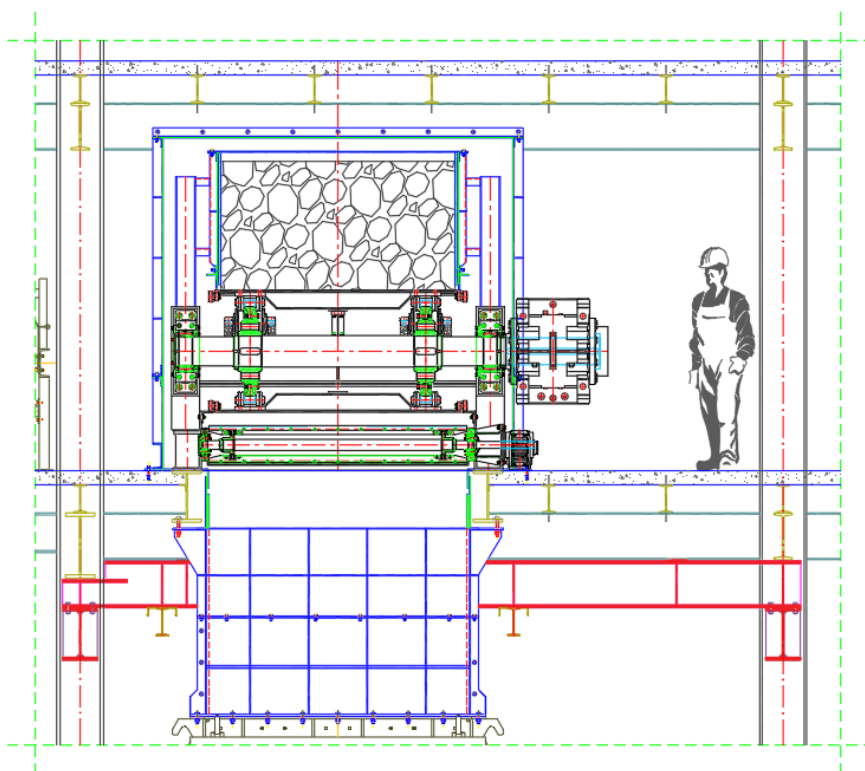


Figure 4 *Structural reinforcement cross section*

The reinforcement design involved installing rolled HEB 450 steel profiles between the main columns of the structure. Transversely oriented HEB 400 profiles were mounted perpendicularly to the axis of the new plate feeders, serving as secondary load-bearing elements. The HEB 450 beams were connected to the columns using end plates

welded with double fillet welds and bolted connections with M20 bolts of strength class 8.8. Additional stiffening plates were welded at the joints between the HEB 450 and HEB 400 profiles as well as at the beam-column interfaces, enhancing the overall rigidity of the assembly and improving stress distribution under dynamic loads.

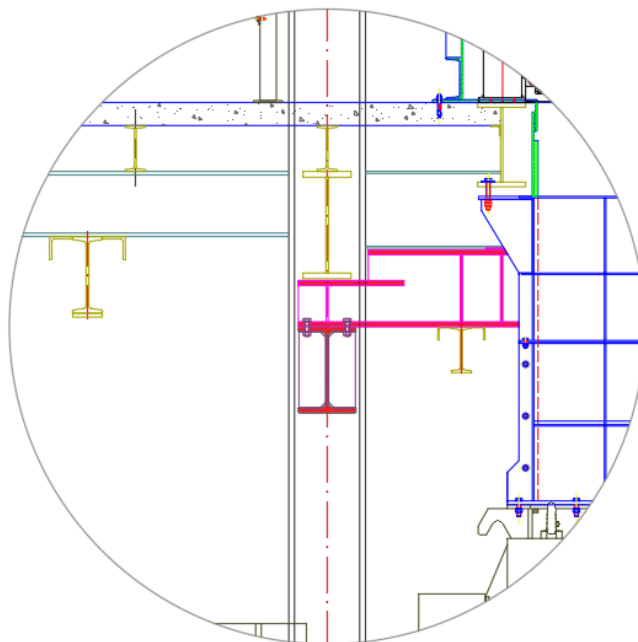


Figure 5 *Structural reinforcement detail*

This step-by-step methodology ensured that the reinforced structure would safely accommodate the higher static and dynamic loads introduced by the plate feeders, without compromising the operational continuity of the facility.

4 CONCLUSION

This paper presents the reinforcement procedure of the supporting structure of the “Drmno” crusher building, which is necessary to achieve the required static and dynamic load-bearing capacity of the level where the feeders are located. The existing belt feeders result in uneven feeding of the jaw crushers, which leads to irregular wear of the hammers and loss of the designed characteristics of the crushed coal.

By replacing the belt feeders with new apron feeders, uniform dosing of run-of-mine

coal across the crusher width has been achieved, resulting in the required crushed coal granulometry and uniform hammer wear.

The reconstruction of the crusher building in the form of steel structure reinforcement was carried out due to the increased weight of the new equipment to be installed in place of the existing one. The necessary load-bearing capacity of the level, from which the old equipment was removed and the new equipment installed, was achieved, and the overall stability of the structure was improved.

The reinforcement of the “Drmno” crusher building was carried out after dismantling the existing belt feeders and unloading the structure. Only after the reinforcement was completed and the required load-bearing capacity achieved, the installation of the new apron feeders was carried out.

Key advantages of the adopted solution include:

- **Ease and speed of installation**, due to the use of standardized, prefabricated rolled steel profiles;
- **Improved load-carrying capacity** to safely support the increased equipment weight;
- **Minimized operational downtime**, as reinforcement was completed prior to equipment installation;
- **Structural integrity and stability**, achieved through proper joint detailing and welded stiffeners.

REFERENCES

- [1] S. Tošić, Calculation of Continuous Transportation Appliances and Lifting Devices, Faculty of Mechanical Engineering Belgrade, 1994. (in Serbian)
- [2] Technical Mining Project for the Reconstruction of the Feeding System of Existing Crushers at the Drmno Open-Pit Mine to Achieve the Designed Parameters of Crushed Coal – Construction Project, 2025.
- [3] Technical Documentation of Plate Feeders, Technical Instructions, and Photographs from Assembly and Commissioning, 2025.
- [4] Standard SRPS EN1993 – 1 – 1 / NA: 2021.

*Jelena Stefanović^{*1}, Zoran Avramović^{*2}, Silvana Dimitrijević^{*3}, Jelena Đorđević^{*4},
Miloš Živanović^{*5}, Nikola Jovanović^{*6}*

EVALUATION OF THE CORROSION RESISTANCE OF STEEL ELEMENTS FROM ELECTROLYTIC REFINING PLANT**

Orcid: 1) <https://orcid.org/0000-0001-6418-1814>; 2) <https://orcid.org/0009-0006-7585-976X> ;
3) <https://orcid.org/0000-0003-1670-4275>; 4) <https://orcid.org/0000-0001-5406-0074>;
5) <https://orcid.org/0009-0006-3331-4294>; 6) <https://orcid.org/0009-0008-0982-2576>

Abstract

The aim of this paper is to present a method for determine a model for accelerated corrosion testing of S235 steel. The experiment was conducted in two parts. In the first part, steel specimens were placed in the Electrolytic Refining Plant, in real conditions, in a indoor. This part of the experiment lasted 6 months. In the second part of the experiment, an attempt was made to obtain a model for accelerated corrosion testing that would accurately simulate real conditions in the Electrolysis. The steel specimens were therefore immersed in the electrolyte solution from the Electrolysis for a month. After cleaning the specimens, mass loss measurements were performed, and then these values were used to determine the corrosion rate after extended exposure. The results show that a shorter experimental duration should be chosen for specimens immersed in the electrolyte solution.

Keywords: corrosion, accelerated corrosion testing, steel specimens, indoor corrosion, immersion, corrosion rate

1 INTRODUCTION

The study of corrosion rates in indoor atmospheres has become relevant in recent years due to structural failures that have occurred on electronic equipment racks and in warehouses. Therefore, it is necessary to analyze this problem in more detail and use accelerated corrosion testing methods in order to obtain relevant data about the steel structure elements.

All corrosion damage affects the load-bearing capacity of steel structures, and there

fore increases maintenance costs. Laboratory corrosion tests are intended to provide approximate results similar to corrosion tests at atmospheric stations, only in a shorter time. The goal is to obtain the same results in a shorter time, thereby achieving significant savings not only in time, but also in the cost of monitoring processes in industrial plants. By comparing experimental results (in the laboratory and in the field, in industrial plants) the realistic capabilities of the model in assuming

^{*} Mining and Metallurgy Institute Bor, Alberta Ajnštajna 1, 19210 Bor, Serbia,
E-mail: jelena.stankovic@irmbor.co.rs

^{**} This work was financially supported by the Ministry of Science, Technological Development and Innovation of the Republic of Serbia, Contract No. 451-03-136/2025-03/200052.

the onset and progression of corrosion are assessed. By obtaining good matches, demanding and time-consuming corrosion testing experiments can be eliminated.

Corrosion resistance tests are performed in real operating conditions or at atmospheric corrosion stations. These are specially selected places, most often with an industrial atmosphere, where samples are exposed and changes in them due to corrosion are monitored. Tests at corrosion stations are long-term, so accelerated laboratory tests are often used, during which corrosion damage occurs in a relatively short time. Acceleration of corrosion processes is achieved by the action of aggressive components, imposing a certain electrode potential, increasing temperature and humidity, etc. The results of accelerated laboratory tests must be compared with data obtained during operation, in order to obtain an appropriate correlation with corrosion behavior in real conditions.

Several authors have chosen the specimens immersion method to define the accelerated corrosion process. The acceleration of the corrosion process is achieved by continuous or alternating immersion of specimens in solutions of a certain composition, at a certain temperature. This is the technically simplest method for accelerated corrosion testing. The time required to achieve the desired level of material damage due to corrosion depends on the corrosion resistance of the metal itself and on the chemical composition of the solution in which the specimen is immersed. The tests are most often performed in chloride solutions (NaCl , FeCl_3), usually with the addition of an oxidizing agent (H_2O_2 , KCrO_4). Depending on the chemical composition of the test solution, the test can be used to simulate corrosion effects.

Frazão et al. [1] conducted a study to evaluate the corrosion and biocorrosion of ASTM A283 carbon steel exposed to a S10 diesel oil/tap water system under static conditions for 90 days. The results revealed that water in the diesel oil can be a negative factor in the corrosion and biocorrosion process. A decrease in the corrosion rate was observed during 90 days of immersion in the two-phase system, which was associated with the formation of a layer consisting of corrosion products and biofilms during the experiments, which made it difficult for the electrolyte to reach the base metal. Garbatov et al. [2] used specimens from a box girder made of ship plate, which was corroded in seawater, in the Baltic Sea. The box girder was placed in a large tank, seawater was continuously pumped into the tank. To increase the degradation due to corrosion, accelerated anodic polarization of the metal surface was used. The anodic electric current was supplied from an external source. The test lasted 90 days.

These studies, as well as numerous others, show that corrosion testing by immersion of specimens can be modified and adapted to specific environmental conditions to suit the problem being analyzed.

2 EXPERIMENT

Continuous immersion tests of specimens are planned during the experimental part. In this study, electrolyte solutions from electrolysis were used as a corrosion medium, thus fulfilling the condition that the solution corresponds to the industrial environment in which the test is performed (Figure 1). The experiment was performed at room temperature, in the laboratory of the Institute of Mining and Metallurgy Bor. The immersion of the specimens was continuous, for a period of one month. Label of these specimens in this paper are A.



Figure 1 *Continuous immersion testing of specimens*

Other set of specimens were placed inside an electrolytic refining plant, Electrolysis, (EF) in closed conditions (Figure 2). Here, the conditions inside the facility are constant in terms of temperature, relative humidity and concentration of pollutants in the air. Blowers were placed inside the electrolysis plant to permanently ventilate the facility. During the experiment,

the temperature inside the facility ranged between 13 °C and 18 °C. The atmosphere also contained electrolytes from aerosols. The higher indoor humidity, which was always higher than 80%, was mainly due to the open electrolytic cells and the high electrolyte temperature (58 ± 2 °C) [3]. The exposure of the specimens (steel tubes) lasted for 6 months.



Figure 2 *Interior of the electrolysis plant; view from the interior balcony where specimens were placed (left) and the ground floor with the pools where the electrolysis of copper anodes were carried out*

3 CLEANING OF SPECIMENS FROM CORROSION PRODUCTS

Cleaning solutions are prepared from chemicals of “pro analysis” purity and distilled water or water of appropriate purity. After any cleaning procedure, the specimen must be washed with distilled water and dried immediately. Chemical cleaning procedures

involve exposing corrosion test specimens to a specific chemical solution that removes corrosion products with minimal dissolution of any base metal. Chemical cleaning of the specimen surface is often preceded by light brushing of the test specimens to remove corrosion

products that are not adhering to the substrate [4].

On weathered specimens, the products were first removed mechanically and then chemically, for a time specified in the standard. Reference specimens were subjected

to the same procedure, as recommended by the standard, to account for mass losses due to exposure to the base material. Table 1 shows the content of chemicals used for cleaning the specimens, as well as the duration of immersion.

Table 1 *Cleaning specimens from corrosion products according to standard SRPS C.A5.005 [5]*

Tag	Material	Chemical	Time	Temperature	Note
C.3.5	S235	500ml hydrochloric acid (HCl, $\rho=1,19$ g/ml), 3,5g hexamethylenetetramine, distilled water up to 1000 ml	10 min	20 to 25 °C	In certain cases, a longer exposure time to the solution may be required.

4 CORROSION RATE

The rate of mass loss increases continuously due to the increase in the time for corrosion to attack the structural elements or due to the increase in the factors affecting corrosion. Generally, after 6 months of exposure, most of the specimen surfaces were 100% covered with corrosion products. According to ISO 9226:2012 [6] after determining the initial total specimen area and the mass loss during the corrosion test, the average corrosion rate in the first year can be obtained.

Long-term predictions of the corrosion rate (C) follow the well-known kinetic expressions for most experimental atmospheric corrosion data [7]:

$$C = r_{corr} t^b \quad (1)$$

The equation is used to describe the corrosion effects obtained during corrosion tests of different durations, at different locations, where C is the corrosion rate after t years, r_{corr} is the corrosion rate in the first year of exposure in grams per square meter

per year ($(g/(m^2 \cdot a))$) and b is an exponent, which represents the dependence on the type of atmosphere in which the steel element is exposed. It should be noted here that the prediction of the corrosion rate depends on the correct determination of r_{corr} , which is determined through this study, while the value of b is taken as the average value of the time exponent from regression analyses of long-term atmospheric corrosion testing programs ISO CORRAG, according to ISO 9224:2012 [8] and has a value of 0.523. The exponent b is a function of atmospheric factors (relative humidity, temperature, duration of precipitation, sulfur dioxide content in air, chloride, PM particles, etc.). The recommendation of many authors is $b=0.77$ for industrial environments (while for marine environments $b=0.78$, and for urban environments $b=0.48$ in the first 4 years, and later $b=0.09$). The corrosion rate of S235JR steel is shown in Table 2.

Table 2 *Corrosion rate and mass loss values of thickness specimens 6 mm*

Nominal thickness of specimens	Label of specimens	Mass loss (g)	Mass loss ratio r	r_{corr} ($g/(m^2 \cdot a)$)
6 mm	A	28,195	0,079	280,95
	EF	0,98	0,003	9,775

The equation (1) can be applied for a period of up to 20 years. At some point, after 20 years, the corrosion process stabilizes, the corrosion rate becomes linear. The corrosion rate decreases with time, stabilizing after 4-6 years. The corrosion process enters the stabi-

lization zone when the corrosion rate changes by less than 10% in one year compared to the previous one [7,8].

Table 3 provides calculated maximum corrosion attack after extended exposure up to 20 years.

Table 3 Determination of the degree of corrosion using a linear model for 20 years

	gr/m ²	A	EF
	$C = r_{corr} t^b$	0.079	0.003
1	1	0.079	0.003
2	1.437	0.113	0.004
3	1.776	0.140	0.004
4	2.065	0.163	0.005
5	2.32	0.183	0.006
6	2.553	0.202	0.006
7	2.767	0.218	0.007
8	2.967	0.234	0.007
9	3.156	0.249	0.008
10	3.334	0.263	0.008
11	3.505	0.277	0.009
12	3.668	0.290	0.009
13	3.825	0.302	0.010
14	3.976	0.314	0.010
15	4.122	0.325	0.010
16	4.263	0.336	0.011
17	4.401	0.347	0.011
18	4.534	0.358	0.011
19	4.664	0.368	0.012
20	4.791	0.378	0.012

5 CONCLUSION

From the mass loss in Table 2 and corrosion rate after extended exposure in Table 3, it can be concluded that the tests by continuous immersion of the specimens in the electrolysis solution are useless in terms of simulating atmospheric corrosion, because they lost too much mass, which means that

the immersion time was assumed to be too long when defining the accelerated corrosion model. If we observe the change in mass over time, with the same linear model used to determine the corrosion rate of S235 steel, it can be concluded that the specimens A immersed in the electrolysis solution for 1

month couldn't be used to calibrate the parameters for specimens EF after 20 years of exposure. In future work, immersed specimens should be analyzed after a shorter time, for example after 10 and 20 days, in order to make the mass loss and corrosion rate, more consistent with the results obtained at the indoor corrosion stations EF.

REFERENCES

- [1] D. Frazão, I. de Melo, M. Montoya, S. Filho, Biocorrosion on Surface of ASTM A283 Carbon Steel, Exposed in Diesel S10 and Tap Water, *Materials Research*, 20 (2) (2017) 808-818.
- [2] Y. Garbatov, C. Guedes Soares, J. Parunov, J. Kodvanj, Tensile strength assessment of corroded small scale specimens, *Corrosion Science*, 85 (2014) 296–303.
- [3] J. Stefanović, Z. Mišković, S. Dimitrijević, Z. Marković, M. Spremić, Experimental analysis of atmospheric corrosion of steel S235JR in industrial environment, *Hemijska industrija*, 79 (1) (2025) 19-30.
- [4] J. Stefanović, S. Dimitrijević, S. Filipović, J. Đorđević, Evaluation of the corrosion resistance of steel elements in the industrially aggressive environments using the accelerated corrosion testing methods, *Mining and Metallurgy Engineering Bor*, 3-4, (2021) 53-60.
- [5] S.C.A5.005:1989, *Korozija metala i legura - Postupci za uklanjanje produkata korozije sa uzoraka za ispitivanje korozije*, Beograd: Institut za standardizaciju Srbije, 1989. (In Serbian)
- [6] Corrosion of metals and alloys — Corrosivity of atmospheres — Determination of corrosion rate of standard specimens for the evaluation of corrosivity (ISO/DIS Standard No. 9226), International Organization for Standardization, Geneva, Switzerland, 2012.
- [7] M. Morcillo, B. Chico, I. Díaz, H. Cano, D. de la Fuente, Atmospheric corrosion data of weathering steel. A review, *Corrosion Science*, 77 (2013) 6-24.
- [8] Corrosion of metals and alloys — Corrosivity of atmospheres — Guiding values for the corrosivity categories (ISO/DIS Standard No. 9224), International Organization for Standardization, Geneva, Switzerland, 2012.

MINING AND METALLURGY INSTITUTE BOR		ISSN: 2334-8836 (Štampano izdanje)
UDK: 622		ISSN: 2406-1395 (Online)
UDK: 681.51:622.271/.33(045)=111	Received: 03.06.2025.	Original Scientific Paper: Management- Project Management
DOI: 10.5937/mmeb2501081J	Revised: 11.06.2025.	
	Accepted: 12.06.2025.	

*Nikola Jovanović^{*1}, Jelena Stefanović^{*2}, Miloš Živanović^{*3}, Zlatko Pavlović^{*4},
Nikola Miljković^{*5}, Zoran Avramović^{*6}*

METHODOLOGICAL APPROACH TO MANAGING THE DEVELOPMENT OF A MAIN MINING DESIGN: A CASE STUDY OF THE X-RAY PLANT AT THE GACKO OPEN-PIT MINE^{**}

Orcid: 1) <https://orcid.org/0009-0008-0982-2576>; 2) <https://orcid.org/0000-0001-6418-1814>;
3) <https://orcid.org/0009-0006-3331-4294>; 4) <https://orcid.org/0000-0001-8102-1820>;
5) <https://orcid.org/0009-0008-0982-2576>; 6) <https://orcid.org/0009-0006-7585-976X>

Abstract

The paper presents an approach to managing the development of the main mining project for an X-Ray sensor-based coal sorting plant under complex technical and organizational conditions at the Gacko open-pit mine. The project team was virtual in nature, consisting of members from multiple countries and disciplines. Through the application of modern project management tools (OBS, WBS, MS Project), the efficiency of planning, control, and risk management was analyzed. The results highlight the importance of a multidisciplinary and digitally integrated approach in the implementation of complex mining projects.

Keywords: mining design, project management, virtual team, multidisciplinary, X-Ray sorting, risk management

1 INTRODUCTION

Modern engineering and mining designs are characterized by a high degree of complexity, large scopes of work, increased budgets, and significant uncertainties [1]. Multidisciplinary approach is a key component, as it involves expertise from various scientific fields, including mining, geology, mechanical engineering, electrical engineering, civil engineering, and others [2]. Additionally, mining projects are marked by long implementation periods and dynamic environments, which require flexible and adaptable management approaches [3].

This paper analyzes a case study of the development of the main mining design for an X-Ray coal sorting plant in Gacko, which was entirely executed by a virtual project team. The paper presents the project management methodology through the definition of team structures, resource and time planning, risk management, and implementation control.

2 THEORETICAL FRAMEWORK

Project management in the context of the mining industry relies on standards such as

^{*} Mining and Metallurgy Institute Bor, Alberta Ajnštajna 1, 19210 Bor, Serbia
E-mail: nikola.jovanovic@irnbob.co.rs

^{**} This work was financially supported by the Ministry of Science, Technological Development and Innovation of the Republic of Serbia, Contract No. 451-03-136/2025-03/200052.

PMBOK [4] and IPMA reference models, which involve a phased approach (initiating, planning, executing, controlling, and closing) and specific tools (WBS, Gantt charts, responsibility matrices). Multidisciplinary projects require the alignment of various disciplines through clearly defined division of work and responsibilities, while working in virtual teams demands intensive digital communication and process standardization [5-7].

3 DESIGN JUSTIFICATION

Coal exploitation in the Gacko Basin is transitioning from fields A, B, and part of C to the Central and Eastern fields [8]. Mining operations in the Central Field are conducted under challenging conditions: increased depth of coal seams, more complex geomechanical and hydrogeological conditions, a higher stripping ratio, greater variability in coal quality, and the presence of numerous waste rock interlayers. These circumstances require the modernization of the coal processing

system, which led to the need for designing an X-Ray sorting plant [8-9].

4 PROJECT TEAM STRUCTURE AND ORGANIZATION

The virtual project team included [10]:

- A project manager,
- Lead designers for individual sections (civil, mechanical, electrical, and mining engineering),
- An administrative associate.

The team members came from six different companies across four countries [10]. By integrating the OBS (Organizational Breakdown Structure) and WBS (Work Breakdown Structure), a responsibility matrix was developed in accordance with the Consortium Agreement [8].

5 TIME AND RESOURCE PLANNING

The responsibility matrix is shown in Figure 1.

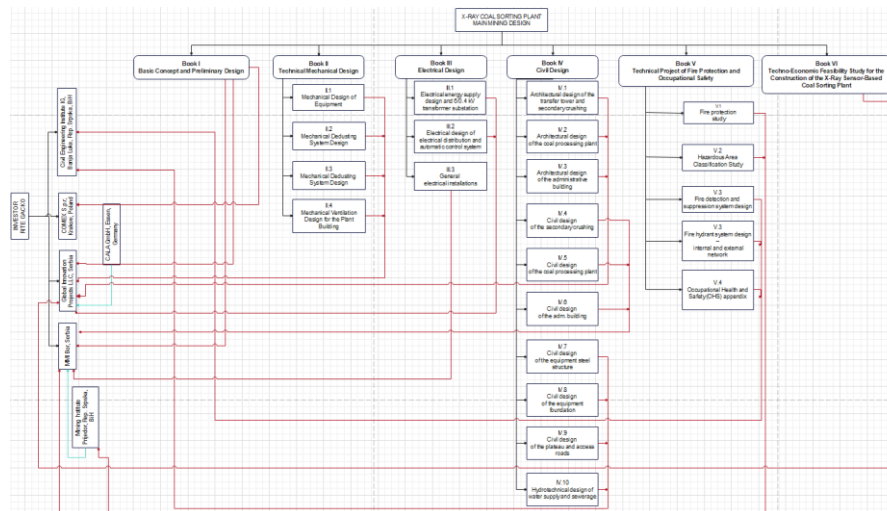


Figure 1 Responsibility Matrix for Main Mining Design

Planning was carried out using MS Project software, up to the third level of the Work Breakdown Structure (WBS), corresponding to individual design volumes. Plans were

developed for summary activities, key milestones, and the start of implementation. The total project duration was eight months. Progress was monitored on a monthly basis,

and evaluations were conducted during regular online meetings [11,12].

Design progress control was one of the key aspects of management, especially in the context of working in a virtual environment. During the project, monthly progress evaluations were conducted with the participation of all project team members via online meetings. The discussions included:

- analysis of the achieved progress,
- deviations from the plan (if any),

- adjustment of upcoming steps according to actual working conditions.

Figure 2 shows progress after three months of work. The diagram shows that the project flow followed the planned timeline, with minor deviations that did not impact overall implementation efficiency. This result indicates a well-established control and coordination system within the team, as well as successful resource planning in relation to the complexity of the task.

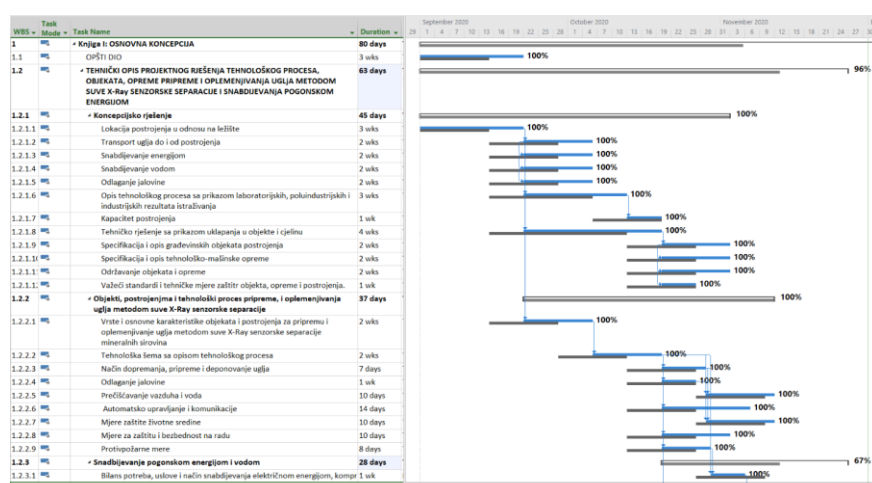


Figure 2 Evaluation of Design Progress. (Adapted from Jovanović et al., 2023, p. 90.)

6 RISK ANALYSIS AND CHALLENGES

The management of the main mining design for the X-Ray sensor-based coal sorting plant in Gacko took place under conditions of pronounced technical and organizational complexity. The key challenges arose from multidisciplinary, the virtual nature of the team, and the geological specifics of the deposit. Identified risks were classified as technical, organizational, regulatory, resource-related, and market-related.

Technical risks included uncertainties regarding the applicability of X-Ray technology to coal of variable quality, as

well as the harmonization of documentation across disciplines [10]. The virtual team, composed of six companies from four countries, faced challenges related to coordination, knowledge management, and differences in professional standards.

Risks were assessed using a probability and impact matrix, and responses included preventive and corrective measures. Monitoring was conducted monthly through online evaluation sessions, enabling timely detection and remediation of deviations.

The risk analysis applied the probability-impact matrix with defined

responses such as mitigation, transfer, and acceptance. Key challenges involved documentation coordination, terminology standardization, and constraints caused by the COVID-19 pandemic [6].

7 CONCLUSION

The development of the main mining design for the X-Ray sensor-based coal sorting plant at the Gacko open-pit mine represents a representative example of managing a complex, multidisciplinary engineering project under specific geological, technical, and organizational conditions.

The use of a virtual project team composed of experts from various fields and countries proved to be an effective solution in the context of modern challenges related to mobility and digitalization. The efficient integration of WBS and OBS structures, along with a clearly defined responsibility matrix, enabled precise management of tasks and responsibilities, as well as progress monitoring in accordance with the plan.

The application of modern planning software tools (MS Project), regular progress evaluations, and a proactive risk management approach contributed to the project's completion within the planned timeframe, without any significant deviations.

The results of this project confirm the importance of an multidisciplinary approach and systematic project management in the implementation of next-generation mining and engineering designs. Furthermore, the experiences gained from this project can serve as a foundation for improving work methodologies in similar contexts, particularly regarding remote team management and adaptation to environmental changes throughout multi-phase project cycles.

REFERENCES

- [1] D. Baccarini, The concept of project complexity – a review, *International Journal of Project Management*, 14(4) (1996) 201–204.
- [2] D. Bogdanović, D. Stojković, *Multi-disciplinarnost u projektovanju rudarskih sistema*, Rudarski glasnik, 2006.
- [3] H. Kerzner, *Project Management: A Systems Approach to Planning, Scheduling, and Controlling*, Wiley, 2018.
- [4] PMI *A Guide to the Project Management Body of Knowledge (PMBOK Guide)*, 6th Edition, Project Management Institute, 2017.
- [5] D.I. Cleland, L.R. Ireland, L. R. *Project Management: Strategic Design and Implementation*, McGraw-Hill, 2007.
- [6] M. Kojić, *Virtuelni timovi i izazovi upravljanja projektima u novim uslovima*, *Menadžment u teoriji i praksi*, 11(1) (2021).
- [7] J.R. Turner, *Handbook of Project-Based Management*, McGraw-Hill., 2009.
- [8] *Main mining project of the X-Ray sensor-based coal sorting plant*, Internal technical document, Mining and Metallurgy Institute Bor, 2020.
- [9] A. Jovanović, M. Bugarin, *Application of the sensor sorting technique in processing of primary and secondary raw materials*, *Proceedings, 50th International October Conference on Mining and Metallurgy*, Bor Lake, Bor, Serbia, 2018, pp. 9-14.
- [10] N. Jovanović, N. Miljković, A. Jovanović, *Upravljanje izradom multidisciplinarnog glavnog rudarskog projekta postrojenja za oplemenjivanje uglja na površinskom kopu Gacko*, U V. Obradović (Ur.), *Zbornik radova XXVII Internacionalnog kongresa iz upravljanja projektima – Interdisciplinarnost kao ključna karika projektne profesije*, IPMA, Srbija, 2023, pp. 84–91.
- [11] .M. Nicholas, H. Steyn, *Project Management for Engineering, Business and Technology*, Routledge, 2020.
- [12] A.J. Shenhar, D. Dvir, *Reinventing Project Management: The Diamond Approach to Successful Growth and Innovation*, Harvard Business Press, 2007.

Marija Jonović^{*1}, Lidija Barjaktarović^{**2}, Dejan Bugarin^{*3}

MAXIMIZING OPPORTUNITIES BY LEVERAGING THE STRATEGIC RISK MANAGEMENT WITHIN THE SCIENTIFIC INSTITUTE^{***}

Orcid: 1) <https://orcid.org/0009-0000-8418-2523> 2) <https://orcid.org/0000-0002-9103-4614>
3) <https://orcid.org/0000-0002-5630-8595>

Abstract

The research is based upon the insights derived from the conclusions of Jonović et al. (2024) and aims to evaluate the effectiveness of Strategic Risk Management (SRM) linked to the COSO ERM (Committee of Sponsoring Organizations Enterprise Risk Management) framework. Implemented within a scientific institute of significant importance to the Republic of Serbia, the SRM is examined for its ability to identify the weaknesses, address threats, and leverage opportunities. The goal is to identify the risk factors and mitigate them through the SRM as a concept closely related to the COSO ERM framework. The primary research includes a SWOT (Strengths, Weaknesses, Opportunities, and Threats) analysis survey conducted from June 26 to July 1, 2024, with a sample of 214 respondents and a response rate of 55.6% (119 respondents). The results highlight a sustainable business strategy and effective application of the SRM in the institute.

Keywords: Nationally significant Institute, COSO, ERM, SRM, SWOT Analysis

Note: Having in mind data protection of the Institute, the authors will not mention the name of the Institute in the research (for the future text it will be used Institute).

1 INTRODUCTION

This study is based upon the conclusions of Jonović et al. (2024) [1], presented at the 55th International October Conference in 2024, held in Kladovo, organized by the Mining and Metallurgy Institute Bor and Technical Faculty in Bor, University of Belgrade. Expanding on their research, this paper provides the new insights into the impact of the Strategic Risk Management (SRM) on a scientific research institute (whose identity remains undisclosed to

maintain confidentiality) that has adopted an Integrated Management System (IMS) guided by the principles of the COSO ERM (Committee of Sponsoring Organizations – Enterprise Risk Management) framework. The subject of the paper emphasizes the importance of effective SRM through the application of the COSO ERM framework combined with the SWOT (Strengths, Weaknesses, Opportunities, and Threats) analysis, highlighting key strengths (moti-

^{*} Mining and Metallurgy Institute Bor, Alberta Ajnštajna 1, 19210 Bor, Serbia,
E-mail: marija.jonovic@irmbor.co.rs

^{**} University of Singidunum, Danijelova 32, 11000 Belgrade, Serbia

^{***} This work was financially supported by the Ministry of Science, Technological Development and Innovation of the Republic of Serbia, Contract on realization and financing of the scientific research work of the Mining and Metallurgy Institute Bor in 2025, Contract No.: 451-03-136/2025-03/ 200052.

vated workforce), weaknesses (equipment and working conditions), opportunities (research impact and collaborations), and threats (budget cuts and talent retention) of the Institute. Furthermore, the research was conducted at an Institute of national importance for the Republic of Serbia, funded by the state budget and possesses intangible resources — the human factor as its greatest potential, with research results holding the significance for society as a whole. In recent years, uncertainty and levels of risk have been increasing both in individual lives and operations of business entities. The reasons for this lie in a turbulent environment where the technological innovations advance rapidly, dynamic nature of business demands the greater seriousness in decision-making, globalization, the global crises resulting in significant losses for all participants in the financial market, COVID-19 pandemic, ongoing crisis in Ukraine, conflict between Israel and Hamas, along with the other negative impacts [2]. Risks are an integral part of operations of any organization. The objectives of risk management within a company are: 1) company can survive losses and sustain further growth thereafter, 2) efficient functioning in a risky environment, and 3) permanent compliance with regulations. Accordingly, the risk management is a dynamic, continuous, and ever-evolving process extending through the implemented organizational strategy [3]. Risk is a condition in which there is a possibility of a negative deviation from desired outcome, expected or hoped for [4]. Finally, the aim of this research is to determine to what extent the SRM, within the ERM process, functioning as an integrated rather than a separate part of the COSO ERM risk management model maximizes opportunities and mitigates risks in the scientific institute. The ERM, as outlined by the COSO in 2017, refers to the integration of culture, skills, and practices with the processes of strategic planning and performance. It serves as the foundation for

organizations to effectively manage risks while achieving, safeguarding, and enhancing value. The definition underscores the ERM emphasis on [5]:

- Understanding and incorporating the organizational culture,
- Building and enhancing the capabilities,
- Implementing the structured practices,
- Aligning the risk management with strategy and performance objectives,
- Addressing the risks in the context of business goals and strategies,
- Establishing a clear connection between the risk management and value creation

Understanding how scientific research organizations operate is a complex task, as it requires simultaneously considering the characteristics of researchers, the organizational traits of the research institution itself, and features of the specific industry sector [6]. The proposed model for strategic management in research organizations, known as the "double-loop learning system" according to Arveson integrates the strategic planning and performance evaluation. The model involves two interconnected components: the internal and external system. The internal system focuses on activities directly related to scientific research, while the external system encompasses common activities characteristic of most organizations. Efficient management of the external system supports the smooth conduct of scientific research, reduces delays, and enables the optimal use of available resources. The key idea is not improvement of the research system itself but the modernization of management structures that support the scientific research activities. [7]. It can be said that the SRM involves the identification, evaluation, and management of risks and uncertainties, influenced by both internal and external factors, which may prevent an organization from achieving its strategic goals and objectives. Its primary aim is to safeguard and enhance the value for all stakeholders. As a fundamental element of the ERM, it serves as

an essential foundation for this broader framework. This definition, which also includes the ERM, is based on six key principles [8]:

- It is a process of identifying, evaluating, and managing the risks and events, both internal and external that could jeopardize the achievement of strategic goals and organizational plans.
- Its primary goal is to preserve and enhance the value for shareholders and all relevant stakeholders.
- It represents an essential part and critical element of the overall risk management system at the organizational level.
- As a part of the ERM, this process is implemented through the activities of boards of directors, management, and other key participants.
- It requires a strategic approach to risk, which involves analyzing the impact of internal and external events or scenarios on the organization ability to execute its plans.
- It is a continuous process that must be integrated into all phases of strategic management, from its formulation to execution and monitoring

This definition and principles can be tailored for an organization to develop its own action plans for improving the ERM, with a focus on strategic risks. The contribution of this study lies in the fact that the SWOT analysis identified deficiencies that, with the optimal management strategy, can be turned into business opportunities. Preventive measures are the adoption of current strategy by the managers in order to solve the real problems. Preventive strategies are aimed at the optimal business models that bring the new values, new products and services and new markets [9].

Based on the information presented earlier, the central hypothesis of this study can be stated as follows H0: The implementation of the IMS based on the COSO ERM framework, in combination with the SWOT analy-

sis, enhances the effectiveness of SRM, enabling the scientific institute to make timely and strategically planned actions aligned with a sustainable business strategy.

The paper is organized into four sections: the opening chapter introduces the study, the second details the methodology, the third focuses on the findings of the primary research, and the final chapter offers the conclusion.

2 METHODOLOGY

The primary research, the SWOT analysis, composed of anonymous survey forms on the topic "Maximizing Opportunities by Leveraging SRM within the Scientific Institute," contains the most significant questions about the potentials for improvement in the Institute, as well as the highest-rated questions.

Various methodological approaches were used for conducting the SWOT analysis during the preparation of the anonymous survey: interviews with employees, quantitative methods for the SWOT analysis, illustrative methods for presenting the research results, and the deductive method for drawing conclusions. The SWOT analysis was conducted to assess the current state of the Institute and identify the potential areas for improvement (both risks and opportunities). The SWOT analysis is a valuable tool in strategic planning as it helps the strategies of organizations structure in accordance with the business requirements [10]. Accordingly, this research presents a SWOT analysis developed with the aim of enhancing the strategic risk management within the Institute. The comprehensive survey structure and combination of methodological approaches clearly contribute to the quality of the results. The SWOT analysis, as a primary survey, will be illustrated in Chapter 3.

This primary survey consisted of four parts (which represents elements of the SWOT, i.e. Strengths, Weaknesses, Opportunities, and Threats), with six questions (36 questions in total; in range of top-rated or lowest-rated). The survey consists of the following elements: 1) potential strengths

within the Institute internal context; 2) potential weaknesses within the Institute internal context; 3) potential opportunities in the Institute external environment; 4) threats in the Institute external environment. Respondents answered the questions by selecting one of five possible ratings. The answers were analyzed using a Likert scale from 1 to 5 (where a rating of 1 means strongly disagree, 2 disagree, 3 neutral, 4 agree, and 5 strongly agree). The anony

mous survey with the closed-ended questions was conducted from June 26, 2024, to July 1, 2024, on a sample of 214 respondents. Out of the total number of respondents, 119 employees completed the survey, of which 86 are PhD holders (72.27%), 31 have a Master's degree (26.05%), and 2 respondents have university-level education (1.68%), resulting in a response rate of 55.6% (presented by Figure 1).

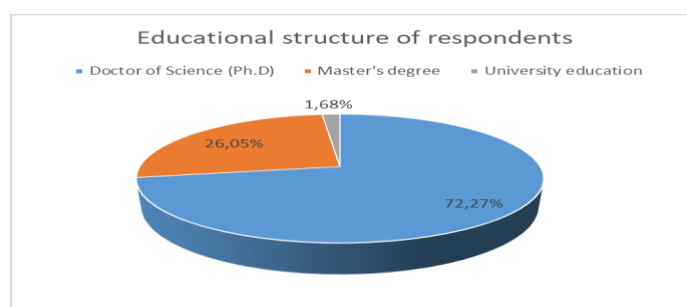


Figure 1 Overview of the educational structure of respondents

3 RESULTS AND DISCUSSION

The results, obtained from the SWOT analysis, conducted on the basis on the survey for potential strengths and weaknesses of the internal context, as well

as opportunities and threats of the external context of the Institute, are presented in the following illustrations in Figures 2, 3, and 4, 5 and Table 1 created on the basis of the conducted survey.

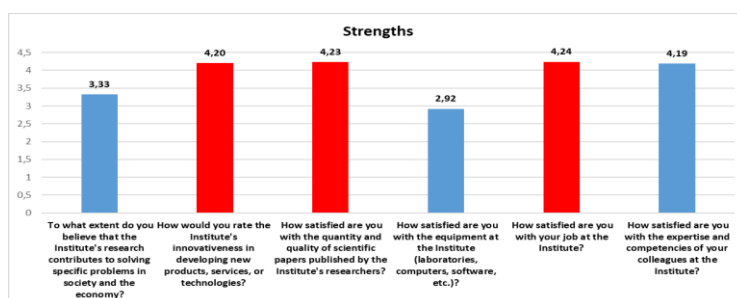


Figure 2 Potential Strengths of the Institute Internal Context (Source: authors)

Legend: Possible strengths: >4.20 ; Sustainable context: $>2.60 < 4.20$; Possible weaknesses: <2.60

Figure 2 illustrates the potential strengths of the Institute internal business context. Based on the survey data, the lowest average

score of 2.92 was given to the question about satisfaction with the Institute equipment (laboratories, computers, software, etc.),

indicating a need for modernization. The highest average score of 4.24 was for satisfaction with the job at the institute, proving that the employees at the institute

highly appreciate and are very satisfied with their work. The average score of 3.85 indicates a sustainable business context.

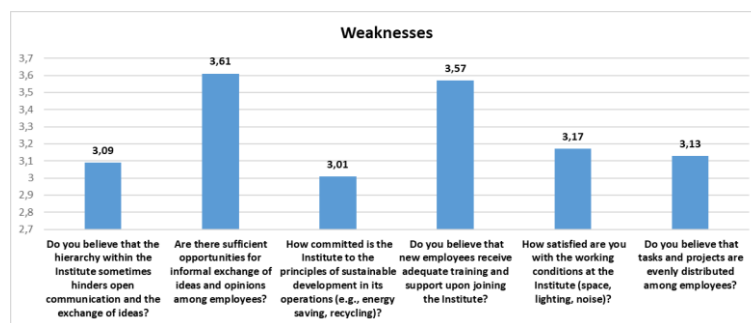


Figure 3 Potential Weakness of the Institute internal context (Source: authors)

Legend: Possible strengths: >4.20 ; Sustainable context: $>2.60 < 4.20$; Possible weaknesses: <2.60

Figure 3 shows the potential weaknesses of the Institute internal business context. Analyzing the responses to questions about the potential weaknesses in the internal context, the lowest average score of 3.01 was obtained for question regarding satisfaction with working conditions (space, lighting, noise). This indicates a sustainable context but shows a room for improvement. The Institute should focus more on improving the working environment and conditions. The

highest average score of 3.61 was obtained for opportunities for informal exchange the ideas among employees, indicating a sustainable business cooperation. The average survey score of 3.26 proves a sustainable business context. Despite this, it is suggested to improve the working conditions, hold workshops on sustainable development, and provide better support and training for the new employees.

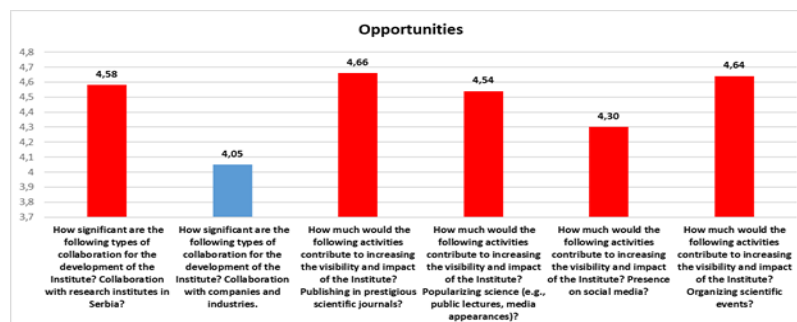


Figure 4 Potential Opportunities of the Institute external context (Source: authors)

Legend: Possible strengths: >4.20 ; Sustainable context: $>2.60 < 4.20$; Possible weaknesses: <2.60

Figure 4 presents the potential opportunities of the Institute external business context. An average score of 4.05 on question about the importance of collaboration with compa-

nies and industry highlights the opportunities available to the Institute. The highest average score of 4.66 was given to the question about the significance of publishing scientific papers

in prestigious scientific journals, showing the outstanding external opportunities that researchers can utilize to improve the Institute operations. The average survey score of 4.46

indicates the exceptional potential external opportunities. It can be concluded that the Institute should be focused on re-cognizing these opportunities.

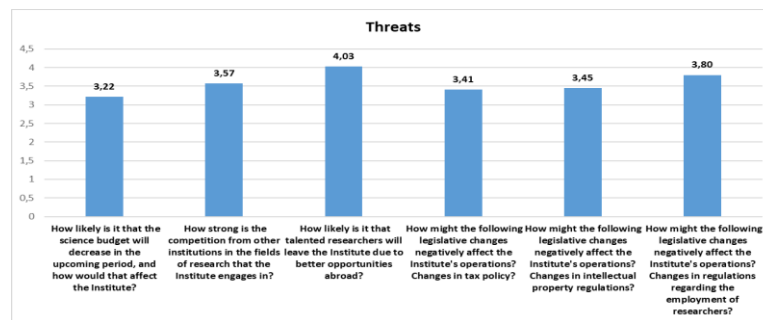


Figure 5 Potential Threats of the Institute external context (Source: authors)

Legend: Possible Threats: >4.20; Sustainable context: >2.60<4.20; Possible opportunities: <2.60

Figure 5 depicts the potential threats of the Institute external business context. The findings highlight two areas requiring the strategic attention from the Institute. While the moderate concern regarding the potential decrease in the science budget (average score: 3.22) indicates a sustainable context, it also suggests the importance of proactive measures to mitigate this risk. Efforts such as lobbying for favorable policies and diversifying funding sources are recommended to ensure resilience and minimize negative impacts. The higher concern over the likelihood of talented researchers leaving for better conditions abroad (average score: 4.03) underscores the urgent need for the Institute to implement the retention strategies. This may include offering the competitive incentives, professional growth opportunities, and fostering a supportive work environment. Overall, the average score of 3.58 demonstrates the Institute ability to resist the potential threats effectively. However, the focused actions to retain talent and address budgetary risks will further strengthen its strategic position and long-term sustainability.

The H0 hypothesis of this primary research: The implementation of the IMS

based on the COSO ERM framework, in combination with the SWOT analysis, enhances the effectiveness of the SRM, enabling the scientific institute to make timely and strategically planned actions aligned with a sustainable business strategy is confirmed by the fact that the SWOT analysis shows a sustainable business context with an average score of 3.79.

4 CONCLUSION

The survey results provide a comprehensive insight into the Institute internal and external context. It is important to emphasized that the H0 (stated as follows: The implementation of the IMS, based on the COSO ERM framework in combination with SWOT analysis, enhances the effectiveness of the SRM, enabling the scientific institute to undertake timely and strategically planned actions aligned with a sustainable business strategy) is confirmed by the findings of the SWOT analysis, which indicates a stable and sustainable business environment, as reflected by the average score of 3.79. Strengths shows that the highest satisfaction with the job at the Institute (average score: 4.24) reflects a highly moti-

vated workforce. Employees value their work, sustainable and productive organizational culture. which is a core strength that contributes to a

Table 1 SWOT analysis of Strategic context report of the scientific Institute

SWOT Analysis		
Internal context	STRENGTHS How satisfied are you with your job at the Institute? (4.24) How satisfied are you with the quantity and quality of scientific papers published by the Institute researchers? (4.23) How would you rate the Institute innovativeness in developing the new products, services, or technologies? (4.20) How satisfied are you with the expertise and competencies of your colleagues at the Institute? (4.19) To what extent do you believe that the Institute research contributes to solving the specific problems in society and economy? (3.33) How satisfied are you with the equipment at the Institute (laboratories, computers, software, etc.)? (2.92)	WEAKNESSES How committed is the Institute to the principles of sustainable development in its operations (e.g., energy saving, recycling)? (3.01) Do you believe that the hierarchy within the Institute sometimes hinders open communication and exchange of ideas? (3.09) Do you believe that the tasks and projects are evenly distributed among employees? (3.13) How satisfied are you with the working conditions at the Institute (space, lighting, noise)? (3.17) Do you believe that the new employees receive adequate training and support upon joining the Institute? (3.57) Are there sufficient opportunities for informal exchange of ideas and opinions among employees? (3.61)
	OPPORTUNITIES How much would the following activities contribute to increasing the visibility and impact of the Institute? Publishing in prestigious scientific journals? (4.66) How much would the following activities contribute to increasing the visibility and impact of the Institute? Organizing scientific events? (4.64) How significant are the following types of collaboration for the development of the Institute? Collaboration with research institutes in Serbia? (4.58) How much would the following activities contribute to increasing the visibility and impact of the Institute? Popularizing science (e.g., public lectures, media appearances)? (4.54) How much would the following activities contribute to increasing the visibility and impact of the Institute? Presence on social media? (4.30) How significant are the following types of collaboration for the development of the Institute? Collaboration with companies and industries. (4.05)	THREATS How likely is it that the science budget will decrease in the upcoming period, and how would that affect the Institute? (3.22) How might the following legislative changes negatively affect the Institute operations? Changes in tax policy? (3.41) How might the following legislative changes negatively affect the Institute operations? Changes in the intellectual property regulations? (3.45) How strong is the competition from the other institutions in the fields of research that the Institute engages in? (3.57) How might the following legislative changes negatively affect the Institute operations? Changes in regulations regarding the employment of researchers? (3.80) How likely is it that the talented researchers will leave the Institute due to better opportunities abroad? (4.03)

Source: Authors created data on the basis of the survey conducted

Weaknesses indicates that areas such as satisfaction with equipment (average score: 2.92) and working conditions (average score: 3.01) require the immediate improvement. Modernizing facilities and creating a more

supportive work environment should be priorities to address these internal challenges. Additional support and training programs for the new employees will also strengthen the Institute internal operations. Opportunities

provide an insight that the external context reveals the exceptional potential, such as the significance of publishing in the prestigious scientific journals (average score: 4.66) and collaboration with the companies and industries (average score: 4.05). These opportunities present a clear pathway for enhancing the Institute research impact and partnerships. Threats highlighted challenges such as the potential decrease in the science budget (average score: 3.22) and likelihood of talented researchers leaving for better opportunities abroad (average score: 4.03) highlight critical risks. To address these threats, the Institute must actively lobby for supportive policies, diversify funding sources, and implement competitive retention strategies to secure its talent pool. It is important to mention that the limitations of the analysis include the use of anonymous questionnaires with closed-ended responses, which restricts the range and adaptability of the answers provided. Likewise complex problems can be reduced to overly simplistic terms, which can result in the loss of important nuances and interdependencies.

The Institute exhibits a solid foundation, with strengths and opportunities that outweigh the identified weaknesses and threats. However, to maintain its sustainability and achieve strategic growth, it is vital to invest in modernizing the infrastructure, retaining talent, and leveraging external opportunities through strategic collaborations and enhanced research visibility. Addressing these areas strategically will strengthen the Institute position and ensure its long-term success. Future research directions should adopt a systematic approach to analyzing the organizational conditions that support the mission and vision of the Institute. Additionally, they should analyze financial parameters related to profitability, as well as the success of strategic risk management.

REFERENCES

- [1] Jonović, M., Barjaktarović, L., Stevanović, M., Bugarin, D., Transforming Risks into Opportunities Through the Strategic Management of a scientific institute, Proceedings – International October Conference on Mining and Metallurgy - 55th IOC 2024, Kladovo, Mining and Metallurgy Institute Bor & Technical Faculty Bor, University of Belgrade, Serbia, 2024, pp. 435- 440.
- [2] Jonović, M., Operational Risk Management on the Example of MMI, (Master's Thesis), Singidunum University, Belgrade, 2023.
- [3] Barjaktarovic, L. Risk Management. Singidunum University, Belgrade, 2015, p.37.
- [4] Vaughan, E., Vaughan, T., Fundamentals of Insurance - Risk Management, MATE (JOHN Wiley & Sons, Inc.), Zagreb, 1995.
- [5] COSO ERM Integrating with Strategy and Performance, 2017, accessed 14/8/2024, https://www.coso.org/_files/ugd/3059fc_61ea5985b03c4293960642fdce408eaa.pdf.
- [6] Laliene, R., Sakalas, A., Conceptual Structure of R&D Productivity Assessment in Public Research Organization, Economics and Management, 19(1) (2014) 25-35.
- [7] Arveson, P., Strategic Management of Scientific Research Organizations, J. Wash. Acad. Sci., vol. 98, 3 (2012) 31–42.
- [8] Frigo M.L., Anderson R.J., Strategic Risk Management: An Example for Directors and Management Teams, Strategy and Execution, 2010.
- [9] Miletić, S., Bogdanović, D., Kostov, A., Building a Strategy for Mining and Metallurgy Companies During the COVID-19 Pandemic, Journal Mining and Metallurgy Engineering Bor, 1 (2022) 41.
- [10] Valentin, E.K., SWOT Analysis from a Resource-Based View, Journal of Marketing Theory and Practice, 9(2) (2001) 54-68.

INSTRUCTIONS FOR THE AUTHORS

Journal **MINING AND METALLURGY ENGINEERING BOR** is published four times per a year and publishes the scientific, technical and review paper works. Only original works, not previously published and not simultaneously submitted for publication elsewhere, are accepted for publication in the journal. The papers should be submitted in both, Serbian and English language. The papers are anonymously reviewed by the reviewers after that the editors decided to publish. The submitted work for publication should be prepared according to the instructions below as to be included in the procedure of reviewing. Inadequate prepared manuscripts will be returned to the author for finishing.

Volume and Font size. The work needs to be written on A4 paper (210x297 mm), margins (left, right, upper and bottom) with each 25 mm, in the Microsoft Word later version, font Times New Roman, size 12, with 1.5 line spacing, justified to the left and right margins. It is recommended that the entire manuscript cannot be less than 5 pages and not exceed 10 pages.

Title of Work should be written in capital letters, bold, in Serbian and English. Under the title, the names of authors and institutions where they work are written under the title. The author of work, responsible for correspondence with the editorial staff, must provide his/her e-mail address for contact in a footnote.

Abstract is at the beginning of work and should be up to 200 words, include the aim of the work, the applied methods, the main results and conclusions. The font size is 10, italic.

Key words are listed below abstract. They should be minimum 3 and maximum of 6. The font size is 10, italic.

Basic text. The papers should be written concisely, in understandable style and logical order that, as a rule, including the introductory section with a definition of the aim or problem, a description of the methodology, presentation of the results as well as a discussion of the results with conclusions and implications.

Main titles should be done with the font size 12, bold, all capital letters and aligned with the left margin.

Subtitles are written with the font size 12, bold, aligned to the left margin, large and small letters.

Figure and Tables. Each figure and table must be understandable without reading the text, i.e., must have a serial number, title and legend (explanation of marks, codes, abbreviations, etc.). The text is stated below the figure and above the table. Serial numbers of figures and tables are given in Arabic numbers.

References in the text are referred to in angle brackets, exp. [1, 3]. References are enclosed at the end in the following way:

[1] Willis B. A., Mineral Processing Technology, Oxford, Pergamon Press, 1979, pg. 35. (for the chapter in a book)

[2] Ernst H., Research Policy, 30 (2001) 143–157. (for the article in a journal)

[3] www: <http://www.vanguard.edu/psychology/apa.pdf> (for web document)

Specifying the unpublished works is not desirable and, if it is necessary, as much as possible data on the source should be listed.

Acknowledgement is given where appropriate, at the end of the work and should include the name of institution that funded the given results in the work, with the name and number of project, or if the work is derived from the master theses or doctoral dissertation, it should give the name of thesis / dissertation, place, year and faculty where it was defended. Font size is 10, italic.

The paper works are primarily sent by e-mail or in other electronic form.

Editorial address : Journal MINING AND METALLURGY ENGINEERING BOR
Mining and Metallurgy Institute
1 Alberta Ajnštajna, 19210 Bor
E-mail: nti@irmbor.co.rs; ana.kostov@irmbor.co.rs
Telephone: +381 (0) 30/435-164; +381 (0) 30/454-108
We are thankful for all authors on cooperation